UNIVERSITE DE LILLE1 – SCIENCES ET TECHNOLOGIES

Ecole Doctorale de Biologie-Santé

Thèse en vue de l'obtention du grade de

DOCTEUR EN BIOLOGIE

Spécialité: Biochimie et Biologie Moléculaire

Epigenetic mechanisms and post-translational modifications play a key role in the cell cycle regulation of *Alphaproteobacteria*

Soutenue par

Antonella Fioravanti

Le 2 Octobre 2014

Thèse dirigée par Dr. Emanuele Biondi

Composition du jury :

Prof. Jean-François Bodart	Président du Jury
Prof. Xavier De Bolle	Rapporteur
Prof. Patrick Viollier	Rapporteur
Prof. Frédéric Barras	Examinateur
Dr. Vincent Villeret	Examinateur
Dr. Emanuele Biondi	Directeur de thèse

Thèse préparée au « Comparative systems biology of signal transduction laboratory »

Institut de Recherche Interdisciplinaire (IRI) – USR3078 CNRS (Villeneuve d'Ascq)

To my brother Emmanuele,
because anything is possible if you really want it.

...don't wait to finish university, to fall in love, to find a job, to marry, to have children, to see them grow up, to lose that ten kilos, to wait for Friday night or Sunday morning, for it to be spring, autumn, summer or winter.
There isn't a better moment to be happy than this, happiness is the way, not the destination. Work as if you don't need money, love as if you never have been hurt, and dance as if nobody can see you.
Remember that the skin wrinkles, hairs become white and the days become years, but the important things don't change, and your power, your belief, doesn't age. Your spirit is the feather duster that sweeps away every web. Behind every finishing line there is a new start. Behind every result there is a new challenge. Until you'll live, feel alive. Go on, even when everybody expects you to give up.

Mother Teresa of Calcutta

Abstract

Epigenetic mechanisms and post-translational modifications play a key role in the cell cycle regulation of *Alphaproteobacteria*

In *Caulobacter crescentus,* the model organism for the bacterial cell cycle*,* many regulators interconnected at multiple levels, are involved in the control of cell cycle progression. This remarkable circuitry is responsible at every cell division for the generation of two different cell types: a vegetative G1-phase (swarmer) cell and a replicative S-phase (stalked) cell. The master response regulator of cell cycle, CtrA, represses in the phosphorylated form the origin of chromosome replication and activates the expression of tens of genes that are crucial for cell cycle progression. CtrA is phosphorylated by the CckA/ChpT phosphorelay at the new pole of the predivisional cell. The spatial organization of CckA suggests that in predivisional cells CtrA-P levels should be higher at the swarmer new pole. Moreover, after CtrA degradation at the G1-S transition, *ctrA* is transcribed thanks to another master cell cycle regulator, named GcrA, the role of which was still enigmatic at the beginning of this PhD. Here we report the study of epigenetic mechanisms, involving the combined activity of GcrA and the methyltransferase CcrM, and post-translational modification of CtrA that play a key role in the regulation of this asymmetrical cell division.

In this thesis we present the discovery of the functional interaction between the enigmatic cell cycle regulator GcrA and the N6-adenosine methyltransferase CcrM, both highly conserved proteins among *Alphaproteobacteria*, that are activated early and at the end of S-phase, respectively. We used a combination of ChIP (chromatin-immunoprecipitation), biochemical and biophysical experimentation and genetics to show that GcrA is a dimeric DNA-binding protein that preferentially targets promoters harbouring CcrM methylation sites. After tracing CcrM-dependent N6-methyl-adenosine promoter marks at a genome-wide scale, we showed that these marks recruit GcrA *in vitro* and *in vivo*. Moreover, we found that, in the presence of a methylated target, GcrA recruits the RNA polymerase to the promoter, consistent with its role in transcriptional activation and activates directly the transcription of several promoters *in vitro* together with the RNA polymerase. Since methylation-dependent DNA-binding is also observed with GcrA orthologs from other *Alphaproteobacteria*, such as *Brucella abortus* and *Sinorhizobium meliloti*, we conclude that GcrA is the founding member of a new and conserved class of transcriptional regulators that function as molecular effectors of a methylation-dependent (non-heritable) epigenetic switch that regulates gene expression during the S-phase of cell cycle. Finally GcrA is also able to interact with a newly characterized protein, named GcrA Interacting Protein X (GipX), that has an essential role in *Caulobacter* and that may plat a role in the regulation of GcrA activity and cell wall metabolism.

Finally, regarding the post-translational modification of CtrA, the protein structure of ChpT and the development of a biosensor able to detect the phosphorylation level of CtrA *in vivo* are described in this thesis. In particular the sensor exploits the ability of response regulators to dimerize upon phosphorylation. The receiver domain of CtrA (CtrA-REC) was individually fused with CFP and YFP, purified and phosphorylated *in vitro*; the phosphorylation-dependent dimerization of the sensor was demonstrated by FRET measurements. Next we confirmed the functionality of this sensor *in vivo* by expressing both fusions at the same time in *Caulobacter* cells measuring the FRET signal in a synchronized population and in different genetic backgrounds. These results open the possibility to use this method to study *in vivo* the phosphorylation of response regulators in other bacterial systems.

L'épigénétique et les modifications post-traductionnelles jouent un rôle essentiel dans la régulation du cycle cellulaire chez les *Alphaproteobacteria*

Caulobacter crescentus est l'organisme modèle d'étude du cycle cellulaire chez les *Alphaproteobacteria*. Le contrôle de ce cycle cellulaire implique un réseau complexe d'effecteurs pouvant interagir à différents niveau de régulation. Chaque cycle de division utilise ce circuit moléculaire pour aboutir à la formation de deux cellules filles différentes : une cellule flagellée en phase G1, et une cellule pédonculée en phase S qui entame immédiatement un nouveau cycle de réplication de l'ADN. Le principal régulateur du cycle cellulaire asymétrique est CtrA, qui dans sa forme phosphorylée inhibe la réplication de l'ADN en se fixant à l'origine de réplication du chromosome et active la transcription de dizaines de gènes indispensables à la progression du cycle cellulaire. CtrA est phosphorylé par le phospho-relais CckA/ChpT, localisé au pôle flagellé de la cellule prédivisionnelle. L'organisation spatiale de CckA suggère qu'à ce stade, les formes phosphorylées de CtrA seraient majoritairement présentes au pôle flagellé. De plus, CtrA est dégradé lors de la transition G1-S pour être ensuite retranscrit grâce à l'action d'un autre régulateur majeur appelé GcrA, dont le rôle était très peu connu au début de ce travail. Nous décrivons ici l'étude des mécanismes épigénétiques, qui impliquent la combinaison des activités de GcrA et de la méthyltransférase CcrM, ainsi que l'étude des modifications post-traductionnelles de CtrA, dans la régulation du cycle cellulaire asymétrique.

Dans ce travail, nous avons mis en évidence l'interaction fonctionnelle entre GcrA et le N6-adenosine méthyltransférase CcrM, protéines toutes deux hautement conservées chez les *Alphaproteobacteria* et activées respectivement au début et à la fin de la phase S. La combinaison d'expériences de biochimie, de biophysique, d'immunoprécipitation de la chromatine et de génétique nous a permis de révéler que GcrA est une protéine dimérique qui se fixe à l'ADN, et qui montre une affinité préférentielle, à la fois *in vitro* et *in vivo*, pour les promoteurs qui ont été méthylés par CcrM. Nous avons également montré que GcrA active la transcription des gènes sous le contrôle de ces promoteurs, en recrutant l'ARN polymérase. La fixation à l'ADN dépendante de la méthylation est également observée avec les orthologues de GcrA présents chez d'autres *Alphaproteobacteria*, telles que *Brucella abortus* ou *Sinorhizobium meliloti*. GcrA est donc le membre fondateur d'une classe jusque-là inconnue de facteurs de la transcription méthylation-dépendants impliqués dans la phase S du cycle cellulaire. Enfin GcrA interagit également avec une protéine récemment caractérisée et appelée GipX. Le gène codant pour cette protéine est essentiel à la croissance de *Caulobacter*, et cette protéine pourrait jouer un rôle dans la régulation de l'activité de GcrA et dans la biosynthèse de la paroi bactérienne.

Enfin, concernant l'étude des modifications post-traductionnelles de CtrA, nous décrivons également la structure protéique de ChpT ainsi que le développement d'un biosenseur capable de détecter les niveaux de phosphorylation *in vivo*. Ce biosenseur est basé sur la capacité des régulateurs de réponses à dimeriser lorsqu'ils sont phosphorylés. Nous avons construit deux protéines de fusion basées sur le domaine receveur de CtrA étiquetées dans un cas avec une CFP et la YFP dans un second cas. Ces protéines ont été d'abord purifiées et phosphorylées *in vitro* afin de confirmer la dimérisation dépendante de la phosphorylation par mesure de FRET. Nous avons ensuite validé la fonctionnalité de ce biosenseur *in vivo*, en exprimant les deux protéines de fusion dans des populations de bactéries synchonisées ainsi que dans des souches présentant des contextes génétiques différents. Nos résultats ouvrent la possibilité d'étendre cette méthode pour l'étude *in vivo* de la phosphorylation des régulateurs de réponses dans d'autres systèmes bactériens.

Table of contents

Introduction

Asymmetric cell growth

Understanding how cell proliferation and division are controlled by complex regulatory networks is a fundamental problem of biology and a basement of several applied research developments in human/veterinary medicine and the biotech industry.

In eukaryotes, the asymmetrical cell growth, that is the cell elongation and the division process producing distinct daughter cells with different morphologies and/or physiologies, is highly investigated and a well-recognized process. Cell division asymmetries can be observed among eukaryotes from single-cell organisms, like protists and unicellular fungi, to multicellular species, where asymmetrical cell fates underlie complex developmental processes (Macara *et al*., 2008; Neumuller *et al*., 2009; Sharma *et al*., 2008; Tajbakhsh *et al.,* 2009).

Such asymmetry among the prokaryotes was for a long time less studied and understood than in eukaryotes. In the past, bacterial cell division was long thought to be mostly symmetrical, as a result of a simple binary fission generating identical daughter cells. However nowadays, after the emergence of new bacterial model systems too, the concept that asymmetry proves integral to the process of cell growth and division is well established for bacteria and eukaryotes alike.

It is known, in fact, that even in apparently symmetric rod-shaped bacteria such as *Escherichia coli*, *Pseudomonas aeruginosa*, *Shigella flexneri* and *Listeria monocytogenes*, where the cell wall growth occur throughout the cell, in a dispersed mechanism (see Fig. 1; Kysela *et al*. 2013), cells are indeed asymmetrical with a new pole created during the last cell division and an old pole made by older material (Fig. 1a). More evident morphological asymmetries are observed in numerous bacterial groups, where cellular growth occurs at cellular poles as in *Actinobacteria* (Chauhan *et al*. 2006; Flärdh et *al.* 2003; Kang *et al.,* 2008; Letek *et al.,* 2008; Nguyen *et al*., 2007; Ramos *et al*., 2003; Meniche *et al*., 2014), or in the *Bacillus* genus in which, under certain starvation conditions, cells can divide asymmetrically as part of a developmental pathway that produce spores (Tan *et al*., 2014; Paredes-Sabja *et al*., 2014). A remarkable type of polar growth is found among the *Alphaproteobacteria,* such as in the *Rhizobiales* order*,* in which cells grow by generation of buds at the new pole (Brown *et al.,* 2012). Budding bacteria divide following

unequal cell growth; the mother cell is able to replicate the DNA producing new daughter cells possessing distinct morphological and/or functional properties (Fig. 1b) (Brown *et al.*, 2012; Macara *et al.*, 2008; Hallez et al., 2004).

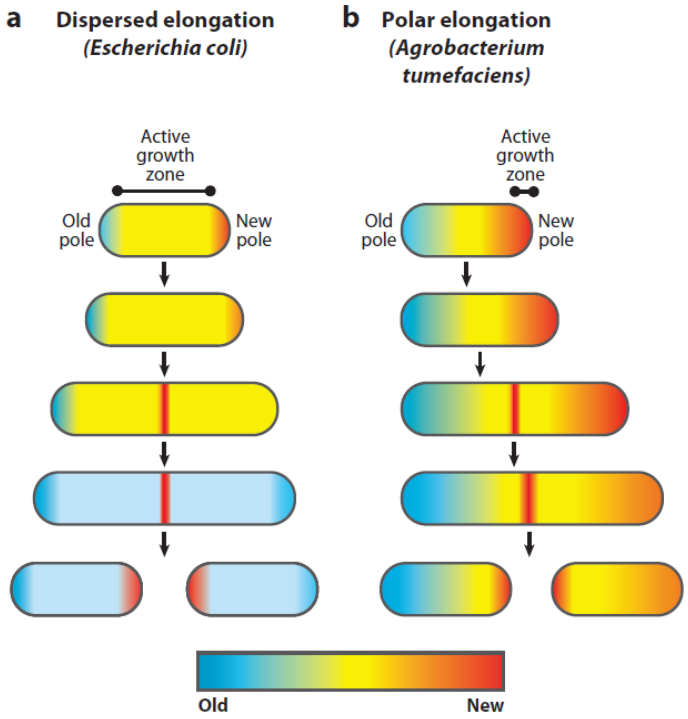

Figure 1. Asymmetry generated during cell growth. (a) Scheme of dispersed cell elongation: new cell wall material is inserted into the existing network of the wall, generating an active growth zone (yellow). The mixture of newer and older patches of wall material in the cylindrical sidewall is present everywhere except the poles. New peptidoglycan (red) is synthesized at the mid-cell to enable cell division. With cell division, each daughter cell contains a new pole and an old pole, giving rise to cellular asymmetry. **(b)** Scheme of polar elongation: new cell wall material is inserted into existing peptidoglycan at the new pole defining an active growth zone (red). A gradient of cell material from old to new is generated as the old half is not experiencing cell wall growth. Following elongation, new peptidoglycan (red) is synthesized at the mid-cell to enable cell division. After cell division, one daughter cell inherits newer cell material (orange), whereas the other daughter cell contains old material (blue) (from Kysela *et al.,* 2013).

A model organism for the study of asymmetrical cell cycle: Caulobacter crescentus

In bacteria, several model organisms have been studied in order to understand the complex regulation that controls cell division and among them, *Caulobacter crescentus* is definitely one

of the most interesting cases and excellent model system for studying cellular differentiation (Brun and Janakiraman 2000, Poindexter 1964). The Gram-negative, aquatic alphaproteobacterium *C. crescentus,* undergoes asymmetric division producing two progeny cells with identical genome but different developmental programs: the sessile ‘‘stalked’’ cell that immediately enters in another replication cycle and the flagellated ‘‘swarmer’’ cell that swims away before differentiating into the stalked morphology and re-entering into the division cycle when the environmental conditions are permissive. Thus the progression through the cell cycle results in a sequential series of changes of the cellular morphology and requires the coordination of processes including chromosome replication, chromosomes segregation, polar morphogenesis, cell growth, and cell division. Like most eukaryotes, *C. crescentus* replicates its chromosome only once during the cell division cycle, therefore the G1, S, and G2 phases are distinguishable (Fig. 2a).

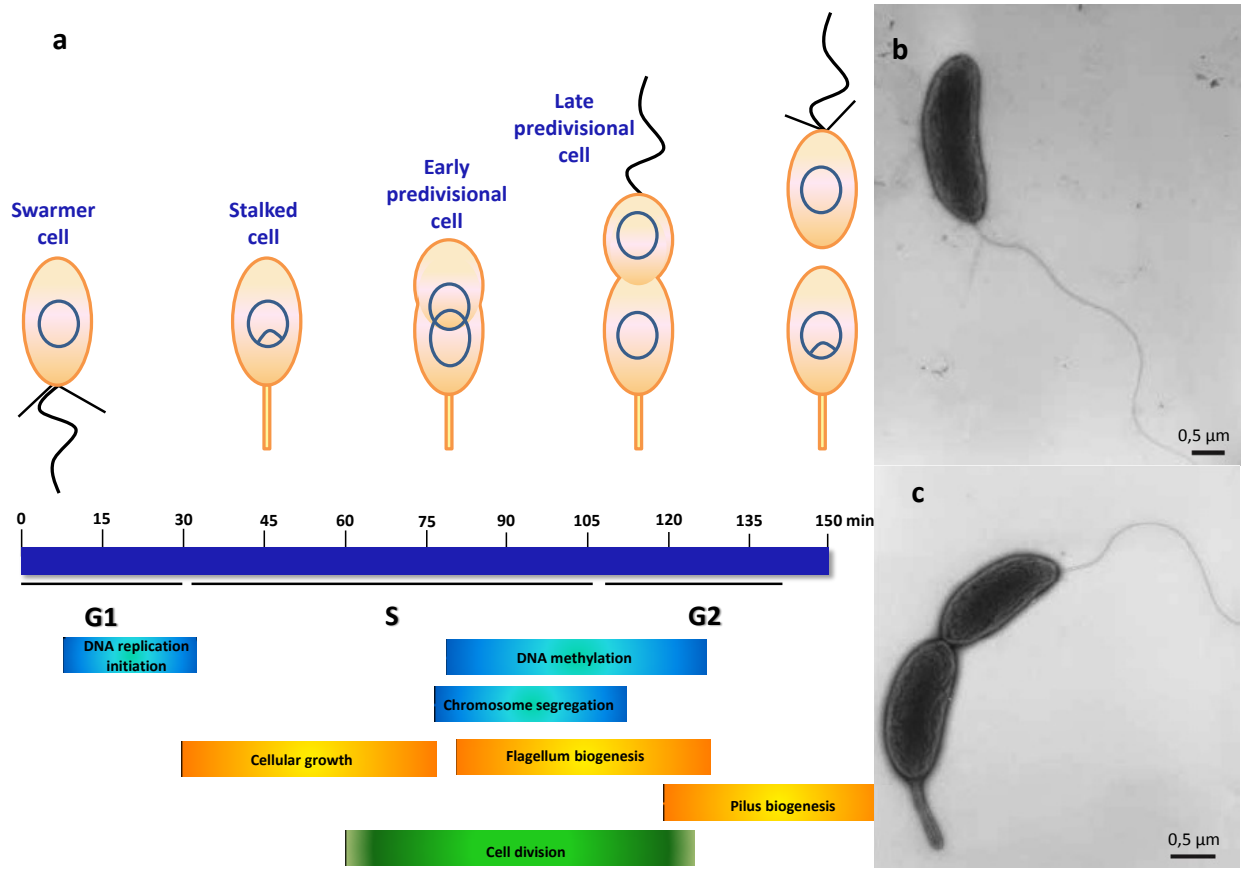

Figure 2. Cell cycle progression in *C. crescentus*. (a) Schematic representation of the cell cycle progressing in minimal medium. The motile swarmer cells differentiate into stalked cells at the G1–S transition by losing their polar flagellum and pili, growing a stalk at that site and initiating DNA replication. The replication of the chromosome is represented by ‘θ’ structures, while circles represent quiescent chromosomes. Colored bars at the

bottom of the panel indicate timing of gene transcription for functionally related sets of genes. Electron micrographs of a *Caulobacter* swarmer cell **(b)** and predivisional cell **(c)** prepared by negative staining with uranyl acetate (from Skerker and Laub 2004).

The chemotactic swarmer cell, that has a polar flagellum and pili and is incapable of chromosome replication, differentiates into a stalked cell after a "gap" period (G1), which depends on the environmental conditions. Cellular differentiation involves ejection of the flagellum, retraction of the pili, and synthesis of a stalk at the same pole that previously contained the flagellum. This polar stalk, which the sessile cell is named after, possesses at its edge an extremely strong polar adhesive structure called the “holdfast” that allows the cell to stick to surfaces during the progression of the cell cycle. At the beginning of S phase, the stalked cell initiates chromosome replication, followed by synthesis of a flagellum at the pole opposite to the stalk and eventually cell division. Flagellum rotation is activated just prior to cell separation. After cell division, pili are synthesized on the new swarmer cell. The stalked cell, acting effectively as a stem cell, undergoes a new round of chromosome replication and cell division.

Thanks to the existence of visible morphological landmarks, which are changing as the cell progresses through the cell cycle (stalk, flagellum and pili); this bacterium in the past years has become an excellent model organism for the study of cell cycle in bacteria. In addition to these landmarks, this organism is a model because of its once-and-only-once DNA replication behavior per cell cycle but also because cultures of *C. crescentus* can be easily synchronized, yielding an almost pure population of swarmer cells (Evinger *et al*., 1977).

Indeed the mechanisms that are driving the progression of the cycle have been examined at the molecular levels in individual cell types throughout the cell cycle reconstructing a fine and complex regulatory circuitry that includes tens of factors. A description of these regulatory mechanisms is provided in the next sections.

Establishment of cellular asymmetry: Global cell cycle regulation in C. crescentus

The generation of *C. crescentus* cells with different morphologies and replicative potentials requires a complex and tightly regulated process. Much of the internal circuitry that drives and

coordinates these adjustments is composed by bacterial two component systems (Stock *et al.*, 2000).

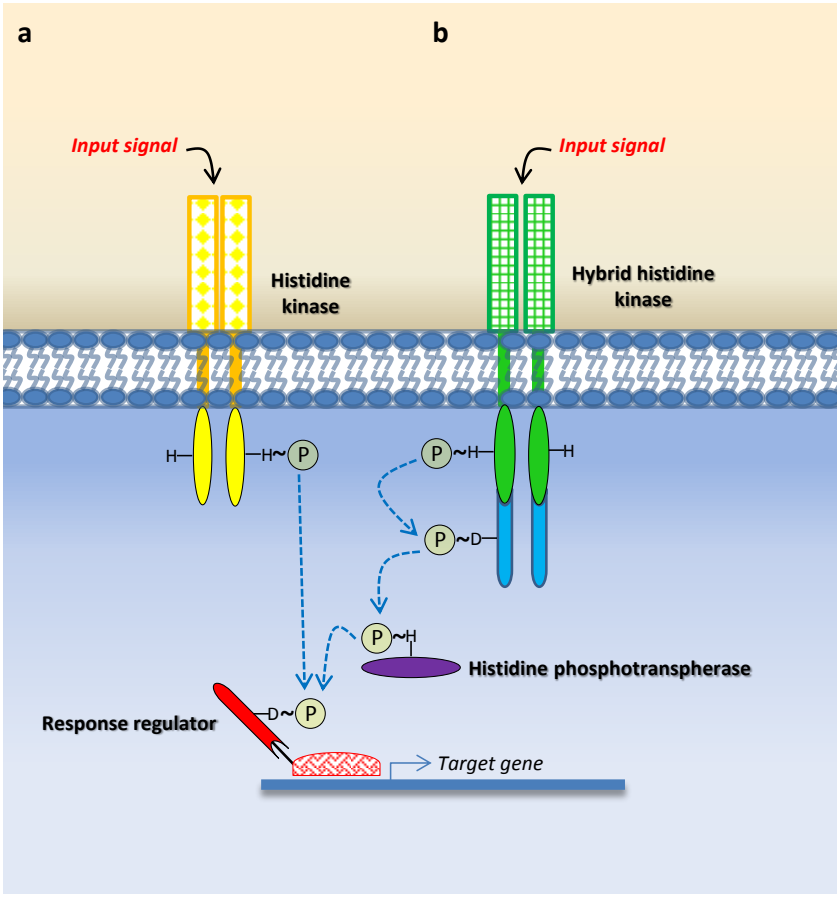

Figure 3. Schematic representation of phosphorylation cascades. (**a**) The classic two-component system, in which upon external activation of the histidine kinase the phosphate (P) is transferred to a response regulator that is going to affect the transcriptional activity of target genes. (**b**) A representation of the less frequent phosphorylation cascade by phosphorelay, in which the phosphate is shuttled from a hybrid histidine kinase, that has both a histidine kinase domain and a receiver domain (homologous to response regulators), to a histidine phosphotransferase that then phosphorylates the response regulator (See text for more details).

Two partners are composing the classic two-component system: a histidine kinase (HK) and a response regulator (RR) (Fig. 3a). The HK is usually composed by two parts, a signal-sensing portion and a kinase portion. The signal sensing part is usually containing transmembrane segments. In response to a signal, the kinase portion auto-phosphorylates itself on a conserved histidine residue upon ATP hydrolysis. The phosphoryl group is then transferred to a conserved aspartate on the receiver domain of the RR, which affects the action of an associated output

domain. RRs are frequently transcription factors, and phosphorylation makes them competent to bind DNA and regulate positively or negatively the transcription of target genes. Less frequently, histidine kinases have a receiver domain of their own; these HK are considered as "hybrid histidine kinase", in which case the phosphoryl group is passed first to this receiver domain and then to a histidine phosphotransfer (Hpt) protein before finally reaching the response regulator, forming a pathway called phosphorelay (Fig. 3b). The function of the Hpt seems to allow either the integration of another histidine kinase into the pathway leading to the response regulator and/or splitting the pathway from a single histidine kinase to multiple response regulators through promiscuity of the Hpt. For two-component and phosphorelay systems, the histidine kinase is usually localized at the membrane, with the sensing domain able to sense signals outside the membrane. An extracellular signal controls the autophosphorylation of the HK domain and consequently the phosphotransfer to the response regulator, which often uses a DNA binding domain as an output.

Taking advantage of the genomic information Laub and coworkers identified at the genome scale level all genes that are cell cycle regulated (Laub *et al.,* 2000). In this first global transcription analysis of synchronized *C. crescentus* cells, 553 genes were identified (19% of the genome) whose messenger RNA levels varied as cell cycle is progressing (Fig. 4). A similar numbers of cell cycle regulated genes were also discovered in *S. meliloti* suggesting that the activity of master regulators, such as CtrA, controlling phase-dependent expression of specific cell cycle genes is a conserved feature of *Alphaproteobacteria* (De Nisco *et al.,* 2014). In other words, *Alphaproteobacteria,* such as *C. crescentus* and *S. meliloti*, evolved a regulation of cell cycle progression that involves ca. 500 genes changing expression during the cycle.

This number of genes changing over the cell cycle strongly suggests a complex regulation of transcription that requires the coordination of several crucial cell cycle events. In the next section an overview of the main players accomplishing this remarkable control is provided.

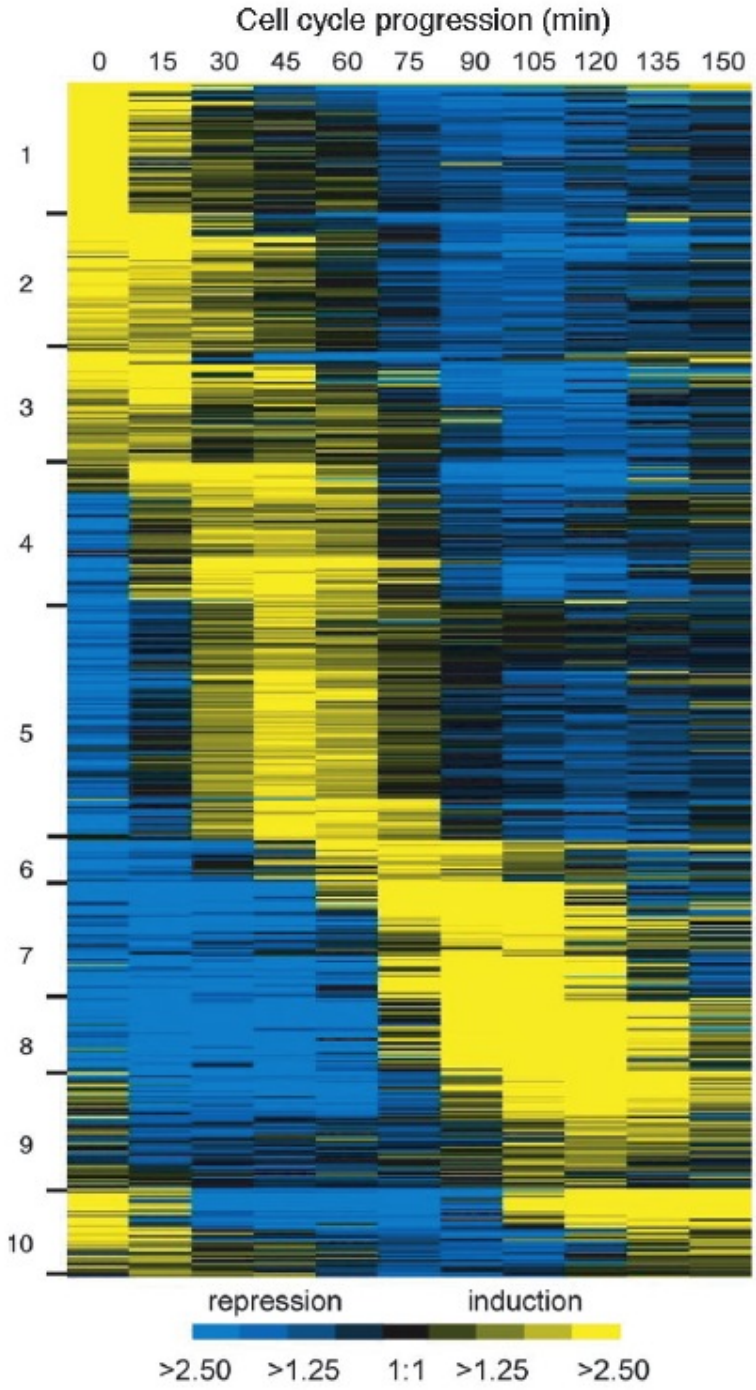

Figure 4. Clustered expression profiles for the *Caulobacter* 553 identified cell cycle-regulated transcripts. Each cluster is numbered from 1 to 10; for an expanded, annotated view of these clusters see Laub *et al.,* 2000; these are organized by time of peak expression. Expression profiles for genes are in rows with temporal progression from left to right, as indicated at the top. Ratios are represented using the color scale at the bottom; from Laub *et al.*, 2000.

The master regulator CtrA

Trying to understand how the intricate gene-expression patterns were regulated and coordinated in different developmental steps, previous works identified the protein CtrA (Cell-cycle Transcription Regulator A) as a key master regulator of cell cycle (Quon *et al*., 1996).

CtrA is an essential transcription factor that acts as response regulator in the phosphorelay composed by the Histidine kinase CckA and histidine phosphotransferase ChpT (Biondi *et al.*, 2006). Once CtrA gets phosphorylated on its conserved aspartate (D51), it undergoes a putative conformational change that increases its affinity for DNA (Siam *et al*., 2000 and 2003). CtrA~P acts either as an activator or repressor for the transcription of cell cycle regulated genes. It was discovered that the 26% of all cell cycle regulated genes have altered transcription due to the direct or indirect activity of CtrA (Laub *et al.,* 2000 and 2002). The CtrA regulon includes gene whose products are required for flagellum assembly and activation, pili biogenesis, holdfast synthesis, stalk biogenesis, DNA methylation, chromosome replication and cell division. The concentration of CtrA itself oscillates through the progression of cell cycle; it is present and phosphorylated in swarmer cells where it binds five sites in the *Cori* region (*C. crescentus* origin of replication) repressing replication initiation (Bastedo *et al*., 2009; Quon *et al*., 1998) and maintaining the cells in G1 state. One of these sites overlaps with a DnaA (essential bacterial chromosome replication initiation factor) binding region, which is required for DNA replication initiation (Marczynki and Shapiro 2002). Only when CtrA gets dephosphorylated and degraded, the S phase can take place in the stalked cells (Domian *et al.*, 1997). Following replication initiation, CtrA is *de novo* synthesized and again phosphorylated, allowing the transcriptional activation of target genes in predivisional cells. Cell division then generates a new swarmer cell that has active CtrA, therefore it cannot initiate replication, and a stalked cell that inactivates and actively degrades CtrA, permitting another round of replication (Fig. 5a). In order to ensure the fidelity of cell cycle progression and generation of functional and morphological asymmetry, CtrA is subjected to multiple levels of regulation (Jenal *et al.,* 1998; Quon et al., 1996; Domian et al., 1997).

1) Post translational modifications

As mentioned before, the specific cell type phosphorylation and degradation of CtrA, is regulated by a double-branched phosphorelay (Biondi *et al.,* 2006) that shares the essential hybrid histidine kinase CckA and the essential histidine phosphotransferase ChpT. ChpT is able to shuttle the phosphoryl group to CtrA, which consequently becomes active, or to another response regulator, called CpdR. This latter protein is a single receiver domain protein lacking the output domain (Biondi *et al.,* 2006; Iniesta *et al.,* 2006). CtrA degradation is performed by the ClpXP ATP-dependent protease (Jenal *et al.,* 1998) at the time of replication initiation, when the protease is localized to the stalked pole by un-phosphorylated CpdR. Following its localization, ClpXP recognizes proteolysis requires a bipartite proteolytic signal in the CtrA sequence that consists in two determinants: the first at the C- termininus of CtrA corresponding to the last 15 amino acid residues (particularly the terminal Ala-Ala), as well as the first N-terminal 56 residues of the CtrA receiver domain (Ryan *et al*., 2002). It was hypothesized that an adaptor protein could be responsible of presenting CtrA to ClpXP, as has been seen for other proteins (Zhou *et al*., 2001); previous studies identify the protein RcdA as factor required for targeting CtrA to the stalked pole in a ClpXP-dependent fashion; this hypothesis was supported by the fact that *rcdA* mutants have stabile CtrA levels during the cell cycle (McGrath *et al*., 2006). In the light of *in vitro* evidence that demonstrates the ability of purified ClpXP to degrade alone the purified CtrA (purified RcdA added to the reaction was not affecting in fact the efficiency of proteolysis) we can conclude that RcdA is not a strict adaptor protein in this process (Chien *et al.,* 2007). Therefore, the role played by RcdA in CtrA proteolysis *in vivo* remains unknown although its role in the CtrA proteolysis is well accepted.

As previously mentioned, both phosphorylation and proteolysis of CtrA are controlled by CckA and ChpT. Like most histidine kinases, CckA is a bifunctional enzyme that harbors both kinase and phosphatase activity (Chen *et al.,* 2009). Consequently, when CckA is not stimulated to autophosphorylate itself (and phosphotransfer to CtrA and CpdR), phosphoryl groups are siphoned back by the phosphorelay to CckA where they are actively eliminated by hydrolysis (Chen *et al.,* 2009).

But which signals/cofactors are controlling CckA activity? CckA is expressed throughout the cell cycle; it is present in the swarmer cell in an active state, while it is located predominantly at the two poles of predivisional cells accomplishing different functions (Jacobs *et al*., 1999). At the swarmer cell pole CckA acts as a kinase, activating CtrA and preventing its degradation by inactivation of CpdR, while, at the stalked pole the phosphatase form of CckA keeps active CtrA levels low and at cell division leads to the sudden dephosphorylation of CtrA and CpdR and therefore to a consequential high level of degradation of the master regulator by ClpPX (Biondi *et al*., 2006; Iniesta *et al*., 2006; Chien *et al*., 2007; Jenal *et al*., 1998). The activity of CckA is positively regulated by the tyrosine kinase DivL (Wu *et al*., 1999; Sommer *et al*., 1991; Tsokos *et al*., 2011), thanks to the direct interaction between these two kinases (Tsokos *et al*., 2011). DivL can be found localized at the swarmer pole of predivisional cells where it is required to recruit CckA and through a protein-protein interaction DivL possibly induces a conformational change of CckA essential for the switch to its active form (Fig. 5b). The ability of DivL to stimulate CckA kinase activity is negatively regulated by the essential single-domain response regulator DivK (Hecht *et al*., 1995).

a

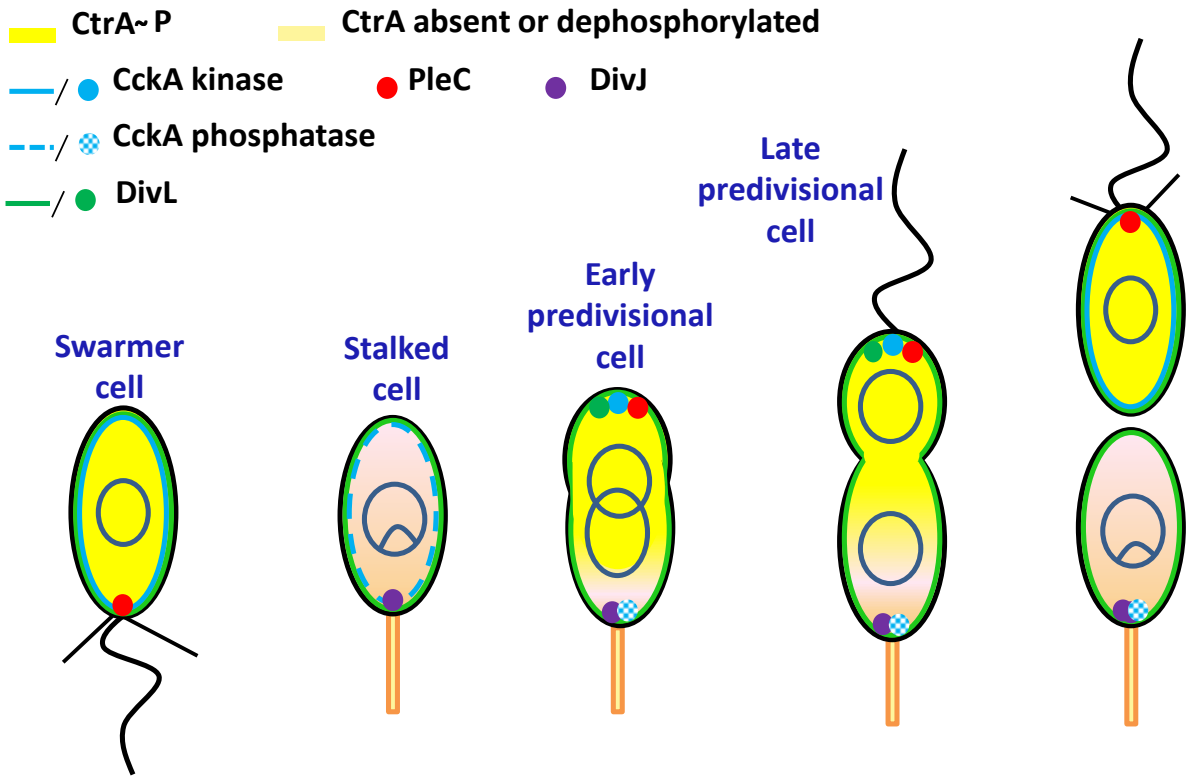

b

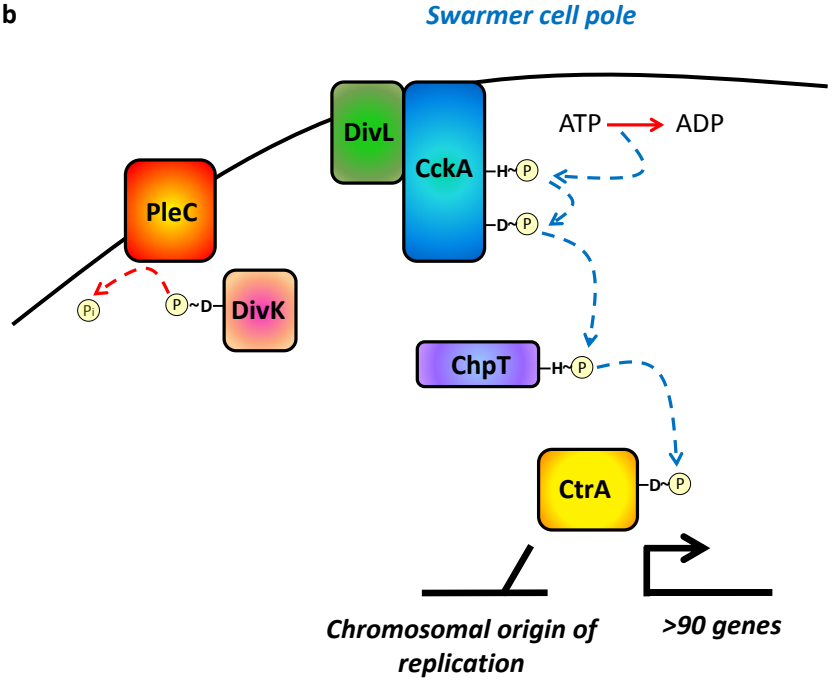

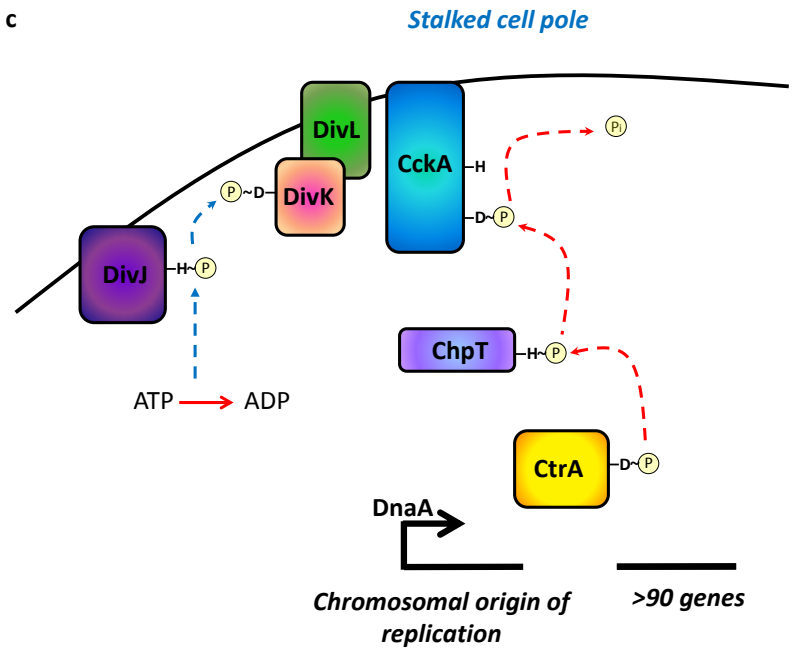

Figure 5. Regulation of CtrA and replicative asymmetry in *C. crescentus*. (**a**) Summary of the regulatory circuitry that controls CtrA in a cell type-specific manner, including the subcellular localization patterns of the histidine kinases CckA, DivL, PleC, and DivJ. (**b**) Model of the two-component signaling pathways and protein–protein interactions that activate CtrA. CckA initiates a phosphorelay that culminates in phosphorylation and activation of CtrA. The activation of CckA as a kinase depends on DivL. PleC keeps DivK un-phosphorylated. (**c**) Phosphorylated DivK can inhibit the CckA–DivL complex interfering with DivL. DivK phosphorylation is controlled by a cognate kinase, DivJ, and a phosphatase, PleC, which localize to opposite poles of the predivisional cell and in the different daughter cells, thereby imposing cell type-specificity on CtrA activation.

The phosphorylated form of DivK binds directly DivL disturbing the interaction CckA-DivL and so inhibiting CckA kinase activity (Fig. 5c) (Tsokos *et al*., 2011). DivK inhibition is controlled at the transcriptional level by CtrA itself, which activates the transcription of *divK* gene, creating a negative feedback loop (Biondi *et al*., 2006). It is proved that DivK and DivL interact in a phosphorylation-dependent manner but it is not clear yet how DivK could precisely affect DivL's ability to promote CckA activity. Phosphorylation of DivK is controlled by the activity of a cognate kinase DivJ and the phosphatase PleC (Paul *et al*., 2008; Jacobs *et al*., 2001; Wheeler *et al*., 1999; Burton *et al*., 1997; Ohta *et al*., 1992).

But how does DivK contribute to asymmetrical distribution of CtrA phosphorylation? PleC is present in swarmer cells where it dephosphorylates DivK, hence allowing DivL and CckA to maintain active and phosphorylated CtrA (Fig. 5a, b). When the swarmer cell differentiates into a stalked cell, PleC is replaced by DivJ, which phosphorylates DivK. Phosphorylated DivK

allosterically activates DivJ resulting in a positive feedback loop that further accelerates DivK phosphorylation (Paul *et al*., 2008) and the consequent down regulation of CtrA, which is a prerequisite for chromosomal replication initiation. The activities of DivK and CtrA are thus inversely related in swarmer and stalked cells (Fig. 5).

In predivisional cells, in which both swarmer and stalked poles are coexisting, CtrA and DivK are phosphorylated thanks to the opposite localization of the phosphatase PleC (swarmer pole) and the kinase DivJ (stalked pole) that depend on polarity factors localized on the membrane, such as SpmX for DivJ (Radhakrishnan *et al*., 2008) and PodJ for PleC (Hinz *et al*., 2003; Viollier *et al*., 2002). Therefore at this stage of the cell cycle the co-localization of specific factors defines a complex spatial arrangement; at the swarmer pole CckA, DivL and PleC will provide a full phosphorylation of CtrA and a complete dephosphorylated form of DivK, while at the opposite site the colocalization of CckA and DivJ will ensure high local concentration of phosphorylated DivK that will induce CckA to act as a phosphatase on CtrA and CpdR.

The fact that in the predivisional cell CckA acts as a kinase at the swarmer pole and as a phosphatase at the stalked pole suggests that phosphorylated CtrA may form a gradient across the cell (Fig. 6), explaining the asymmetrical replicative potential of the two origins (Chen *et al*., 2011).

At the G1-S transition stage of cell cycle the DNA replication is allowed just at the stalked pole where levels of phosphorylated CtrA are lowest, but not at the swarmer pole. This hypothesis was verified by examining DNA replication in individual cells in which the localized origins of replication were fluorescently marked (Chen *et al*., 2011). However no direct measurement of CtrA-P levels in predivisional cells has ever been provided.

Replicative symmetry (both poles origins fired simultaneously with equal probability) was observed in cells lacking active CtrA, or containing fewer CtrA binding sites in the origin (Chen *et al*., 2011). These results indicated that the asymmetrical fates of daughter cells are established before cytokinesis and, more generally, they provide a striking example of the sophisticated spatial patterns of protein activity that can be generated inside bacterial cells.

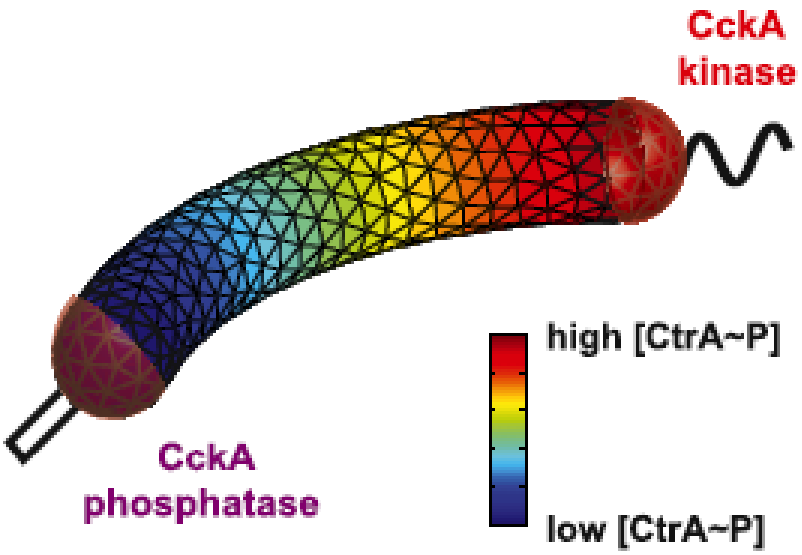

Figure 6. The computational modeling of CtrA~P asymmetry when CckA functions as a kinase at the swarmer pole and as a phosphatase at the stalked pole that was proposed in Chen *et al*., 2011. The modeling is represented in the scheme for a predivisional cell as a 3D curved cylinder with length 4 µm (from Chen *et al*., 2011).

2) Transcription

The different activation of the two promoters (P1 and P2) of *ctrA* is controlling the master regulator transcription during cell cycle (Domian *et al*, 1999). In the next sections we will explore the behavior of these two promoters, and also the role of GcrA.

The P1 is a relatively weak promoter located 122 base pairs (bps) upstream of the *ctrA* translation start site and is active only in the stalked cell for the *de novo* synthesis of CtrA required in the predivisional cell. The P1 promoter contains a GAnTC methylation site and is activated soon after chromosome replication initiation, when the chromosome is hemi-methylated (Marczynski *et al*., 1999; Reisenauer and Shapiro, 2002; Stephens *et al*., 1996).

In 2004 Holtzendorff and coworkers identified a gene encoding a 20 kDa protein of unknown function with striking cell cycle defects when mutated. Interestingly, levels of this protein, named GcrA (global cell-cycle regulator A), oscillated out of phase with CtrA over the course of the cell cycle. While GcrA lacks recognizable functional motifs, chromatin immunoprecipitation assays demonstrated that this protein interacts (directly or not) with some cell cycle-regulated

promoters, including the P1 promoter of *ctrA*. Microarrays analysis showed that this mysterious protein, directly or indirectly, affects transcription of 49 cell cycle-regulated genes in the S-phase of stalked cells (Holtzendorff *et al*., 2004) (a detailed description of this regulator will be provided in the results section as GcrA is an object of this PhD thesis).

When CtrA~P accumulates in the predivisional cell, the P1 promoter gets repressed by CtrA itself, which will activate its own expression through the P2 promoter.

When the chromosome is fully methylated, the P1 promoter is repressed allowing minimal *ctrA* expression prior to a new round of chromosome replication. This second promoter, located 65 bp upstream of the translational start site, is the strongest promoter of *ctrA.* Both promoters are subject to feedback control by CtrA, P1 is repressed (negative feedback) while P2 is activated (positive feedback) in the predivisional cell in the latter part of S phase (Domian *et al*., 1999).

Recently another regulator has been linked to the transcriptional regulation of *ctrA*: MucR1/2 (Fumeaux et *al*., 2004). It has been shown that MucR1/2 complex binds the promoter region of *ctrA* and positively controls its transcription, as the expression of *ctrA* is severely reduced without this regulator.

Finally, methylation of DNA is also regulating *ctrA* transcription, but details about this mechanism will be discussed in the next section.

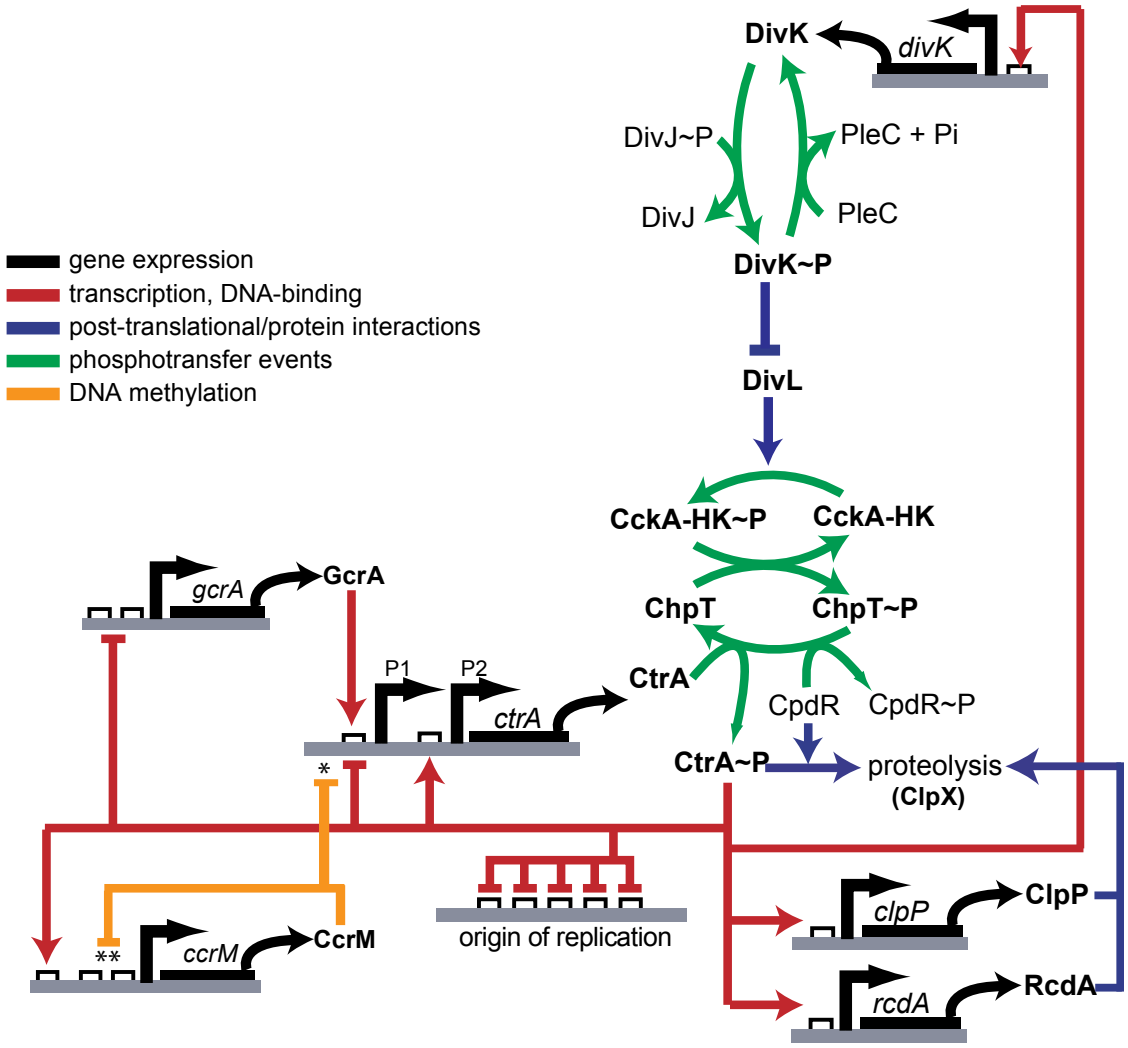

Figure 6. Schematic of the circuit driving cell cycle. Green arrows correspond to phosphorylation reaction; blue connection between DivK and DivL is a protein-protein interaction, while red arrows correspond to transcriptional regulation, which is obviously slower than the other ones, introducing a delay in the circuit (modified from Brilli *et al.*, 2010).

Regulation of DNA replication and methylation machinery

Epigenetic signals, such as methylation of DNA, play an important role in the regulation of gene expression in eukaryotes and, as we will see here and in the Results section of this thesis, in the regulation of *ctrA* expression in *Alphaproteobacteria*. Methylation of adenines at the N6 position (m6A) has been described in Bacteria, Archaea, Protists and Fungi. However, besides being known for its protective role in bacterial restriction/modification systems, m6A also fulfills cellular functions in *Gammaproteobacteria*, including the initiation of DNA replication, transposition, mismatch repair, and virulence gene expression (Marinus *et al*., 2009; Brunet *et al*., 2011; Demarre *et al*., 2010). In the *Alphaproteobacteria* such as *C. crescentus*, *S. meliloti*, *Brucella abortus* and *Agrobacterium tumefaciens*, the solitary methyltransferase CcrM is required for efficient growth, presumably through gene expression control of critical cell cycle genes (Zweiger *et al*., 1994; Stephens et al., 1996; Wright *et al*., 1997; Robertson *et al*., 2000).

The cell cycle role of CcrM was originally characterized in *C. crescentus* (Zweiger et al., 1994; Wright *et al*., 1997) and associated to the master regulator CtrA. As described before, in G1 CtrA~P inhibits DNA replication by repression of the origin of replication (Quon *et al*., 1998) and only upon CtrA proteolysis or dephosphorylation, DnaA-mediated chromosome replication initiation occurs (Hottes *et al*., 2005) committing cells to the S phase. The resynthesis of CtrA requires transcription of *ctrA* that relies on the methylation-sensitive *ctrA*P1 promoter (Domian *et al*., 1999) whose activation depends on GcrA, an enigmatic factor that is encoded in the genomes of *Alphaproteobacteria* and several *Caulophages* (Brilli *et al.*, 2010; Gill *et al.,* 2012; Panis *et al.*, 2012). The *ctrA*P1 promoter is repressed by full methylation of DNA, therefore only when the DNA is replicated, thus hemimethylated, its transcription can start (Reisenauer *et al*., 2002). While in *C. crescentus* GcrA accumulates in early S phase and is confined to stalked cells (Holtzendorff *et al.,* 2004) for the activation of *ctrA*P1, the *ctrA*P2, reinforces *ctrA* transcription later in S-phase. At the end of S-phase phosphorylated CtrA in turn activates transcription of the *ccrM* gene. After the introduction of m6A marks in the context of GAnTC sequences (Zweiger *et al*., 1994) CcrM is proteolyzed prior to cell division by the Lon protease (Wright *et al*., 1997). How the m6A marks, introduced by CcrM, affect transcription is unclear, but the marks are transient as DNA replication converts the (full) methylation on both DNA strands to the hemi-

methylated state, until strands are re-methylated in a distributive manner (Albu *et al*., 2012) once CcrM has accumulated at the end of S-phase (Fig. 7). The time a given genomic locus spends in the hemi-methylated state is thus predetermined by its physical proximity to the origin of replication, a feature that might be exploited to couple activation of certain promoters, such as *ctrA*P1, with replication progression (Reisenauer and Shapiro, 2002). Therefore GcrA and CcrM are implicated in the transcriptional regulation of *ctrA*P1, suggesting linked roles that will be explored in the Results section of this thesis. While an underlying biochemical relationship is also hinted by the analysis of the gene occurrence pattern in the *Alphaproteobacterial* genomes (Fig. 8) (Brilli *et al*., 2010), this link remains experimentally untested.

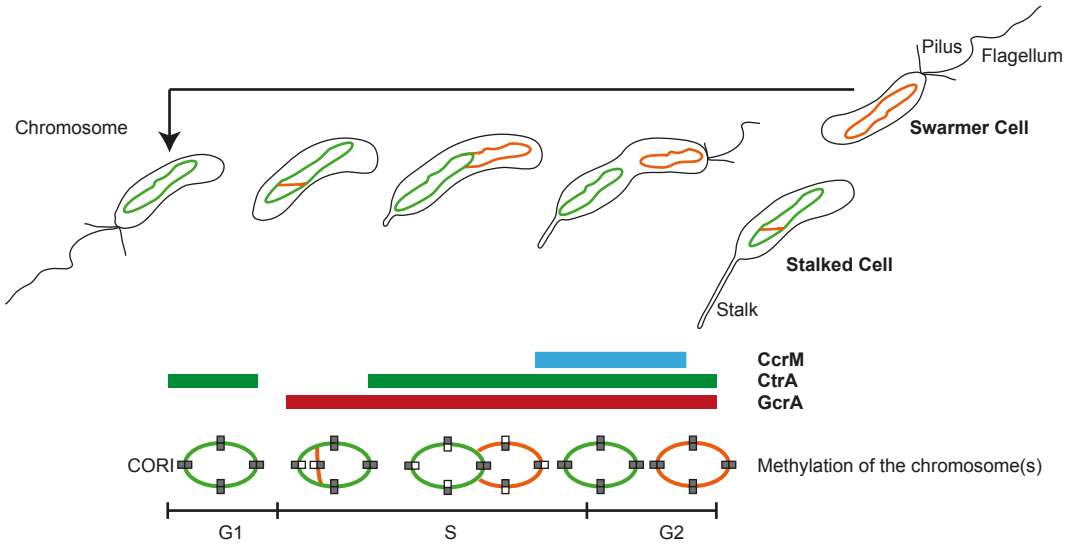

Figure 7. Scheme of chromosome methylation by CcrM during the cell cycle progression in *C. crescentus*. Levels of CcrM, CtrA and GcrA are represented by colored bars.

Conservation across organisms of the cell cycle regulatory circuit

Alpha subdivision of proteobacteria (*Alphaproteobacteria*), which includes *C. crescentus*, is a taxonomic group of bacteria that contains several interesting models for the study of cell cycle progression. This group is a very heterogeneous and includes symbionts of plants (*Rhizobia*), pathogens for animals (*Brucella*, *Rickettsia*) and pathogens for plants (*Agrobacterium*).

The conservation across organisms of this circuit has been studied in *Alphaproteobacteria*, where CtrA is present, using bioinformatics tools (Brilli *et al*., 20010; Fig. 8).

CtrA, even if associated with variable regulatory circuits within *Alphaproteobacteria*, shows conservation of the control of certain functions, such as cell division, motility and signal transduction, especially in cluster A where CtrA is, in fact, the master regulator of cell cycle (Brilli *et al*., 2010). The ability to detect the same functions controlled by CtrA in different organisms also suggests that the prediction capability of CtrA-regulated genes is highly reliable.

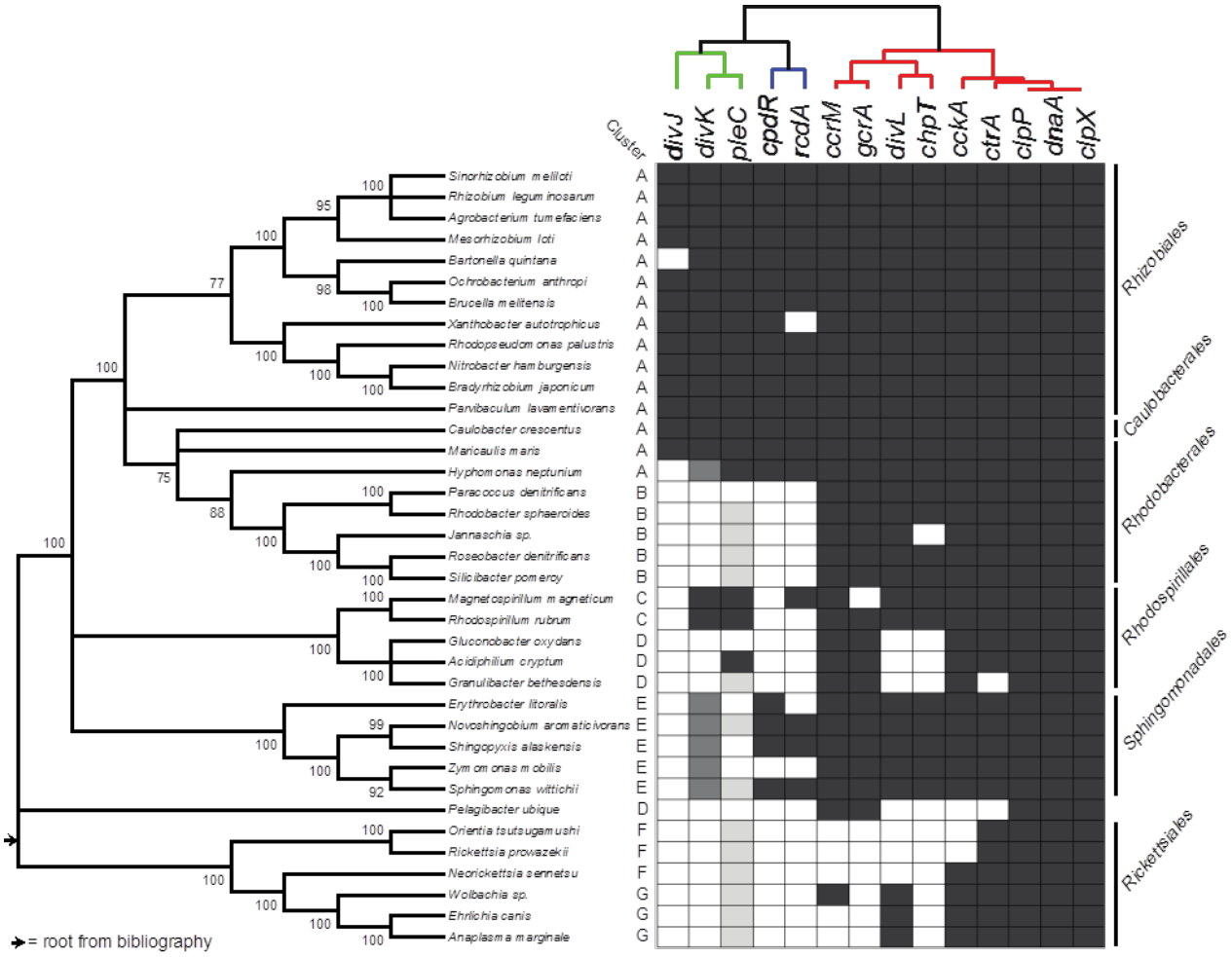

Figure 8. Orthologous genes in *Alphaproteobacteria*. Presence (black) or absence (white) of genes involved in cell cycle regulation in the alphaproteobacterial genomes. Proteins are indicated in the uppermost row and they are ordered on the basis of their co-occurrence patterns. Dark gray cells indicate the presence of an ortholog with respect to the protein corresponding to that column. Medium dark gray cells correspond to DivK proteins in those organisms that have an ambiguous position in the phylogenetic tree; light gray cells correspond to organisms that have PleC but where DivK is absent or in doubt (from Brilli *et al*., 2010).

Several regulators of cell cycle, first identified in *C. crescentus*, were sporadically investigated in other *Alphaproteobacteria*, such as *Agrobacterium*, *Magnetospirillum*, *Brucella* and *Sinorhizobium* (Pini *et al.,* 2013; Mohapatra *et al*., 2014).

What is emerging by an overall interpretation of these results is that cell cycle and asymmetrical division are peculiar features of *Alphaproteobacteria* (Hallez *et al*., 2004), but each organism has evolved also specific features in order to adapt to specific environments.

Although the knowledge of *C. crescentus* cell cycle is now providing self-explained models of its regulation, many gaps are still present. This is particularly true for other models in the *Alphaproteobacteria* in which clearly regulators and modules are present but their different behaviour is not understood yet. Pioneering works on *S. meliloti*, *Agrobacterium* and *Brucella* have provided hints of alternative cell cycle regulation models (Ardissone *et al*., 2012). For example, looking at the DivK module, in *Sinorhizobium* and *Brucella* a more complex situation than *C. crescentus* has emerged, in which DivJ/PleC-like kinases are multiple and sometimes essential, differently from *C. crescentus*, suggesting a more important role in the cell cycle regulation (Pini *et al*., 2013; Hallez *et al*., 2007).

Objectives

As we discussed in the introduction, the study of cell cycle regulation in *C. crescentus* and the comparison of this knowledge to other *Alphaproteobacteria* is a challenging and still surprising field of research. Although in the past 50 years a lot has been discovered about the molecular mechanisms that are driving the cell cycle and asymmetrical division of this bacterium, many questions remain open.

"What is the role of the enigmatic factor GcrA? Is there a link with the methylation of DNA by CcrM?" were some of those intriguing questions; although GcrA has been matter of research since its discovery (Holtzendorff *et al*., 2004), many aspects regarding this protein were still unclear at the beginning of this PhD.

One of the challenges of my PhD work was to understand whether GcrA was able to interact directly with DNA possibly acting as a transcription factor, since an effect on transcription of cell cycle-regulated genes was originally observed (Holtzendorff *et al*., 2004). A study of the biophysical characteristics of this protein was also required to better understand its function, because until then GcrA was defined as a *"protein that lacks recognizable functional motifs"* (Holtzendorff *et al*., 2004). On the other hand, a clarification of the apparent connection with the methylase CcrM (Marczynski *et al*., 1999; Reisenauer and Shapiro, 2002; Stephens *et al*., 1996; Holtzendorff *et al*., 2004) required the setup of a biochemical assay able to detect methylation dependent binding of GcrA on specific targets of DNA.

My PhD work was intended to respond to these ambitious tasks starting from a pure and stable preparation of GcrA. This was the starting point of my work: obtaining the best preparation of the protein in order to perform biophysical and biochemical studies. Once these questions were answered, a comparative study of the knowledge acquired for the *C. crescentus* GcrA to other *Alphaproteobacteria* models was a further goal of this PhD thesis.

More was known about the master regulator CtrA and its regulation, but many unclear aspects remained to be investigated at the beginning of this thesis. At the time I started my PhD, except for the response regulator DivK (Guillet *et al*., 2002), no structural information of proteins involved in the regulation of CtrA, and CtrA itself, was available. Thus, another objective of this

thesis was to perform for the first time a structural study on the cytosolic components of the CckA-ChpT-CtrA phosphorelay with the intent to gain insights at the molecular level on the organization and function of these important proteins. With this information we aimed to understand the mechanisms that lead to the activation or deactivation by phosphorylation and dephosphorylation of CtrA.

Another approach was adopted later in the thesis in order to study *in vitro* and *in vivo* the phosphorylation of CtrA; using the property of response regulators to dimerize upon phosphorylation we aimed to construct a FRET biosensor CtrA tool able to measure phosphorylation levels. This last strategy allowed us to study the phosphorylation event to whom is subject CtrA in the cell and *in vitro*. Especially *in vivo*, this tool was adopted in order to measure for the first time the gradient of phosphorylated CtrA (hypothesized by Tsokos and coworkers in 2011) in predivisional cells, a fundamental event for generation of asymmetry during the cell cycle progression.

Results

The results section is divided in two main sections:

1) The investigation of role played by GcrA in regulating the cell cycle, its connection with CcrM methylation and its interacting proteins, such as RNAP and GipX;

2) The study of the molecular details of CtrA phosphorylation cascade using a structural approach and through the development of FRET-based tools to study CtrA dimerization.

Study of GcrA function and interacting proteins

GcrA is a CcrM methylation–dependent transcription factor controlling cell cycle

1) Production, Purification and Biophysical characterization of GcrA:

GcrA is a conserved protein that lacks primary structural resemblances to known characterized domains. GcrA is a 173 amino acids (aa) long protein, with a high content of positively charged residues, such as arginine and lysine (16.7% of the total aa content) mostly located in the central region (45-80 aa) and an Isoelectric point (pI) of 10.58. Those features may support the ability of GcrA to bind DNA directly through its N-terminal/central part. Consistently, the N-terminal part is also the most conserved region of GcrA at the evolutionary level across orthologs of GcrA shown in the figure 9.

This conservation suggests an important functional role of the region, for example in the specific DNA binding or in putative interactions with other cellular factors.

The aa composition of the protein revealed that 60.6% of the amino acids (aa) are polar and that the 46% of the sequence consist of disorder-promoting residues such as charged residues or prolines and glycines, that are usually frequent in intrinsically disordered proteins (IDPs) (Theillet *et al*., 2013).

```
CLUSTAL 2.1 multiple sequence alignment


Agrobacterium      MNWTDERVEKLKKLWSEGLSASQIAAQLGGVSRNAVIGKVHRLNLPGRVKAGGPVTSARS 60
Sinorhizobium      MNWTDERVEKLKKLWSEGLSASQIAAQLGGVSRNAVIGKVHRLSLPGRAKAGG-STAAAA 59
Brucella           MNWTDERVELLKKLWSEGLSASQIAAQLGGVSRNAVIGKVHRLKLSGRGKTTTAAPRSKK 60
Caulobacter        MSWTDERVSTLKKLWLDGLSASQIAKQLGGVTRNAVIGKVHRLGLSGRAAPSQPARPAFK 60
                   *.******. ***** :******** *****:*********** *.**  .      :

Agrobacterium      APKRTAAPAPRATT--FAGRVNAAPARILTRSNAATALHEEIDIETAQVLDYVPSKNVVT 118
Sinorhizobium      RPKR-ATSAPRAPN--YAARS---VTRTVTRTAGATALKEELAVDLTIDQELQIDRNIVL 113
Brucella           VNTPAAAPRPAVQNNNSGTHTTTMRTATVTKTVGATALQMEYATEVVAETVIKPASDVVV 120
Caulobacter        APRPARPAAQAMPS----------APRRVTPVEAPTS------VPVAAAPAPLPAFRHEE 104
                         ..     .           .  :*   ..*:         .

Agrobacterium      PISRRLTLTELTERTCKWPVGDPLKDDFHFCGCEALESSPYCKFHAKLAYQPVSERRKA- 177
Sinorhizobium      PMSRRLELTELTERTCKWPIGDPLKEEFHFCGNDSPEASPYCTFHARLAYQPSAERRRMR 173
Brucella           PISRHLTLLQLSERTCKWPIGDPLNEDFHFCGNESGEASPYCSYHSRLAFQPTAERRRAR 180
Caulobacter        PGS--ATVLTLGAHMCKWPIGDPSSEGFTFCGRRSSEG-PYCVEHARVAYQPQQTKKKSG 161
                   * *    :  *  : ****:*** .: * ***  : *. ***  *:::*:**   :::

Agrobacterium      ------------
Sinorhizobium      ------------
Brucella           ------------
 Caulobacter        GAELARSLRRYI 173
```

"*" means that the residues or nucleotides in that column are identical in all sequences in the alignment.

":" means that conserved substitutions have been observed.

"." means that semi-conserved substitutions are observed.

Figure 9. CLUSTAL multiple sequence alignment of GcrA orthologous. Aa sequences of *S. meliloti*, *A. tumefacis*, *B. abortus* and *C. crescentus* GcrAs are aligned by ClastalW2 program, showing an higher homology at the N-terminal of the orthologous proteins (from Fioravanti *et al*., 2013).

Prediction of unfolded regions using RONN (Fig. 10a; Yang *et al*., 2005) suggested that two regions 41–105 aa and 145–173 aa of GcrA are disordered, while the software SOPMA (Geourjon *et al*., 2013), suggested that GcrA is partially structured in the N-terminal region (Fig. 10b) with an organization in three predicted alpha helices suggesting a folded structure.

a

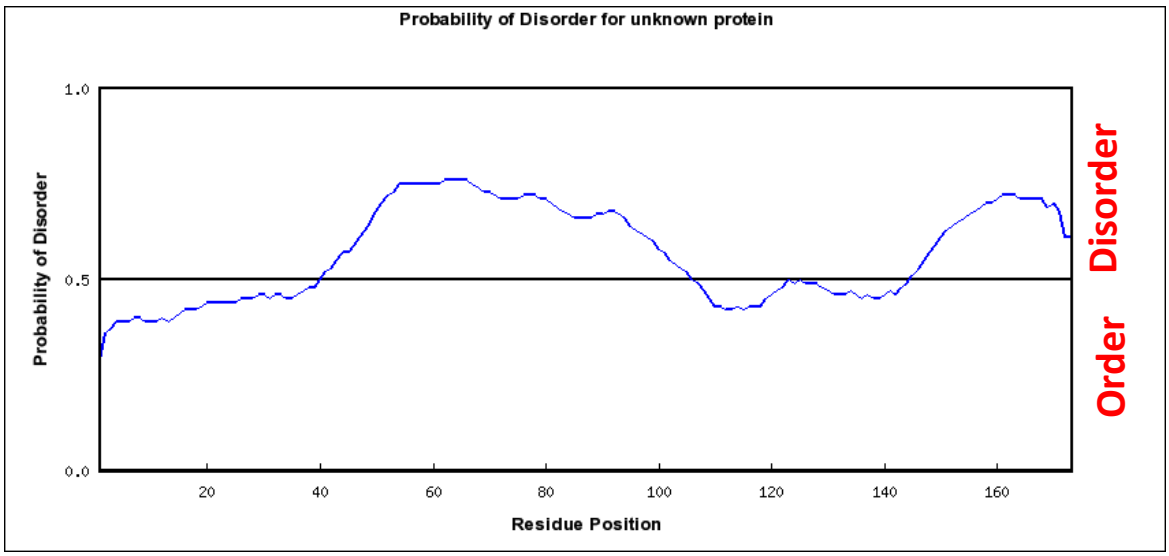

b

```
          10        20        30        40        50        60        70
           |         |         |         |         |         |         |
MSWTDERVSTLKKLWLDGLSASQIAKQLGGVTRNAVIGKVHRLGLSGRAAPSQPARPAFKAPRPARPAAQ
hccchhhhhhhhhhhhttcchhhhhhhhhhcchhhhhhhhhhetccccccccccccccccccccccccc

AMPSAPRRVTPVEAPTSVPVAAAPAPLPAFRHEEPGSATVLTLGAHMCKWPIGDPSSEGFTFCGRRSSEG
ccccccccccccccccccccccccccccccccccttceeeeehccccccccccccccceeetccccccc

PYCVEHARVAYQPQQTKKKSGGAELARSLRRYI
cccchhhheeeccccccccchhhhhhhhhhhh


Legend:
   Alpha helix      (h): 28.90%
   Extended strand  (e): 6.94%
   Beta turn        (t): 3.47%
   Random coil      (c): 60.69%
```

Figure 10. Bioinformatic study of the sequence of GcrA. (a) Prediction of unfolded regions by RONN; to each amino acid residue a PONDR score is assigned and amino acids with a value > 0.5 are considered promoting disorder in that zone of the protein. GcrA can be considered having 3 different zones of order/disorder: an N-terminal ordered zone, a central disordered one and a C-terminal zone that is mainly disordered. (**b**) GcrA secondary structure prediction by SOPMA that confirm the prediction of order/disorder by RONN predicting alpha-helices at the N-terminal and some secondary structure feature at the C- terminal of the protein.

With the goal of investigating the interactions of GcrA both with DNA and its targets *in vivo* and *vitro* we purified an N-terminally hexa-histidine tagged variant of GcrA (His_6-GcrA) from an *E. coli* overexpression strain (BM335) by consequential affinity and gel filtration chromatography and characterized its biophysical properties (see Materials and Methods). SDS-PAGE (Fig. 11) and dynamic light scattering (DLS) analysis (data not shown) indicated a highly pure (>95%) and monodisperse preparation of His_6-GcrA.

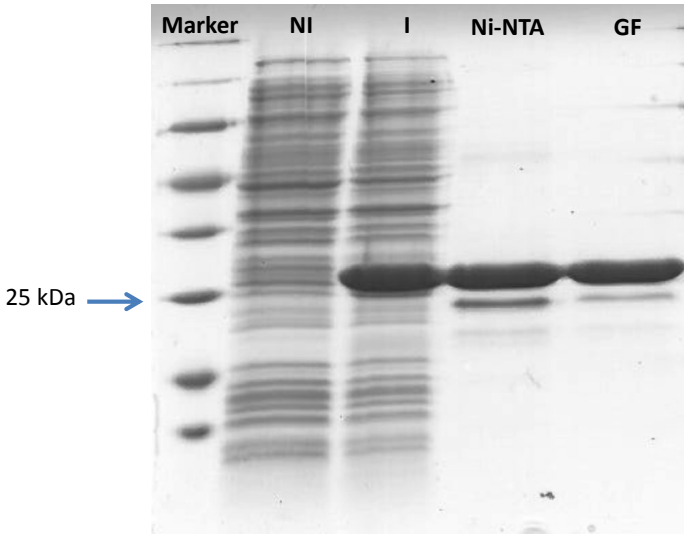

Figure 11. SDS-PAGE gel of the His_6-GcrA production and purification. NI= protein content of BM335 before induction; I= protein content of BM335 after IPTG induction; Ni-NTA= first step of purification by affinity purification (Nickel column); Gel Fi= final preparation of His_6-GcrA after the second step of purification obtained through size exclusion purification (gel filtration column) (from Fioravanti *et al.,* 2013).

To gain insight into the spatial organization of GcrA, we conducted Small Angle X-ray Scattering (SAXS) analysis (See Materials and Methods) that allows the determination of shape, size and oligomerization status of macromolecules in solution (Fig. 12). SAXS estimates the molecular mass of His_6-GcrA at 42 kDa, which corresponds to a dimeric organization. Also the dimensions of His_6-GcrA, by using computed radius of gyration (Rg) and maximum dimension (Dmax) values, combined with the pair-distance distribution function, P(R), shape and the Kratky plot representation, are consistent with an elongated form and partially disordered conformation of His_6-GcrA dimers in solution (See legend of figure 12 for more technical details). Possibly the interaction of GcrA with other proteins and with DNA can induce a stabilization of the disordered regions.

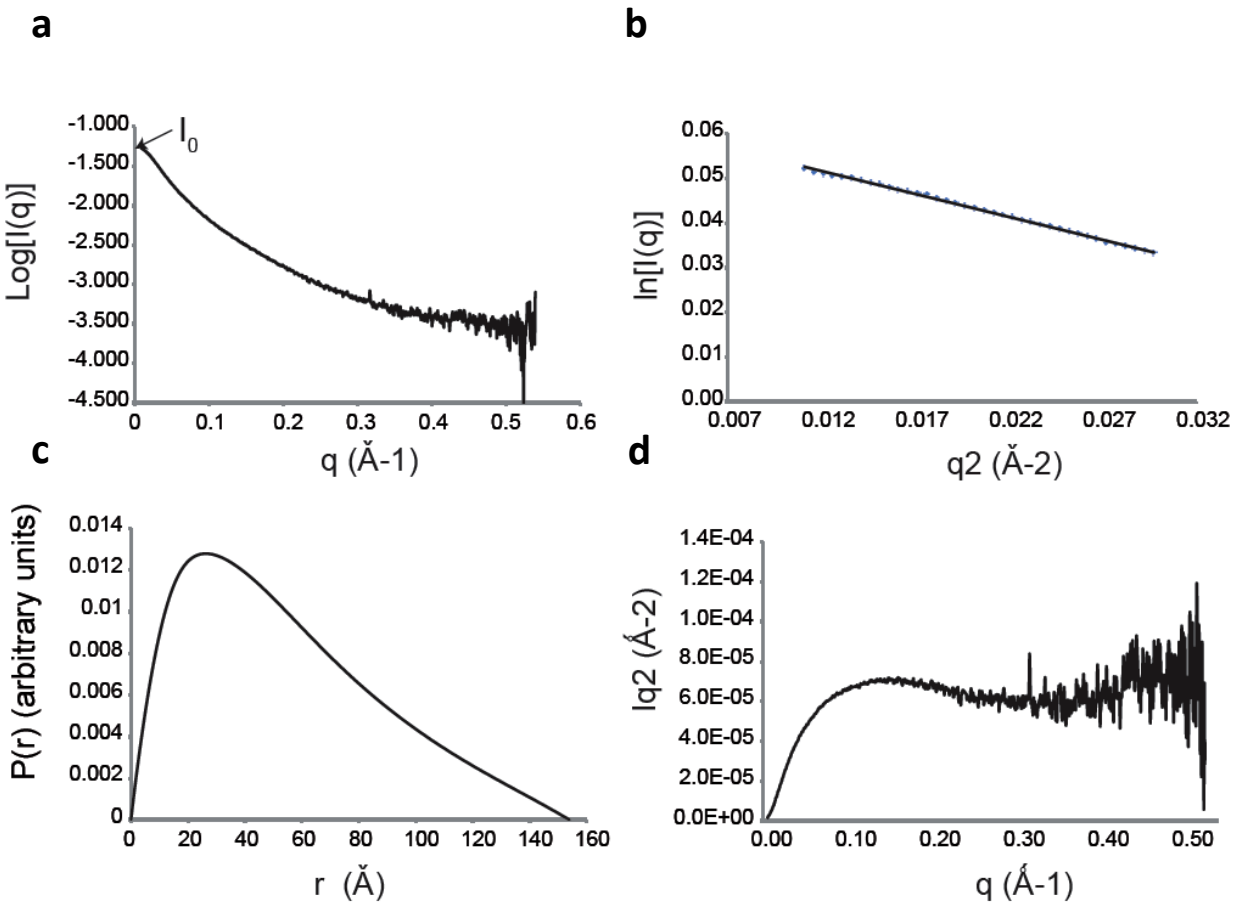

Figure 12. GcrA is partially unfolded dimer with elongated shape. Small angle scattering (SAXS) data from GcrA in solution. **(a)** Experimental scattering curve, Intensity at q = 0 (I_0) obtained by extrapolation of the curve at law value of q is directly related to the Molecular Weight (MW) of the particle that can thus be estimated. For GcrA the estimated MW corresponds to a dimeric organization of the molecule (ca. 42 KDa). **(b)** The Guignier plot, which represents the logarithm of scattering intensity versus q2, is linear over a restricted region attesting that there is no aggregation of GcrA in solution. The radius of gyration (RG) of GcrA (43.45 Å), estimated from the slope, provides information about the average size of the particle. **(c)** The distance distribution function P(r) calculated by the program GNOM (Svergun *et al*., 1992) is a histogram of all interatomic distances r within the molecule. The maximal value of r (Dmax) of GcrA (152 Å) corresponds to the maximal diameter of the protein and gives information on the shape of the particle. In the case of GcrA, P(r) shows that the molecule has a rather elongated shape. **(d)** The Kratky plot representation of the intensity curve (q2I(q) versus q) assess the globular nature of the polypeptide chain. Kratky plot for GcrA shows the typical shape observed for non or partially globular molecules having significant flexibility (from Fioravanti *et al.*, 2013).

Next, we performed limited proteolysis followed by MALDI-TOF mass spectrometry (MS) analysis in order to identify regions of His_6-GcrA that were more resistant to proteolysis indicating its more compact (structured) nature. Two different proteases, Thermolysin and V8

(see Materials and Methods) were used and the most resistant fragments to proteolysis were analyzed by MS (Fig. 13). This analysis suggests that the N-terminal part of GcrA (from 1 to 115 ca.), although containing proteolytic sites for both proteases, was more stable than the C-terminal part; this protection could be consistent with the presence of predicted of alpha helical structures in the N-terminal portion of GcrA or a coiled coil region (predicted by other software, data not shown).

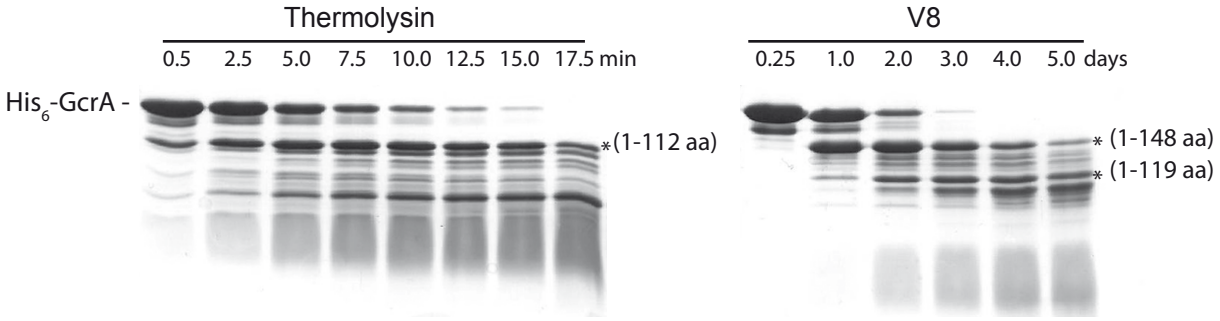

Figure 13. Limited proteolysis of GcrA using Thermolysin (left) and V8 (right). Asterisks correspond to resistant bands that were analyzed by MS and the interval between parentheses is the amino acid region of GcrA (from Fioravanti *et al.,* 2013).

2) Genome-wide occupancy of GcrA at promoters in vivo

In light of these structural features suggesting that the N-terminal domain of GcrA binds DNA, we looked for specific *in vivo* targets of GcrA that could be used to probe DNA-binding of GcrA *in vitro*. Previous non-quantitative chromatin-immunoprecipitation (ChIP) experiments using polyclonal antibodies to GcrA, provided support for the notion that GcrA affects the transcription of cell cycle genes by, directly or indirectly, associating with specific chromosomal sites (Holtzendorff *et al*., 2004). In order to investigate the basis for this selectivity and the underlying mechanism of transcriptional regulation by GcrA in *Alphaproteobacteria*, we subjected ChIP samples from NA1000 wild-type cells to deep sequencing (ChIP-Seq) using Chromatin-bound DNA precipitated by polyclonal antibodies produced against the His_6-GcrA preparation described in the previous section (Robertson *et al*., 2007) (see Materials and Methods). By mapping the reads onto the genome, we determined the binding profile of GcrA on genomic regions.

First, in collaboration with the lab of Patrick Viollier in Geneva, a peak finding strategy to identify regions bound by GcrA with high affinity was used (see Materials and Methods); this analysis allowed to identify 218 peaks that were subsequently associated to the closest genes (Table S2 in Fioravanti *et al*., 2013).

Inspection of the top 50 targets (Fig. 14a) revealed wide peaks (ca. 1 kbp wide, data not shown). We found that half of these GcrA-bound sequences were significantly associated with CcrM methylation sites (GAnTC). To explore this association more in detail, we calculated the average number of methylation sites in 1kbp windows centered on the peaks and found it to be close to 2 (1.78), in comparison with 0.58 sites per random 1kbp genomic regions (Fig. 14b). These results clearly indicate a significant enrichment of methylation sites in genomic regions bound in vivo by GcrA, raising the possibility that methylation enhances GcrA binding to its targets.

Next, in all promoter regions, defined from 300 bp upstream to 100 bp downstream a gene's start codon, the number of ChIp-Seq reads (see Material and Methods) were calculated (Table S3 in Fioravanti *et al.,* 2013). This list of the 161 GcrA-bound promoter regions (Z-score ≥ 2, 89 containing CcrM sites) contained many known GcrA-controlled targets such as *mipZ*, encoding a division regulator (Thanbichler *et al*., 2006), *podJ* encoding a polarity factor (Viollier *et al*., 2002; Hinz *et al*., 2003) and *ctrA* (for an overview see figure 10 of Fioravanti *et al*., 2013). We observed a remarkably small overlap with the genes previously identified as GcrA-dependent by DNA microarrays (Holtzendorff *et al*., 2004). Only 8 genes passed the threshold (Z score ≥ 2), including those encoding CCNA_01542 (ice nucleation protein), CCNA_01556 (LacI family transcriptional regulator), CCNA_01766 (hypothetical protein), CCNA_02005 (inosine-uridine preferring nucleoside hydrolase), CCNA_02086 (sporulation domain containing protein), CCNA_02246 (*mipZ*), CCNA_02401 (encoding a transcriptional regulator) and CCNA_03325 (encoding a hypothetical protein). Since microarrays detect both direct and indirect mRNA abundance changes, it is likely that many genes whose expression was affected by GcrA depletion were, in fact, indirect targets of GcrA presumably under the control of other transcription factors, such as CtrA.

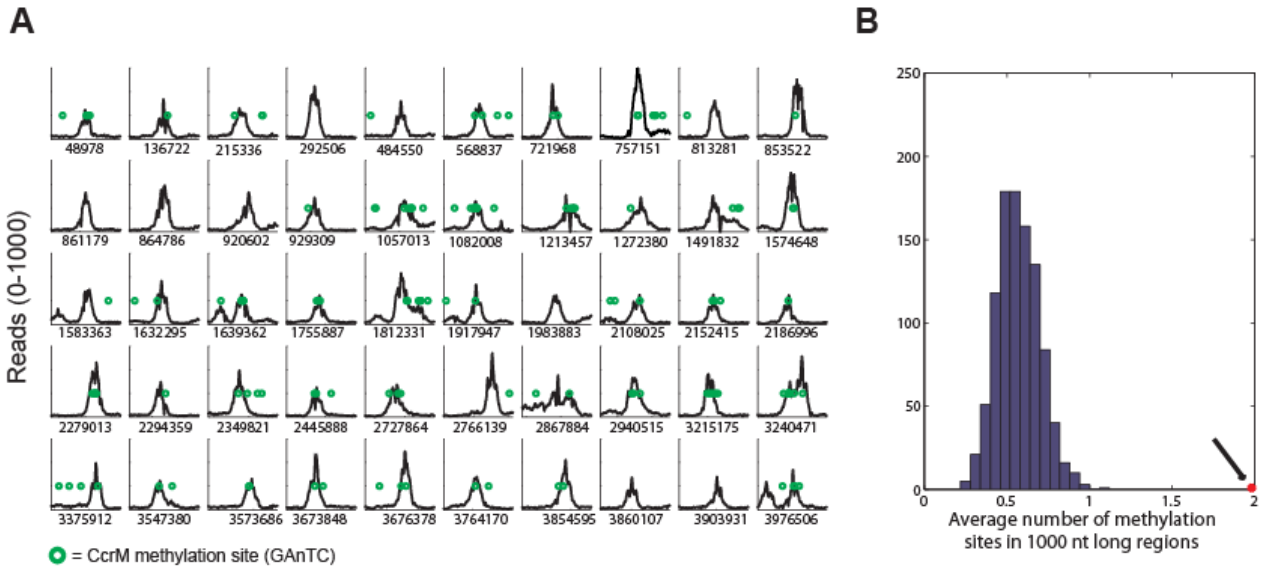

Figure 14. Chromatin Immunoprecipitation and deep sequencing (ChIP–Seq) of GcrA-bound genomic sequences are enriched in methylation sites. (A) Best 50 sequences 2 kbp long from Table S2 of the *C. crescentus* genome that are immunoprecipitated with GcrA antibodies. In each plot the number of reads per nucleotide in 2 kbp is shown. The number below the graphs corresponds to the position in the NA1000 genome of the middle of the 2 kbp region. Methylation sites of CcrM (GAnTC) are represented as green circles. **(B)** A random sampling of 1 kbp sequences reveals a distribution of methylation sites around 0.6, while the GcrA sequences have an average number of 2 (Black arrow) (from Fioravanti *et al*., 2013).

3) GcrA defines a new class of specific DNA binding proteins

In order to test if GcrA binds DNA *in vitro*, we set up an electrophoretic mobility shift assay (EMSA) with His_6-GcrA and regions identified as *in vivo* targets of GcrA by the ChIP-seq experiment described above. We selected 5 regions as EMSA probes, each with distinct features: 1) the preferred target (with the maximum number of reads in table S2 of Fioravanti *et al*., 2013) corresponding to the N-terminal coding sequence of gene CCNA_00697 that has three GAnTC sites; 2) the intergenic sequence between CCNA_00278 and CCNA_00279 that is efficiently bound by GcrA *in vivo*, but has no predicted GAnTC methylation site; 3) the promoter of the gene *mipZ,* which was also discovered previously by microarray as a GcrA-dependent gene and has two juxtaposed GAnTC sites; 4), the P1 promoter of *ctrA* (*ctrA*P1) that has one GAnTC site (there is another GAnTC sequence after the transcription start site of the *ctrA*P2 promoter) and is thought to be activated by GcrA (Holtzendorff *et al*.,2004); 5) a negative control, corresponding to the intergenic region between CCNA_01926 and CCNA_01927 which GcrA binds non-specifically *in vivo* based on ChIP-seq data. Probes were designed as 70-mer

double stranded oligo-nucleotides, in which the central part corresponds to the genomic region with the highest number of ChIP-seq reads.

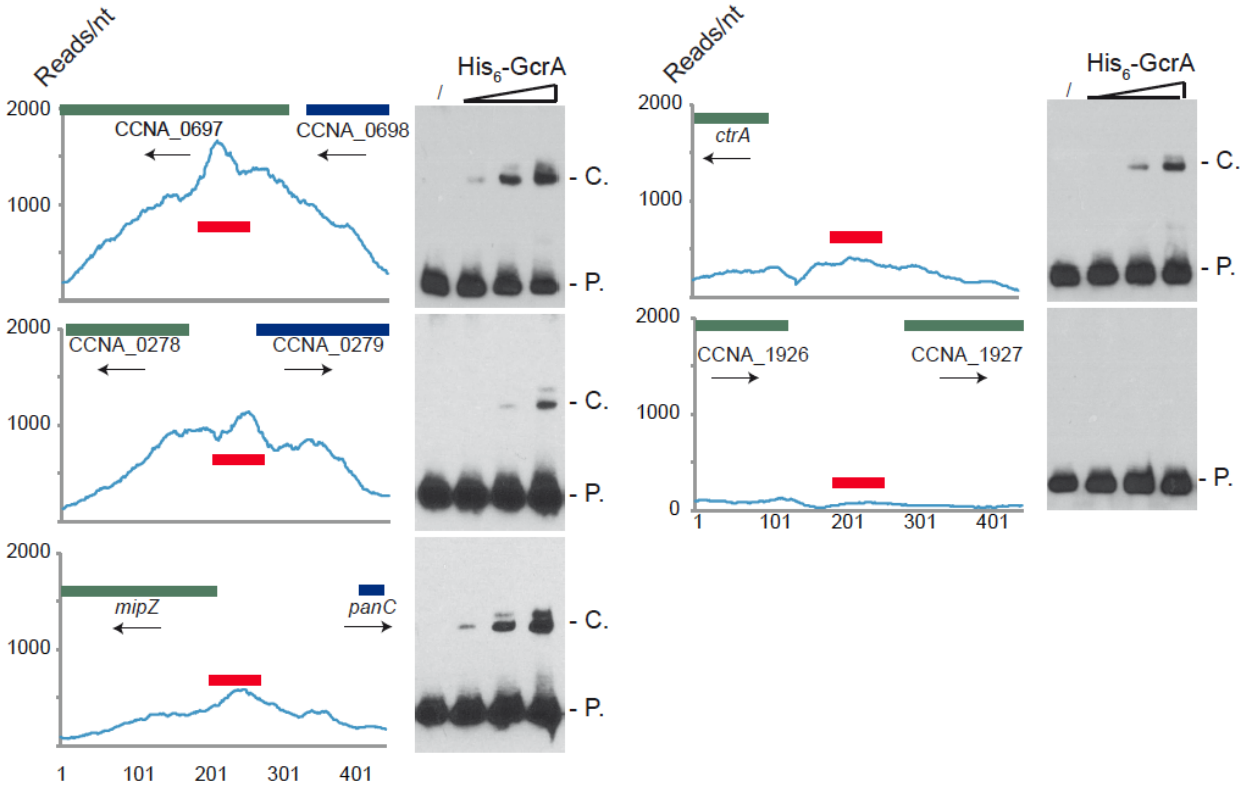

Figure 15. Electrophoresis mobility shift assay (EMSA) of 5 ChIP–Seq regions with His_6-GcrA. EMSA results using increasing concentrations of purified GcrA using probes (red line) design in regions with high number of reads in ChIP-Seq results. From the top to the bottom: 1) the sequence with the maximum number of reads Chip-Seq results, corresponding to the coding sequence of CCNA_00697; 2) the intergenic sequence between CCNA_00278 and CCNA_00279; 3) The promoter of *mipZ*; 4) The promoter *ctrAP1* of *ctrA;* 5) A negative control, corresponding to the intergenic between CCNA_01926 and CCNA_01927. On the right, P. = Probe signal and C. = complex signal (from Fioravanti *et al.*, 2013).

The EMSA (Fig. 15) showed that His_6-GcrA shifted four out of five probes, indicating the formation of a His_6-GcrA•DNA complex with sequences identified by ChIP-Seq, except for the intergenic sequence between CCNA_01926 and CCNA_01927 (i.e., the negative control). All positive probes gave rise to two distinct His_6-GcrA•DNA complexes with similar migration properties, possibly reflecting different oligomeric states of His_6-GcrA with different apparent affinities for the DNA (see below). In particular, probe CCNA_00697 was the most efficiently bound by His_6-GcrA (Kd = 4 ± 0.5 µM); probes *ctrA* (Kd = 6.5 ± 0.5 µM) and *mipZ* (Kd = 8.5 ± 0.5 µM) also showed DNA binding however the complex forms only at a higher concentration of

His_6-GcrA, mirroring, with the exception of the intergenic region between CCNA_00278 and CCNA_00279 (Kd > 9 µM), the *in vivo* binding preference suggested by ChIP-seq (see Fig. S9 in Fioravanti *et al.,* 2013).

The EMSA results also demonstrate that His_6-GcrA binds DNA in a specific fashion *in vitro*. Considering also that the conserved GcrA protein has no homology with known DNA binding proteins at the primary structure level, we conclude that GcrA defines a new class of alphaproteobacterial DNA binding proteins that directly interacts with target promoters to control transcription of many *C. crescentus* S-phase genes, including the gene encoding the master regulator CtrA. Although methylation sites are associated with GcrA-bound regions, GcrA apparently can also bind sequences that do not contain GAnTC methylation sites, based on the methylation-dependent binding experiments described below, we suggest that multiple DNA constrains exist in the GcrA specificity, perhaps involving m6A marks in different sequences contexts or a different type of methylation mark altogether. In this context, it is noteworthy that two putative cytosine methyltransferases are encoded in the *C. crescentus* genome (Nierman *et al.*, 2001; Kozdon *et al*., 2013).

4) DNA binding of GcrA is enhanced by CcrM-dependent methylation

To test if GAnTC methylation modulates the binding of His_6-GcrA to some of its targets *in vitro*, we conducted EMSA competition experiments with the un-methylated region of P_{mipZ}, CCNA_00697 and *ctrA*P1 as biotinylated probes and double stranded synthetic oligos harboring N6-adenosine methylation at GAnTC on either one or both strands as competitors. In these experiments, His_6-GcrA was pre-incubated with the unlabeled competitor DNA, followed by the addition of the biotinylated probe. The more the unlabeled competitor DNA reduces the abundance of the shifted His_6-GcrA•DNA complex, the higher the affinity of His_6-GcrA is for the unlabeled competitor. As shown in figure 16, we observed a clear preference of GcrA for the methylated competitors over the un-methylated one, with those carrying methylation on both strands ("full"-methylation) competing better than either one harboring the methylation on one of the two strands ("hemi"-methylation). Remarkably, in the case of the CCNA_00697 and *mipZ* competitors, hemi-methylation on the "sense" strand is a better competitor than the hemi-

methylated competitor with the modification on the other strand. For promoters of *ctrA* and *mipZ,* the calculated Kds provided quantitative confirmation of the results shown in figure 16 (see also figure S9B and C in Fioravanti *et al.,* 2013).

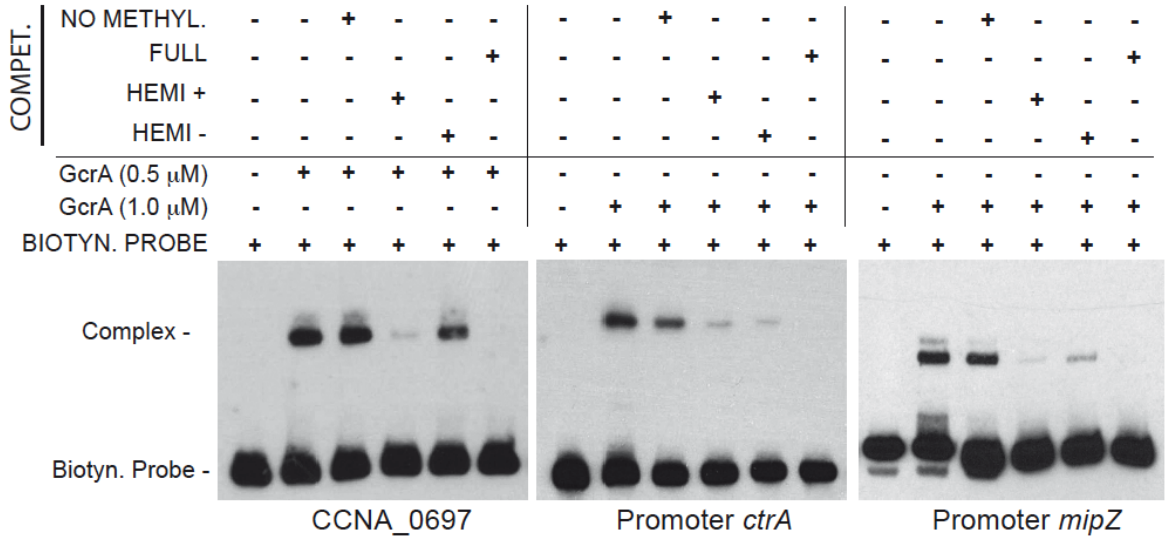

Figure 16. GcrA DNA binding depends on CcrM methylation state. Three regions (CCNA_0697, *ctrA*, *mipZ*) containing methylation sites of CcrM were tested in a competition experiment. Competitor DNA identical to the probe with various methylation states was mixed with biotinylated probes and GcrA in order to evaluate competition. For CCNA_00697 we used 0.375 μM of competitors, while for *ctrA* and *mipZ* promoters we used 1.25 μM. Dissociation constants (Kd) of the methylated probes of *ctrA* and *mipZ* probes are shown in figure S9 of Fioravanti *et al*., 2013 (from Fioravanti *et al*., 2013).

In order to assess if methylation alters the disposition of GcrA on its target DNA, we conducted DNase I protection assay using fully and hemi-(GAnTC) methylated fluorescently-labeled *ctrA*P1 promoter probes. As shown in figure 17A, GcrA protects specific regions of the probe in a methylation-dependent manner, giving rise to a larger region of protection spanning the -35 to the -10 of the *ctrA*P1 promoter with the fully-methylated (*i.e.* on both strands) probe. By contrast, the protection of the hemi-methylated (on the plus strand) probe was confined to a region adjacent to the methylation site itself. Importantly, the un-methylated probe and the hemi-methylated probe carrying the modification on the minus strand did not show protection by His_6-GcrA at any concentration. We conclude that methylation induces different oligomerization or conformational states in strand-specific manner.

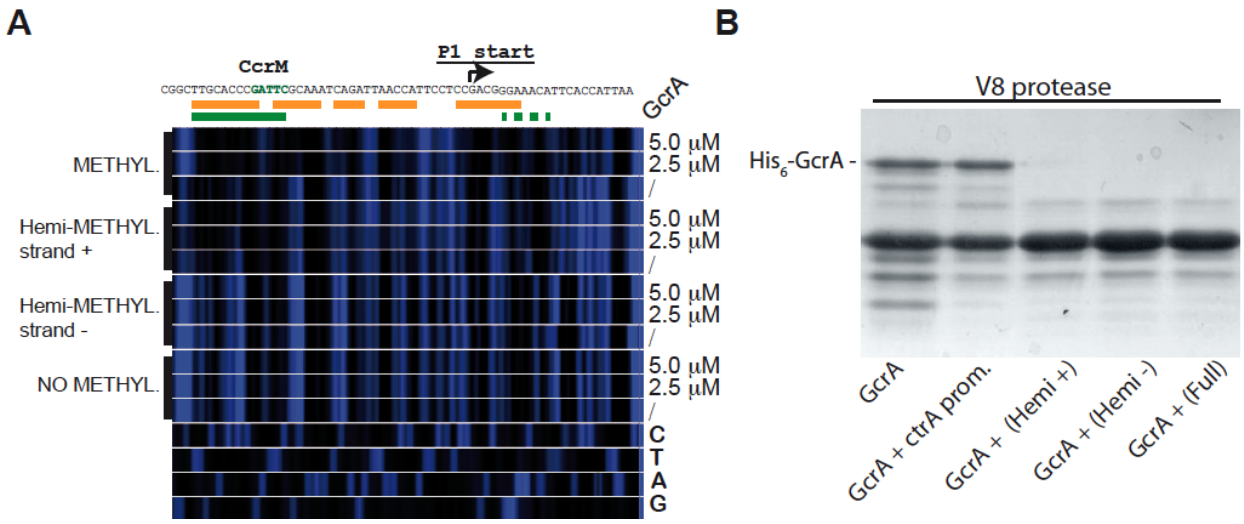

Figure 17. Differential binding of GcrA to different GAnTC methylation states of DNA induces conformational changes of GcrA. (A) DNase I footprinting of the *ctrA*P1 promoter by GcrA. The promoter region was tested in different methylation states with increasing concentrations of His_6-GcrA. The nucleotide sequence of the *ctrA*P1 promoter with the start site and the CcrM methylation site (green) shown on top. In orange, the putative region, protected by GcrA in the fully methylated state. In green the putative region protected in the hemi-methylated strand plus. **(B)** Proteolytic digestion using V8 in presence of DNA. In particular 4 kinds of DNA corresponding to the *ctrA*P1 promoter were tested as reported in the bottom part (from Fioravanti *et al.,* 2013).

Next, we complemented the DNase I protection experiments, with protection experiments of His_6-GcrA by limited proteolysis in the presence or absence of the various methylated *ctrA*P1 probes (Fig. 16B). We found that efficiency of proteolysis is accelerated in the presence of methylated probes, suggesting that conformational rearrangements are induced by the methylated probe to expose protease hypersensitive sites, akin to the DNase I hypersensitive sites of the target DNA that become exposed only when GcrA associates with a methylated target, but not in the presence of the un-methylated site. We also ruled out the possibility that the oligos affected the DNase I activity by incubating another protein (His_6-ChpT) (Fioravanti *et al*., 2012), which was proteolyzed identically with or without the DNAs (data not shown). CcrM-dependent methylation of *ctrA*P1 was previously proposed as an essential element of a transcriptional regulatory switch, culminating in the GcrA-dependent activation of *ctrA*P1 upon the conversion from full- to hemi-methylation (Reisenauer and Shapiro, 2002). Intriguingly, our results reveal that His_6-GcrA binds hemi-methylated versus fully methylated *ctrA*P1 in strikingly different manner, with the latter covering a much larger area. This raises the possibility that

cooperative interactions, induced by the transition from hemi- to full-methylation mediated by CcrM, can lead to a wider and stronger association of GcrA with the target DNA. As His_6-GcrA protects multiple sites in the region from -35 to +7 of fully methylated *ctrA*P1, it may interfere with RNA polymerase holo-enzyme (RNAP) binding at *ctrA*P1; a possibility that must be explored in future work. By contrast, on the hemi-methylated plus strand of *ctrA*P1, His_6-GcrA occupies a 12 nt stretch overlapping the -35 region and adjacent to the GAnTC site and with lower affinity a 12 nt region from +5 onwards. GcrA could compete with RNAP for binding to *ctrA*P1 or alternatively tether it at the promoter, preventing promoter clearance, *i.e.* the switch from transcription initiation to the elongation phase. Furthermore the methylation strand-specificity opens the possibility of an "asymmetric" mechanism of gene regulation, in which only one of the two replicated loci is preferentially bound and transcriptionally regulated by GcrA before re-methylation by CcrM in the pre-divisional cell. Such a regulatory bias could have far reaching consequences in all forms of spatiotemporal and/or of gene-dosage regulation for all living cells, as it has been suggested before for PapI-promoted Lrp binding to hemi-methylated sites in uropathogenic *E. coli* (Hernday *et al*., 2004).

5) GcrA–dependent interactions with RNAP

To explore the models described above, we tested whether GcrA can directly or indirectly associate with RNAP. To this end a pull down assay was performed passing a soluble *C. crescentus* cell lysate, in which DNA was fragmented by a mild DNase I treatment, over a nickel-NTA column that had been pre-loaded or not with His_6-GcrA. Following extensive washes with buffer containing up to 1 M NaCl, we eluted His_6-GcrA and associated proteins with buffer containing imidazole (see Materials and Methods). Blots harboring these samples were then probed with antibodies to the β subunit of core RNAP, revealing that RNAP β in the eluted fraction from the His_6-GcrA pre-loaded column only (Fig. 18).

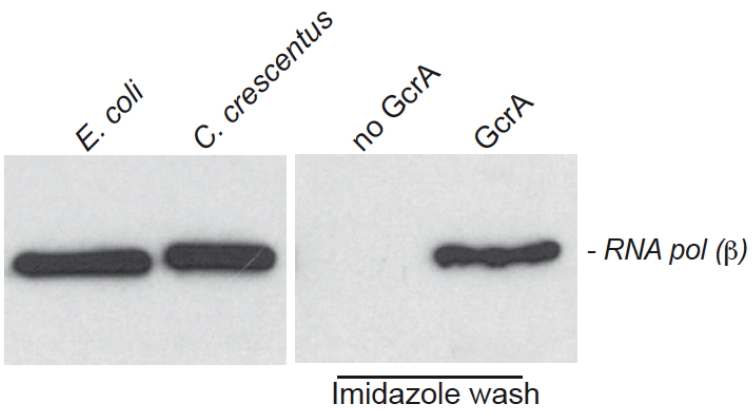

Figure 18. GcrA interacts with RNA polymerase. Immunoblots using RNAP β subunit antibodies on several samples. On the left cellular lysates of E. coli cells and C. crescentus cells, both positives to the antibodies. On the right, samples of *C. crescentus* CB15N cell lysate applied to the column containing His_6-GcrA and subsequently washed with NaCl (up to 1 M) and imidazole in order to remove His_6-GcrA and its putative interacting proteins. This procedure was done also with an empty column ("No GcrA" lane). The nickel column loaded with His_6-GcrA was used to detect the association of GcrA to RNA polymerase (from Fioravanti *et al.,* 2013).

We extended these findings by showing that *E. coli* RNAP core enzyme can associate with the DNA•GcrA complex in an EMSA using *ctrA*P1 promoter. Increasing concentration of RNA polymerase clearly showed the formation of lower mobility complex whose formation was dependent on the presence of GcrA (Fig. 19).

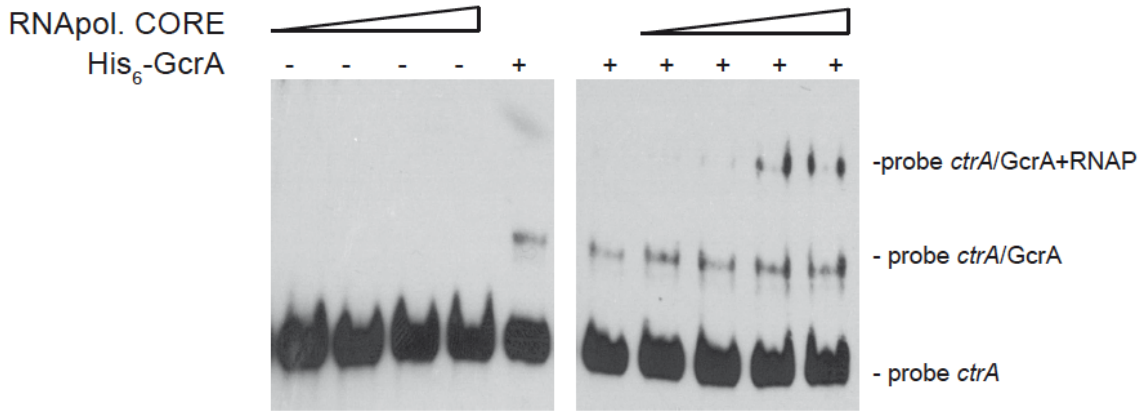

Figure 19. GcrA interacts with RNA polymerase and DNA. *E. coli* RNA polymerase core enzyme is able to bind the GcrA-DNA complex (promoter *ctrA*P1), as visualized by a slower migration rate as the amount of RNA polymerase increased. On the left the same RNA polymerase conditions were tested without GcrA (from Fioravanti *et al.,* 2013).

This interaction of RNAP with GcrA bound to its target was also observed with the *mipZ* promoter (Fig. 20).

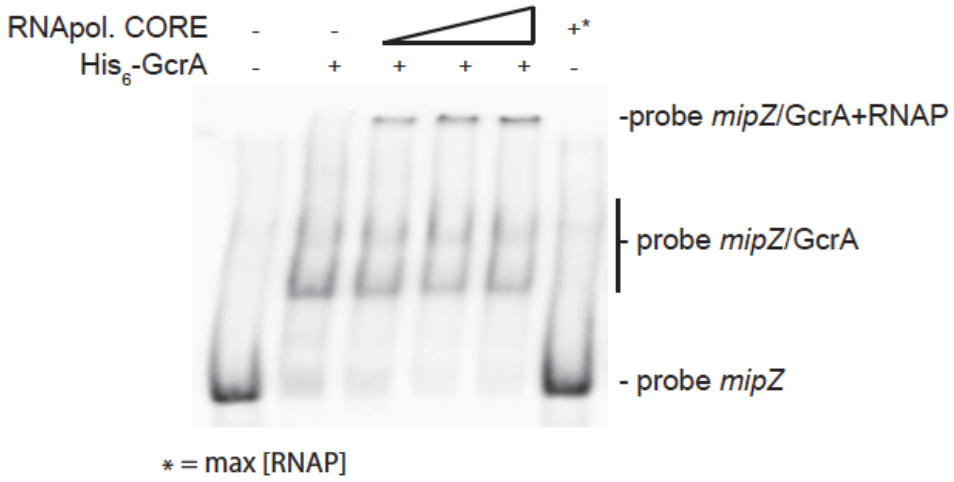

Figure 20. EMSA using *E. coli* RNA polymerase core enzyme. RNAP is able to bind the GcrA-DNA (*mipZ* promoter) complex, as visualized by the formation of a slower migration rate band as the amount of RNA polymerase increased (from Fioravanti *et al.,* 2013).

Taken together, these results indicate that GcrA binds components of the RNA polymerase core complex and they provide a mechanistic explanation for how GcrA might affect gene transcription.

The connection between methylation by CcrM and DNA-binding of GcrA, seen *in vitro*, together with the association of GcrA to RNAP, was also confirmed *in vivo* (see Fioravanti *et al.,* 2013). To this end, in collaboration with the lab of Patrick Viollier, several promoters that have methylation sites and that emerged as *in vivo* targets of GcrA in the ChIP-seq experiments were fused to the promoter-less *lacZ* reporter gene. Also methylation sites were mutated replacing the methylated A with C (GAnTC to GCnTC). Results clearly showed that both GcrA and methylation by CcrM are required for proper transcription of those genes. Both absence of GcrA and mutation of the methylation site reduced the transcriptional levels of several genes, such as *podJ*, *flaY* and *mipZ* (Fioravanti et al., 2013).

6) ***Methylation-dependent DNA binding of GcrA orthologs***

To explore if GcrA-controlled functions are conserved across the *Alphaproteobacteria,* we introduced the GcrA ortholog (Brilli *et al*., 2010) from *Brucella melitensis* biovar *abortus* 2308 (BAB1_0329) and *Sinorhizobium meliloti* Rm1021 (SMc02139) under the control of an xylose-inducible promoter on a low-copy plasmid (Skerker *et al*., 2005) in *C. crescentus,* harboring a temperature sensitive allele of *gcrA* with a Thr→Pro mutation at position 10 and evaluated their ability to support growth at the restrictive temperature (Holtzendorff *et al*., 2004) .

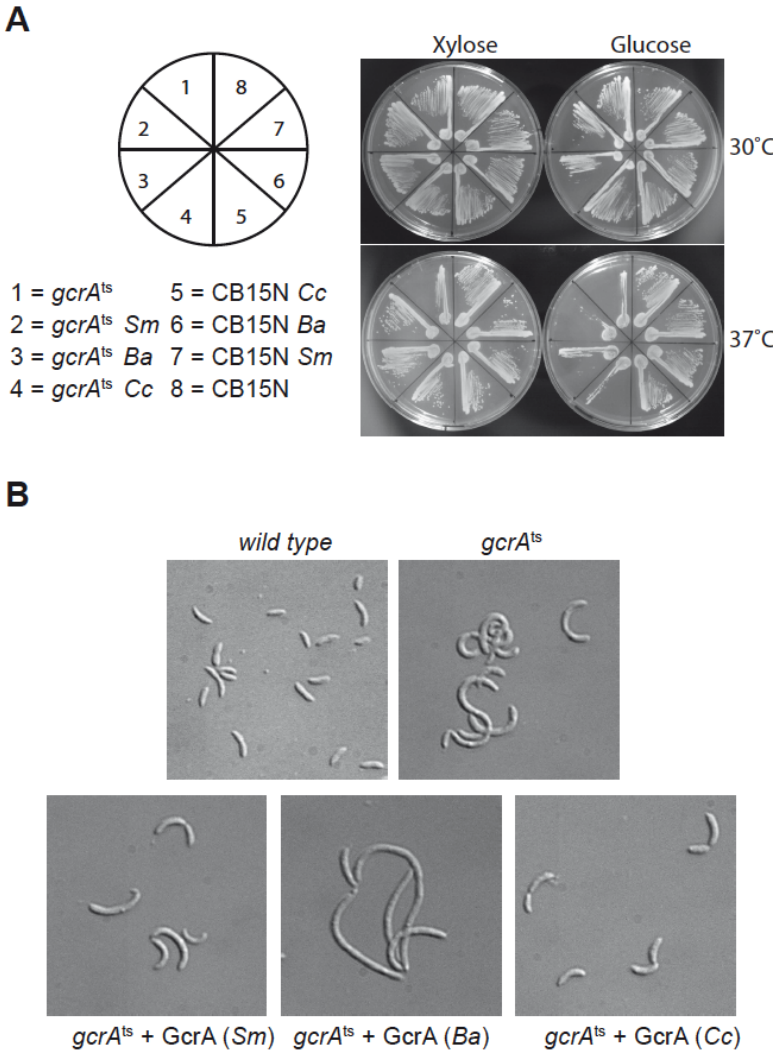

Figure 21. GcrA orthologs in *Alphaproteobacteria*. (A) Genetic complementation of gcrA^{ts} (T10P) allele by *C. crescentus* (Cc), *B. abortus* (Ba) and *S. meliloti* (Sm) *gcrA* orthologs. (B) Orthologs, although able to support viability, caused diverse morphological phenotypes when expressed as the only functional copy of GcrA in *Caulobacter*. Morphologies at 30ºC with and without xylose are not reported since cells appeared normal (data not shown) (from Fioravanti *et al.,* 2013).

As shown in Figure 21, both *B. abortus* and *S. meliloti gcrA* orthologs are able to support viability of the strain *gcrA*^{ts} at the restrictive temperature (37˚C) following induction with xylose. Orthologs of GcrA from *S. meliloti* and *B. abortus*, although able to complement GcrA functions, revealed morphological diversities in *C. crescentus* (Fig. 21B), likely owing to differences in abundance, activity and/or target specificity of these GcrA versions. Regardless, the complementation of the temperature-sensitive phenotype indicates that the function and target site specificity of GcrA orthologs are similar.

We confirmed this result by testing directly the ability of GcrA orthologs to bind the *C. crescentus* target promoters. Therefore *B. abortus* and *S. meliloti* GcrA with an N-terminal His_6 tag were purified from *E. coli* overexpression strains (see Material and Methods; Fig. 22).

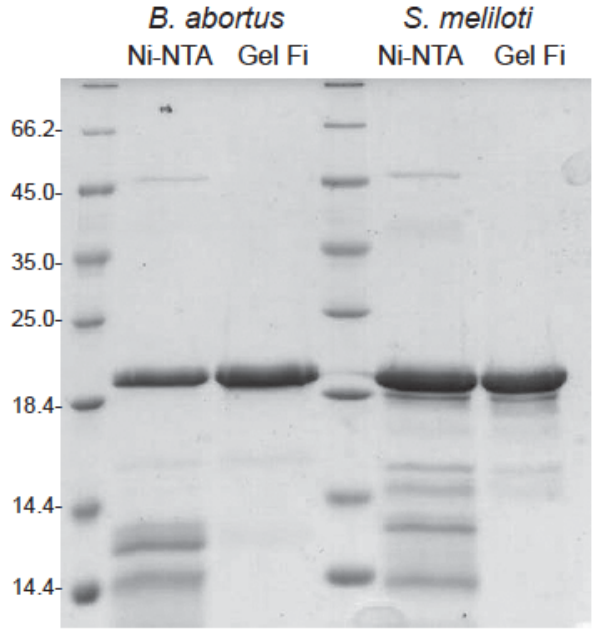

Figure 22. Purification of *B. abortus* and *S. meliloti* GcrA orthologs. SDS-PAGE gels of purifications at different steps: NI-NTA = purification by nickel columns; Gel FI = purification after Gel filtration (procedure is described in Materials and Methods) (from Fioravanti *et al.,* 2013).

EMSA experiments using target sites of *C. crescentus* GcrA revealed that these GcrAs are able to bind DNA efficiently and with the same apparent specificity (Fig. 23). Surprisingly the *B. abortus* and *S. meliloti* GcrA orthologs are able to form multiple complexes with different migration properties, likely due to structural and/or charge differences.

Finally we tested if binding of *B. abortus* and *S. meliloti* GcrAs is also stimulated by GAnTC methylation. EMSAs showed that methylation still affects GcrA binding, as fully methylated probes showed a stronger binding affinity in comparison with hemi-methylated and even more with non-methylated DNA. However the asymmetry in binding efficiency found for certain regions of DNA (Fig. 23B) appeared different in other GcrAs with respect to the *C. crescentus* one.

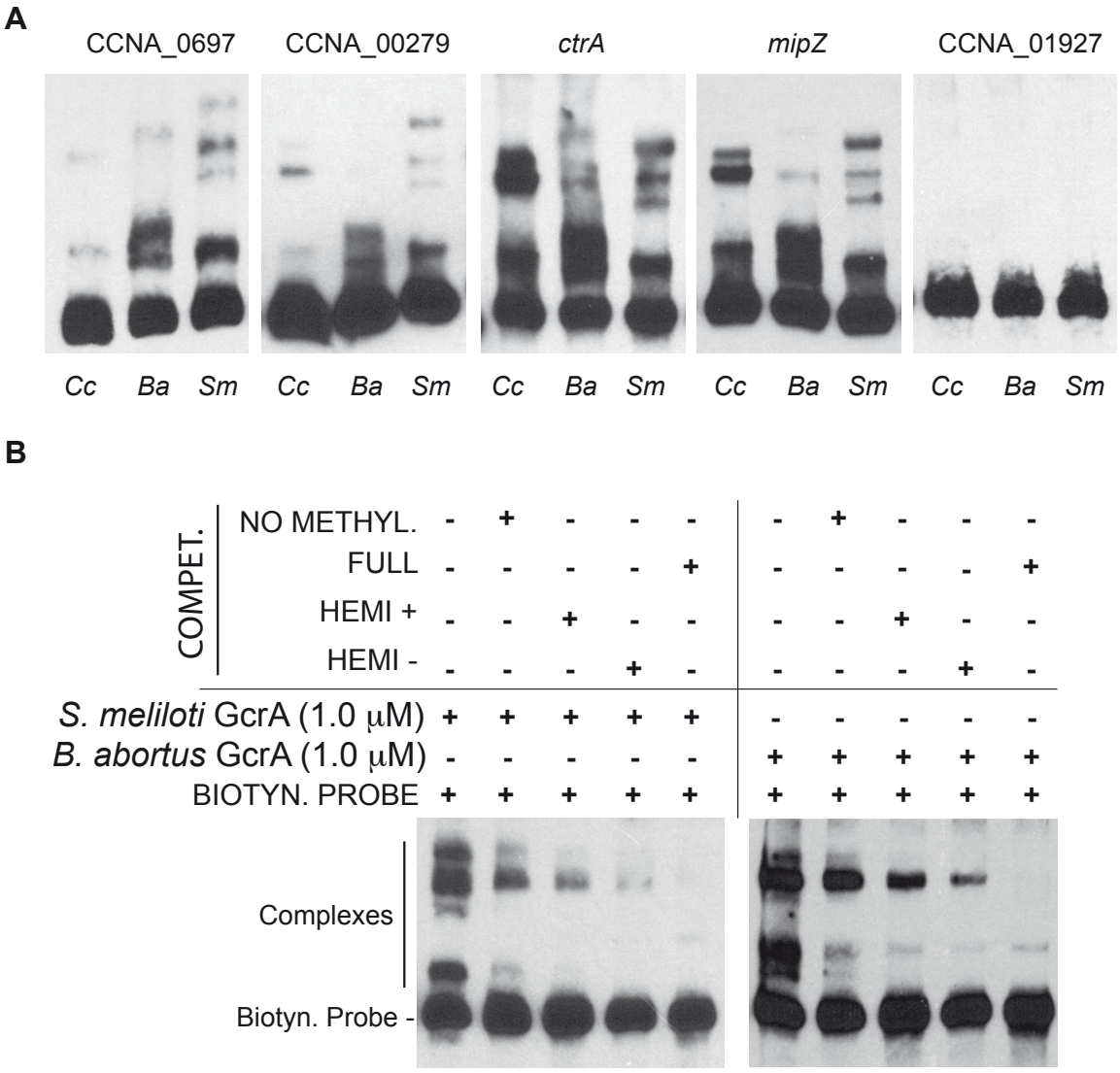

Figure 23. GcrAs in *Alphaproteobacteria* conserve specificity and GAnTC methylation-dependency. (**A**) Both *B. abortus* and *S. meliloti* GcrAs form DNA-protein complexes with similar specificity as observed in *C. crescentus* using probes described in figure 2. (**B**) GcrAs binds with the different methylation states of the *ctrA* probe with a different efficiency as observed for *C. crescentus* GcrA (from Fioravanti *et al.,* 2013).

Study of C. crescentus GcrA interaction with RNAP

In the previous section (see also Fioravanti *et al*., 2013), we explored the capability of GcrA to interact with the RNA polymerase enzyme. In the published article we briefly discussed the technique used to reveal this interaction: a soluble *C. crescentus* cell lysate, in which DNA was fragmented by a mild DNAse I treatment, was loaded into a Ni-NTA column that was pre-loaded with His_6-GcrA. Following extensive washes with buffer containing up to 1M NaCl, we eluted His_6-GcrA and associated proteins with a buffer containing imidazole. With this experiment we found an interaction of GcrA with RNAP and other proteins.

3) Co-immunoprecipitation of GcrA with RNAP

We further explore this interaction by optimizing a co-immunoprecipitation (CoIP) technique using M2 antibodies able to specifically bind an FLAG tag fused to GcrA (see Materials and Methods). Together with Saswat Mohapatra, a strain of *C. crescentus* (EB690) was created; briefly the chromosomal copy of *gcrA* was deleted and M2-*gcrA* (high- copy plasmid) and wild type *gcrA* (single chromosomal copy) were under the xylose promoter. Immunoblots using GcrA antibodies revealed that at low xylose concentration the prevalent form of GcrA is the M2-GcrA, due to the expression by a high copy vector (data not shown).

M2-GcrA was able to bind several proteins. Proteins present only in the lysates containing M2-GcrA were extracted from the SDS-PAGE gel and analyzed by mass spectrometry (Fig. 24). We found that in particular most of the RNA polymerase subunits (alpha, beta and the sigma factor 70) were detected by this procedure confirming results published in the previous article (Fioravanti *et al*., 2013).

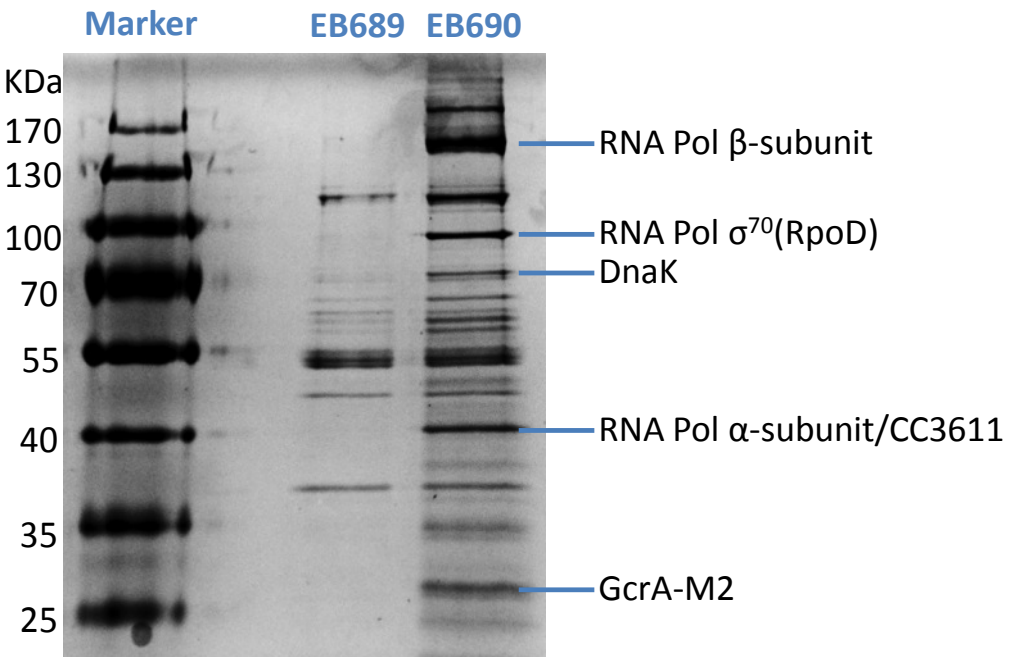

Figure 24. CoIP assay using anti M2 Ab. SDS-PAGE gel silver stained of the CoIP on the *C. crescentus* EB690 (that expresses M2-GcrA) and the negative control strain EB589 (no M2-GcrA). Bands immuno-precipitated with GcrA-M2 were identified by Mass Spec analysis.

4) GcrA is able to activate/repress the expression of ctrAP1

In order to better understand the significance of this different affinity of GcrA for different methylation state of DNA, the *C. crescentus* transcriptional machinery of *ctrA*P1 has been reconstituted *in vitro* (in collaboration with Saswat Mohapatra). As we can see in figure 25, GcrA acts as transcriptional activator of the RNAP holoenzyme, purified from *C. crescentus* (it is partially active also with *E. coli* commercial holoenzyme, data not shown) using the *ctrA*P1 hemimethylated in the positive strand. In the case of a hemimethylated template in the minus strand, this activation is almost negligible, while we can clearly see that an increase of GcrA in presence of a fully-methylated template represses the transcription.

Considering the DNase I footprinting experiments (Fig. 17), in which the maximum coverage of the *ctrA*P1 promoter by GcrA corresponded to the full methylation state, it appears consistent that increasing amounts of GcrA would block the access of RNAP to the promoter P1, resulting in the inhibition of transcription.

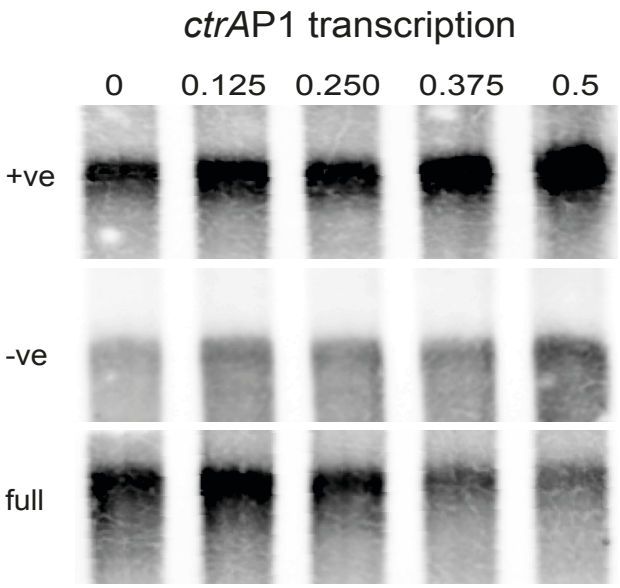

Figure 25. *In vitro* transcription assay using *C. crescentus* RNA polymerase holoenzyme in presence of increasing concentration of GcrA. Transcription of *ctrA*P1 region in different methylation states in presence of increasing concentration of GcrA. The transcription of this region seems to be clearly affected by the amount of GcrA and the methylation state of the DNA [positive (+ve), negative (-ve) hemi-methylated or fully-methylated]. Initial conditions of transcription without GcrA are different, probably due to the preparation of the DNA templates.

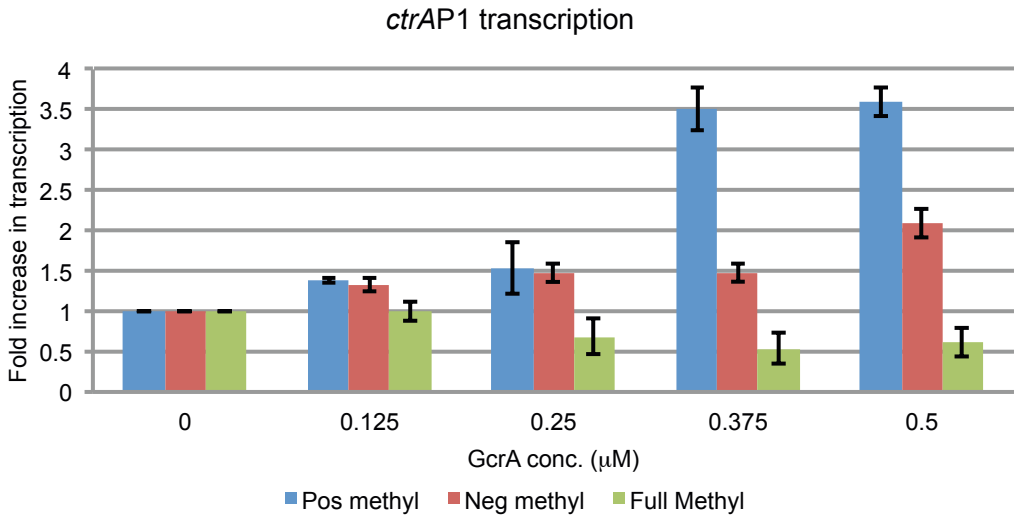

Figure 26. Quantification of the GcrA transcriptional activation for *ctrA*P1. Triplicates of each condition shown in figure 25 were quantified by ImageJ and plot as relative amounts.

We confirmed these observations by quantifying these transcriptional changes shown in figure 26. Triplicates of each condition were quantified using ImageJ and plot, revealing that

transcription increases 3.5 times in the positive hemi-methylation state and only 2 times in the negative thanks to GcrA. The fully methylated template on the contrary decreased its transcription by a factor of 2.

These results, combined with *in vivo* and *in vitro* results obtained previously in the Fioravanti *et al*., 2013, suggest that GcrA is a transcription factor able to repress and activate CcrM methylation dependent gene expression acting in the S-phase of the cell cycle, when DNA replication is taking place and the methylation of the chromosome is progressively changing from fully to hemi- and then to a fully methylation states. In this scenario, we can speculate that GcrA can adapt its role to enhance transcription or repress it in a methylation manner depending on the moment of replication and state of methylation of the chromosome.

Study of the GcrA-Interacting Protein X (GipX)

Other proteins were isolated in the Co-IP experiments showed above, including the chaperone DnaK (no study has been performed yet to confirm this interaction) and the protein CC3611, which is the subject of this section.

CC3611 encodes for a globular 40kDa protein that we preliminarily named GcrA Interacting Protein X (GipX). This protein is predicted, by BLAST analysis, to be a conserved protein in bacteria that corresponds to a Pyridoxal 5'-Phosphate (PLP)-dependent enzyme possibly belonging to the PLP-dependent aspartate aminotransferase superfamily (fold I). These enzymes are usually involved in aminotransferase reactions required to produce amino precursors for cell wall biogenesis (Hwang *et al*., 2004).

Interestingly the CC3611 gene was previously shown to be essential (Christen *et al*., 2011) and its expression was demonstrated to be cell cycle regulated with the highest peak of expression in early S-phase right before the *gcrA* expression. This result suggests the GipX and GcrA co-exist in S-phase. However no functional study on GipX in *C. crescentus* has ever been performed before.

With the intent of investigating the function of GipX and its interaction with GcrA *in vitro,* an N-terminally hexa-histidine tagged variant of GipX (His_6-GipX) was purified from an *E. coli*

overexpression strain by sequential affinity and ion exchange chromatography (see Materials and Methods). SDS-PAGE (Fig. 27) and dynamic light scattering (DLS) analysis (data not shown) indicated a highly pure (>98%) and monodisperse preparation of His_6-GipX.

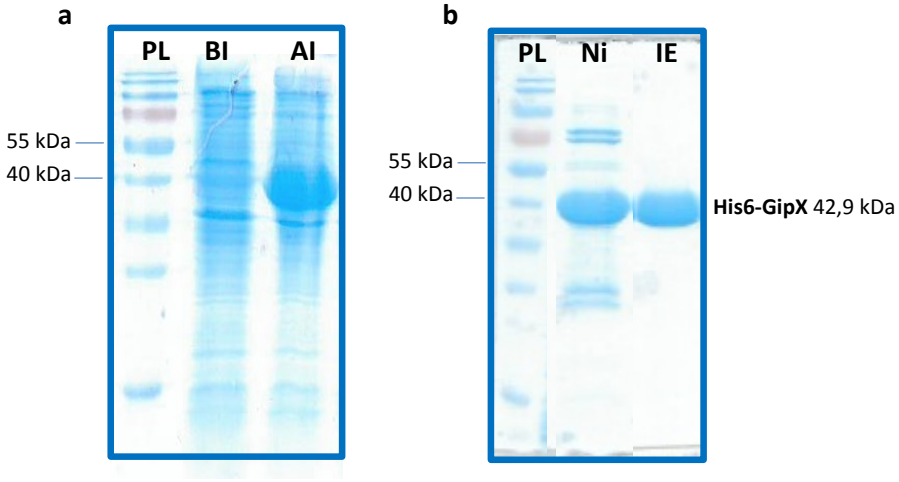

Figure 27. (**a**) **His_6GipX Production** in *E.coli* BL21 (EB793); PL= proteins' ladder, BI = EB793 protein content before induction, AI= EB793 protein content after induction by IPTG; (**b**) **His_6GipX Production** by two steps of purification**;** Ni=first step of purification, affinity column, IE= second step of purification By Ion Exchange column

1) GipX is a homodimer that presents similarities with members of Fold Type 1 aminotransferase family

Finding initial crystallization conditions for a new macromolecule can be a long and complicated research. In the first screening trials, the protein has to be exposed to numerous different chemical agents, concentrations of salts and pH in order to obtain clues for the best crystallization conditions. In order to simplify this search, pre-made crystallizations kits, whose composition is based on known and published data for various proteins, are available. Those kits allow, just using a minimal amount of protein sample, to explore a broad range of buffers, pH, and precipitants in a single experiment. For the His_6-GipX we performed crystallization screenings using the Vapor Diffusion Crystallization method previously described (Fioravanti *et al*., 2012).

To acquire insight into the structural organization of GipX and its function, we conducted crystallization assays on the full length His_6-GipX. With initial crystallization trials, performed using commercial crystallization kits, we obtained multiple crystals of our protein (Fig. 28) and, after optimization (see Material and Methods); we were able to obtain unique crystals (Fig. 28b) suitable for X-rays exposition. Analysis by Synchrotron X-rays allowed us to solve the protein structure with a resolution of 2, 1 Å.

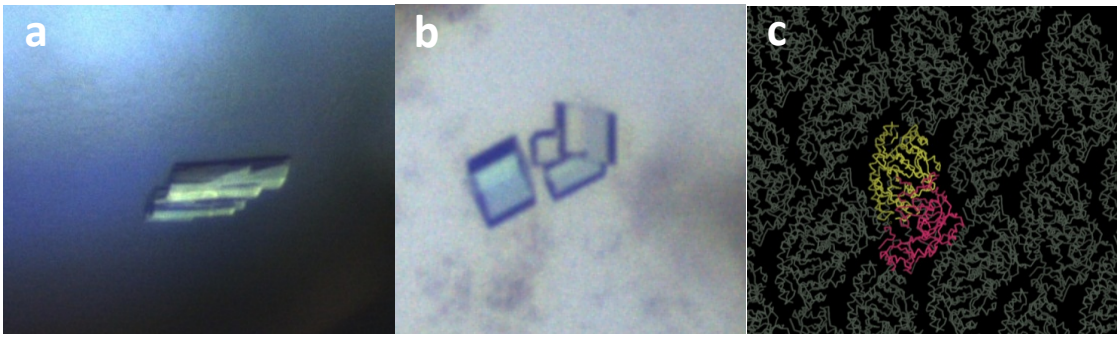

Figure 28. Crystallization of His_6-GipX (a) Initial native crystal obtained in condtion 82 with CryoSuite, Qiagen**;** (**a**) Native His_6-GipX crystal obtained after optimization of crystallization condition; (**c**) Packing of the crystal, with one dimer per unit cell.

Data processing revealed that GipX crystallized as a homodimer in the monoclinic space group $P2_1$, with two molecules (one dimer) in the asymmetric unit (Fig. 28c) with the following unit-cell parameters a = 47.37, b = 89.85, c = 80.90 Å; β=108.9°. Structure was solved by molecular replacement (MR) using the structure of the *Pseudomonas aeruginosa* aminotransferase WbpE as model (PDB entries 3NU7 Larkin *et al.,* 2010).

GipX overall scaffold is similar, as in the case of WbpE, to that of other members in the Fold Type 1 aminotransferase family, in particular to the aspartate aminotransferase (AAT) representing the first and most well studied member (Larkin *et al.,* 2010) (Fig. 29).

As AATs, each monomer of GipX is organized around a β-sheet core (Fig. 29c and d) that is composed of 7 β-strands organized in a β-sheet in the following order: β-1, β-7, β-6, β-5, β-4, β-2, β-3, where β-7 is antiparallel to the others. This β-sheet is bordered on the top and bottom faces by seven α-helices (α-2, α -3, α-5, α -6, α-7, α-8, α-10, α-12 and α -13). At the C-terminal part of the protein, another smaller antiparallel β-sheet is found (β-8, and β-9) surrounded by

six α-helices (α-1, α -9, α-10, α -11, α-14 and α -15), (Fig. 26b, c and d). Each monomer is facing the other and it is in this interface area that it should be the catalytic site of the protein (Fig. 29a).

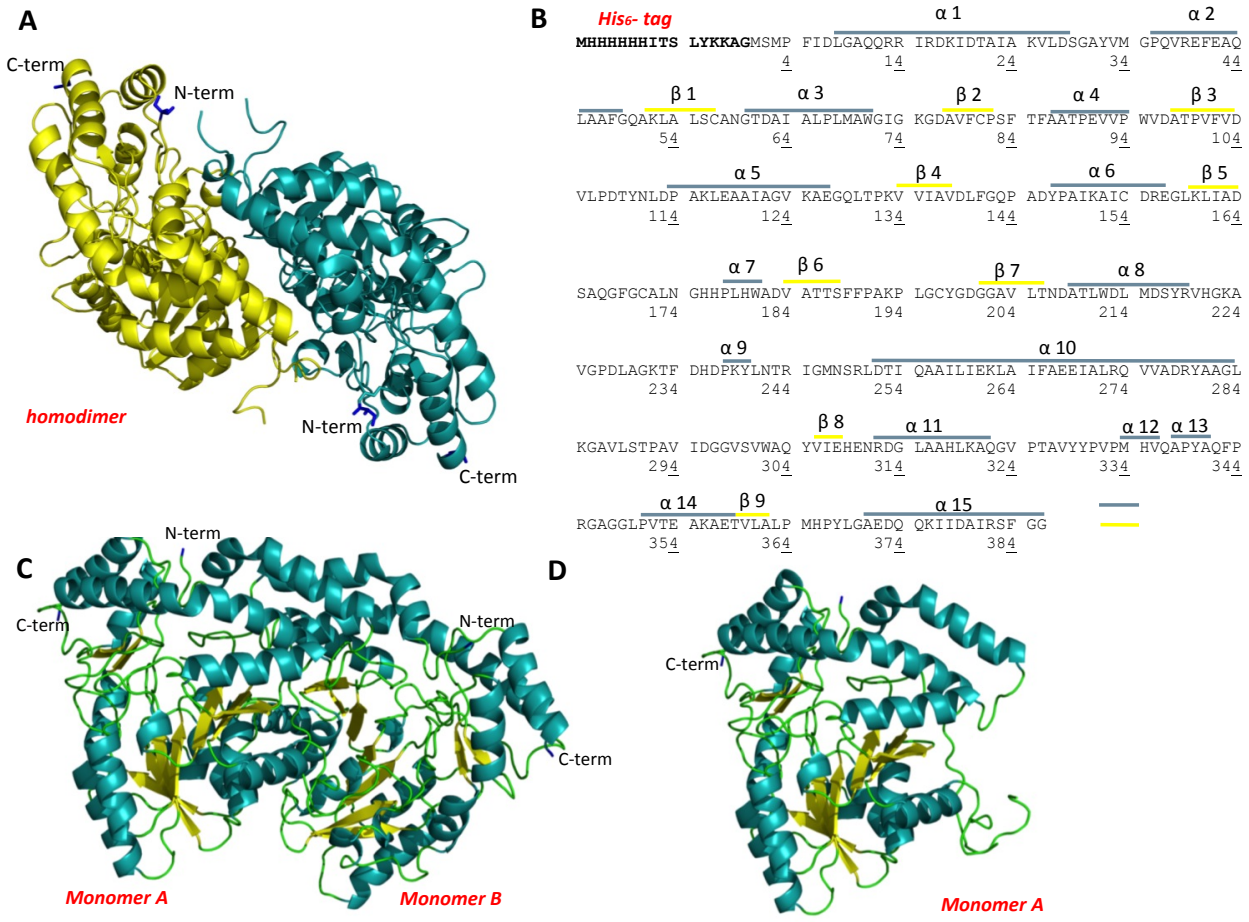

Figure 29. Structure of GipX. (a) Ribbon rapresentation of His_6-GipX homodimer, in cyan blue one dimer, in yellow the other; (**b**) Secondary structure features of the protein are rapresented as colored lines on the primary sequence of the His_6-GipX monomer: alpha-helices in cyan blue, β-sheets in yellow; (**c**) Ribbon representation of His_6-GipX homodimer, where secondary structure features respect the color code of the pannel (**b**) of the figure: alpha-helices in cyan blue, β-sheets in yellow, loops in green; (**d**) Ribbon rapresentation of the monomer A, with the secondary structure color code used in pannel (b) of the figure.

GipX shows a 41% of identity with the model protein WbpE and, as we can see in the figure 30, they can be easily superimposed with a Root-mean-square deviation (RMSD) of atomic positions of 1.66 Å. WbpE is a pyridoxal 5'-phosphate (PLP)-dependent aminotransferase, that belongs to the Wbp pathway (WbpA, WbpB, WbpE, WbpD, and WbpI) responsible for the synthesis of the central carbohydrate of the *P. aeruginosa* PAO1 (O5) B-band O-antigen, ManNAc-(3NAc)A,

which has been shown to be critical for virulence. In particular WbpE is responsible for the conversion of UDP-GlcNAc-(3keto)A and L-glutamate to UDP-GlcNAc(3NH2)A and R-ketoglutarate (R-KG) (Larkin *et al.,* 2010).

Two binding sites have been described in the WbpE catalytic site, a nucleotide sugar-binding site and a cofactor (PLP) binding site. Interestingly, all the residues building these binding sites and that are involved in the interaction of the protein with its substrate and cofactor (in yellow in the alignment, panel B, Fig. 30) are conserved in GipX sequence too, supporting the hypothesis that GipX could act as a PLP-dependent aminotransferase.

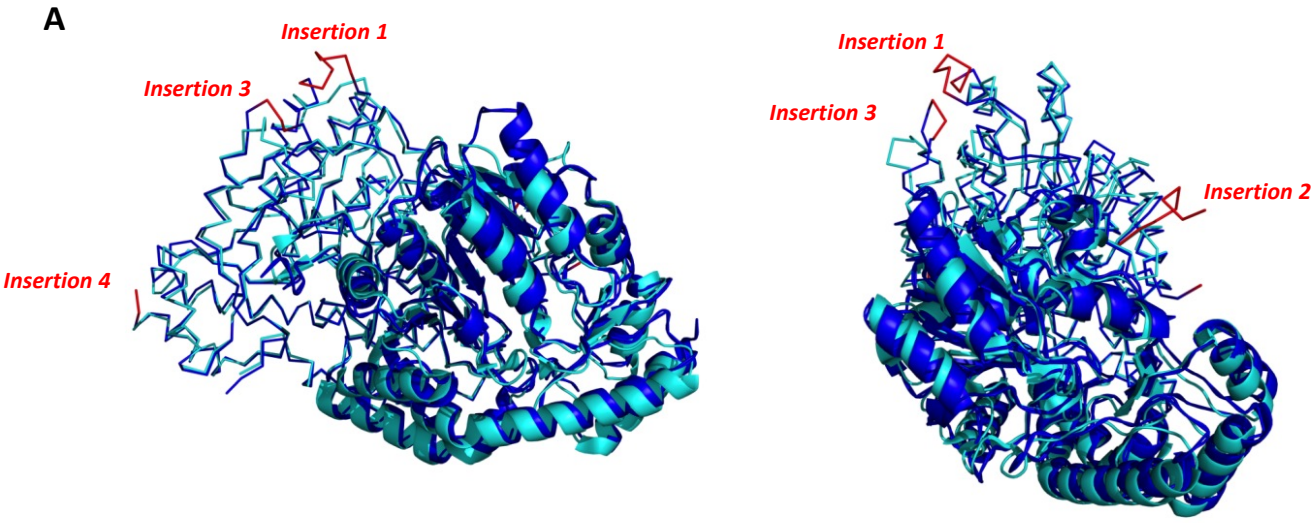

Figure 30. (a) Super imposition of GipX (in blue) **and WbpE** (in cyan blue) **structures** in two different orientations; each monomer is rapresented with a a ribbon rapresentation and a stick rapresentation. In the stick

representation, the four sequence insertions in GipX structure are shown in red**.** (**b**) **GipX and WbpE primary structure alignment** the insertions in GipX compared to WbpE are shown in red, while highlighted residues correspond to conserved catalytic site residues (yellow are the same, red are different); "*" means that the residues are identical in the two sequences, ":" means substitution with a very similar aa, while "." means substitutions with a weakly similar aa. The blue arrow shows the conserved aspartate important in all Fold Type I aminotransferases that is crucial for maintaining the cofactor in its protonated state by a salt bridge between the carboxylate of the Asp and N1 nitrogen atom of the pyridinium ring of PLP.

The presence of a conserved Aspartic acid (Asp or D) in position 163 of GipX sequence is particularly important. This residue (blue arrow in figure 30b) is actually conserved in all Fold Type I aminotransferases and is crucial for maintaining the cofactor in its protonated state, by a salt bridge between the carboxylate of the Asp and N1 nitrogen atom of the pyridinium ring of PLP. This molecular feature is the indispensable condition to enhance the properties of the cofactor as electron-sink.

ClustalW2 alignments of the two protein sequences (Fig. 30b), revealed that 4 insertion regions can be found in the sequence of GipX, when compared to WbpE one. As we can see from the 3D ribbon representation of the two proteins structure (Fig. 30a), these regions correspond to loops and α-helices portions that are exposed on the surface of the protein and that may be involved in interaction with partners of the protein, such as GcrA.

2) GipX is able to compete with DNA in the interaction with GcrA

In order to confirm the interaction that was seen by Co-IP assays between GipX and GcrA and test if this interaction can modulate the binding of His_6-GcrA to some of its targets *in vitro*, we set up an EMSA competition experiments with increasing amount of His_6-GipX in the presence of the positive hemi-methylated region of P_{mipZ} and His_6-GcrA (see Material and Methods).

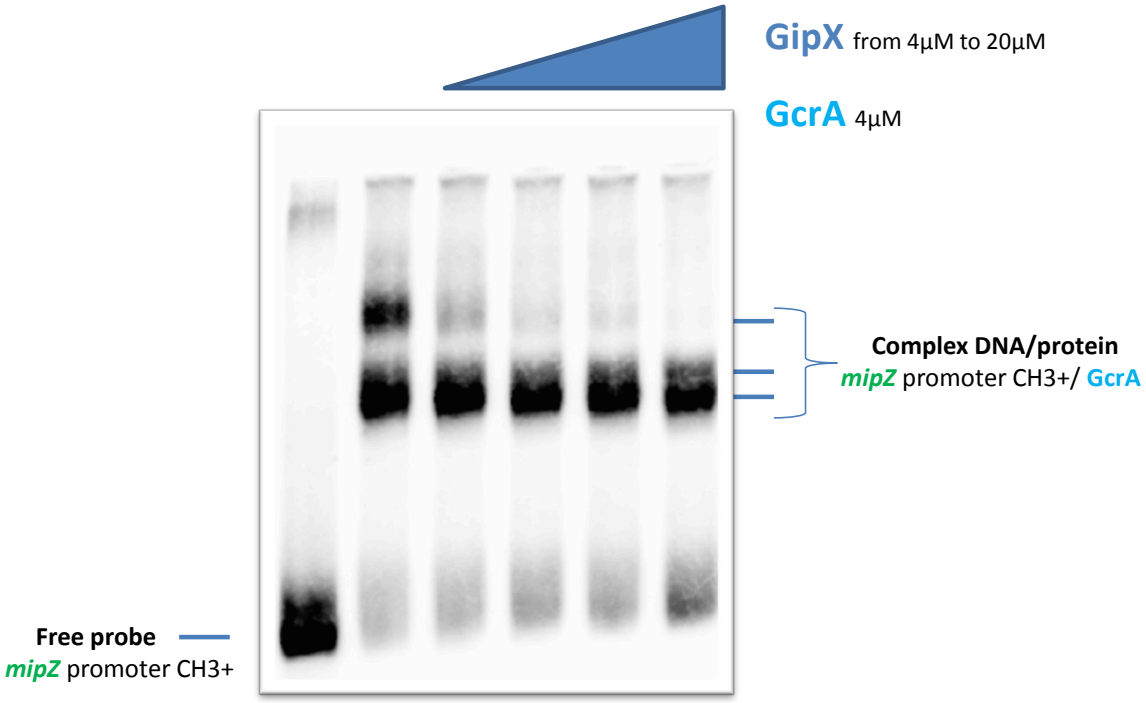

Figure 31. GipX is able to compete with DNA for the interaction with GcrA. EMSA assay of GcrA, *mipZ* promoter in presence of GipX; DNA-GcrA complexes of slower mobility are disappearing in the presence of an increasing amount of GipX in the reaction.

In these experiments, His_6-GcrA was pre-incubated with His_6-GipX, followed by the addition of the biotinylated probe. As we can see in the figure 31, as the amount of GipX is increasing in each sample, the highest complex formed by GcrA/*mipZ* CH_3^+ disappears, while the free probe signal is increasing. As shown in figure 31, we observed that GipX has a preference for GcrA involved in the formation of the highest molecular weight complex with the DNA. In fact, as GipX concentration is increasing, low mobility DNA/GcrA complexes are decreasing together with reappearance of the free probe. This result was also confirmed by using an excessive amount of GcrA (20 µM) in the EMSA reaction. In this condition GcrA is able to trap completely the probe and form a high positively-charged heavy complex that cannot enter in the EMSA gel (Fig. 32). After the addition of GipX in the reaction, the DNA/GcrA complex is freed from GcrA and it can enter in the gel. Those results were reproduced also after the addition of GipX to a preincubated mix of GcrA/DNA, confirming that the interaction between the two proteins can occur in presence or absence of DNA.

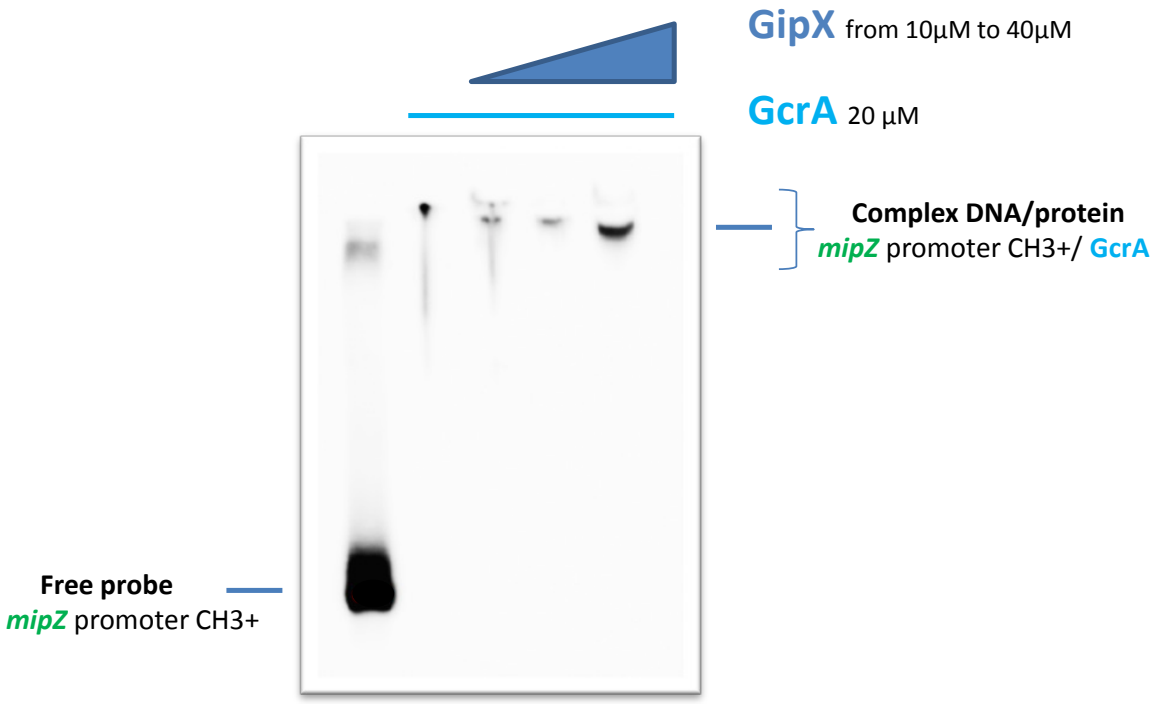

Figure 32. EMSA competition assay. An excess of GcrA is able to form a complex with DNA that cannot enter the polyacrylamide gel. An increasing of GipX concentration in the reaction can free the DNA-GcrA complexes from some GcrA and let the complex enter the gel.

Once the interaction GcrA/GipX was confirmed *in vitro*, we performed a co-crystallization assay between the His-tagged GcrA and GipX in order to explore this interaction at the structural level. Following an initial crystallization screening by commercial kits we identified a condition (different from the condition in which we recovered GipX crystals) where signs of crystallization were observed (see Material and Methods) (Fig.33). Unfortunately these crystals did not diffract by X-ray exposition suggesting that still the crystallization conditions, although very promising, are not still optional. Crystal optimization is still in progress.

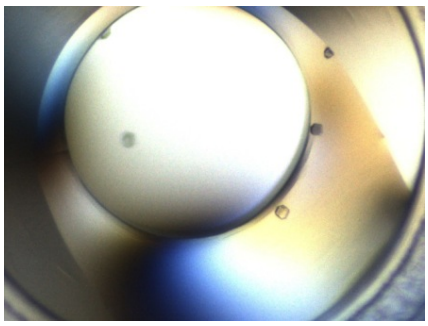

Figure 33. Co-crystallization assays of His_6-GipX and His_6-GcrA. Crystal obtained in condition 74 by CryoSuite kit, Qiagen.

Study on CtrA phosphorylation

Structural study of phosphorylation cascade that activates CtrA

As we discussed in the introduction, the phosphorylation of the cell cycle master regulator CtrA in *C. crescentus* requires the activity of a phosphorelay composed of the membrane hybrid histidine kinase (HK) CckA (Jacobs *et al*., 1999) and the histidine phosphotransferase (Hpt) ChpT (Biondi *et al*., 2006). As for most response regulators (RRs), the active form of CtrA depends on its phosphorylation at a conserved aspartate residue (D51). This phosphorylation event has to happen at the right time and at right place in the cell, especially in predivisional cells in which asymmetrical cell division is established.

In the last years, part of my research has been focused on this phosphorylation mechanism at the molecular level by a structural and biochemical approach (see next section). Moreover I have been involved in the development of tools able to measure CtrA phosphorylation at the cellular level. The results of this part of my PhD (published or not) will be illustrated in the following section.

At the beginning of my PhD, no protein structure of the phosphorelay was solved. The only factor, involved in the regulation of cell cycle in *C. crescentus* for which the structure was determined, was DivK (Guillet *et al*., 2002).

Thus one of the challenges of my PhD consisted in the structural study of cell cycle factors starting obviously from the cytosolic factors ChpT and CtrA.

1) C. crescentus CtrA

No structural information about CtrA has ever been established even if there have been several examples of structures of similar response regulators, such as, for example, PhoP from *Mycobacterium tuberculosis*, a response regulator that binds DNA (Menon *et al*., 2011). This objective has been a challenging step of this PhD project due to the purification low efficiency and the instability of CtrA.

The following section describes only the process of optimization of the protocol of production, purification and crystallization tests of the full-length wild type and D51E mutated versions of CtrA. Any crystal suitable for X-ray analysis has not been obtained yet, but this optimization and standardization of the purification represent, in my opinion, a crucial step for further advancements.

a) Tagging and expression optimization of wild type and D51E CtrA

The full-length DNA fragment of *ctrA* (CC3035 in CB15N genome) wild type (wt) and D51E were cloned into several destination vectors in order to test the effect of different tags (GST, TRX, His_6 and MBP) on the production and solubility of the protein. These plasmids were then used to expressed the CtrAs in BL21(DE3) *E. coli* cells (30°C, 3h in presence of 100 or 500 µM IPTG and at 20°C, overnight in the presence of 100 or 500 µM IPTG) and by auto-induction in Rosetta (DE3) LysS *E. coli* strain. The production of these recombinant versions of the protein was then checked by SDS-PAGE gel and for the best production condition we investigated the solubility using different method of lysis: Lysozyme, Sonication, Bugbuster and Emulsiflex. The best soluble proteins were then purified with Ni-NTA spin kit (data not shown).

We observed that the tagging of the CtrAs (wt and D51E) that gives higher expression and solubility yield is the His_6 tagged at the N-term of the protein.

Next we optimized a protocol of purification obtaining a pure and stable preparation of the two proteins.

For both the CtrA versions we used pET300/NT-DEST (Life Technologies) as destination vector, producing recombinant IPTG-inducible genes that are able to express CtrA fused to an N-terminal His_6 tag (MHHHHHHITSLYKKAG-) generating the strains EB527 (wt CtrA) and EB624 (D51E CtrA). Three different aspects were crucial in the optimization of these protocols of purification: temperature, time and storage buffer.

Both versions of the protein immediately showed an increase in the stability of the protein inversely proportional to the temperature (4°C, 15°C and room temperature). Moreover after several tests, we concluded that also freezing the protein was not possible, as the protein started to precipitate after thawing. We concluded that this was an important limiting feature of

the protein in order to perform crystallization assays as reproducibility of crystallization starting always from the same stock represents an essential step of the procedure.

We also observed that even in the best conditions (optimal buffer and 4°C), after one or two days His_6-CtrA started to precipitate, forcing us to perform in the same day purification, concentration and crystallization assay (See next).

However the optimized purification gave a pure preparation of CtrA as shown in SDS–PAGE gels representing the different steps of production and purification of the two His_6-CtrAs (Fig. 34). The final result of this optimization approach was a procedure that combines the use of an optimized buffer with a combination of Nickel-affinity purification and gel filtration, giving a preparation of this protein pure and suitable for crystallization tests.

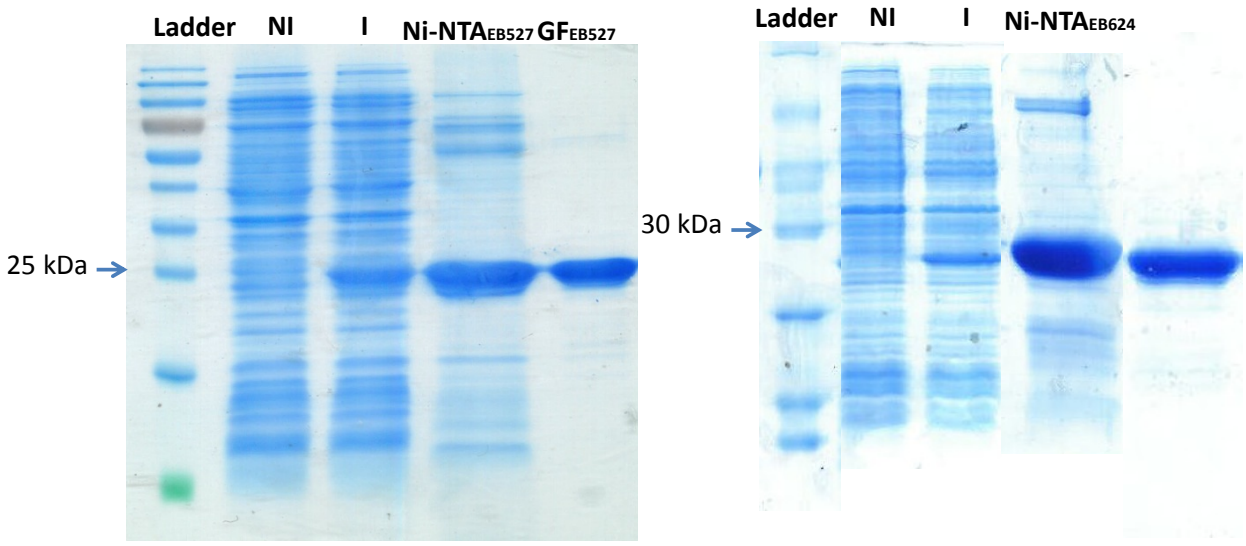

Figure 34. CtrA wild type (EB527) and D51E (EB624) productions and purifications. Both proteins have a molecular weight of 27.7 kDa**; NI** = protein content of not induced cells; I = Protein content of Induced cells by IPTG; Ni-NTA = Eluted protein after the first step of purification by Nickel columns; GF = Eluted protein obtained by Gel filtration purification.

b) Crystallization tests

For the wild type version of CtrA we performed crystallization screening trials using 4 different kits: the CryoSuite (Qiagen), the Pact Suite (Qiagen), pH Clear I and II.

In order to increase the possibility to found a hit, three different concentration (50, 100 and 150 µM) of protein were tested for each condition (1152 drops). The crystallization trails have

been replicated at two different temperatures (4 and 15 °C). Plates during the crystallization were monitored regularly to have an idea of kinetics, and the results were classified for the presence of precipitates or crystallization nuclei or clear solutions. However, none of the conditions we followed allowed production of a suitable crystal. We obtained a crystal in presence of 0.1 M Tris and 4.0 M Sodium chloride (pH Clear) for 100 µM of the protein that did not diffract. At the moment the D51E version of CtrA has been tested at two different concentrations (50 and 100 µM) with the CryoSuite (192 drops), but no successful crystallization condition has been found yet. We noticed for this variant of the protein a different behavior in comparison with the wild type version; in fact, the CtrA D51E organizes itself in fibers.

1152 conditions for CtrA (EB527) and 192 for the D51E version (EB624) were tested, using a robotic crystallization system (Droplet by Cybio robot). Observations of crystallization tests of CtrA wild type revealed that most of the conditions showed precipitation, ca. 20% were instead clear, suggesting that the concentration of the protein used was appropriate. Three conditions revealed primordial nucleation phenomena that we could not optimize. Just one condition formed a crystal, which was not diffracting. Also in the case of D51E observation of crystallization tests revealed that most of the conditions showed precipitation suggesting that the concentration of protein should be appropriated, but no conditions has been found yet.

2) *C. crescentus ChpT*

Histidine phosphotransferases (HPTs) are usually monomeric proteins that form a typical structure named a four-helix bundle (Biondi *et al*., 2006; Xu *et al*., 2009). In *Bacillus subtilis*, however, the four-helix bundle structure of Spo0B is achieved by the parallel association of the helical hairpins of two subunits (Varughese *et al*., 1998). ChpT does not belong to any class of known HPTs. Its N-terminal histidine 33 (His33) shuttles the phosphate, while the C-terminus weakly resembles an ATP-binding domain (Biondi *et al.,* 2006). This organization suggests a possible similarity to histidine kinase structures. However, previous biochemical studies have shown that ChpT has no capability to autophosphorylate its His33 using ATP (Biondi *et al*., 2006; Chen *et al*., 2009), suggesting other roles for the C-terminal domain. Despite the importance of ChpT in cell-cycle regulation in *C. crescentus* and its novelty in the signal transduction field, no structural analysis has been carried until our work. More recently the structure of ChpT was also solved giving the same results (Blair *et al*., 2013).

a) *ChpT is a homodimer that adopts the domain architecture of the intracellular part of class I histidine kinases*

To acquire a deeper knowledge about the spatial organization of ChpT and its function, we conducted crystallization assays on the full length His_6-ChpT (Materials and Methods for production and purification procedures Fig. 35A). With initial crystallization trials (performed using commercial crystallization kits) we identified a primordial nucleation phenomenon of our protein (Fig. 35B). The optimization of the nucleation conditions and the optimal concentration of the protein (see Material and Methods), led us to obtain unique crystals suitable for X-rays exposition, solving the protein structure within a resolution of 2.2 Å (figure 35C and D).

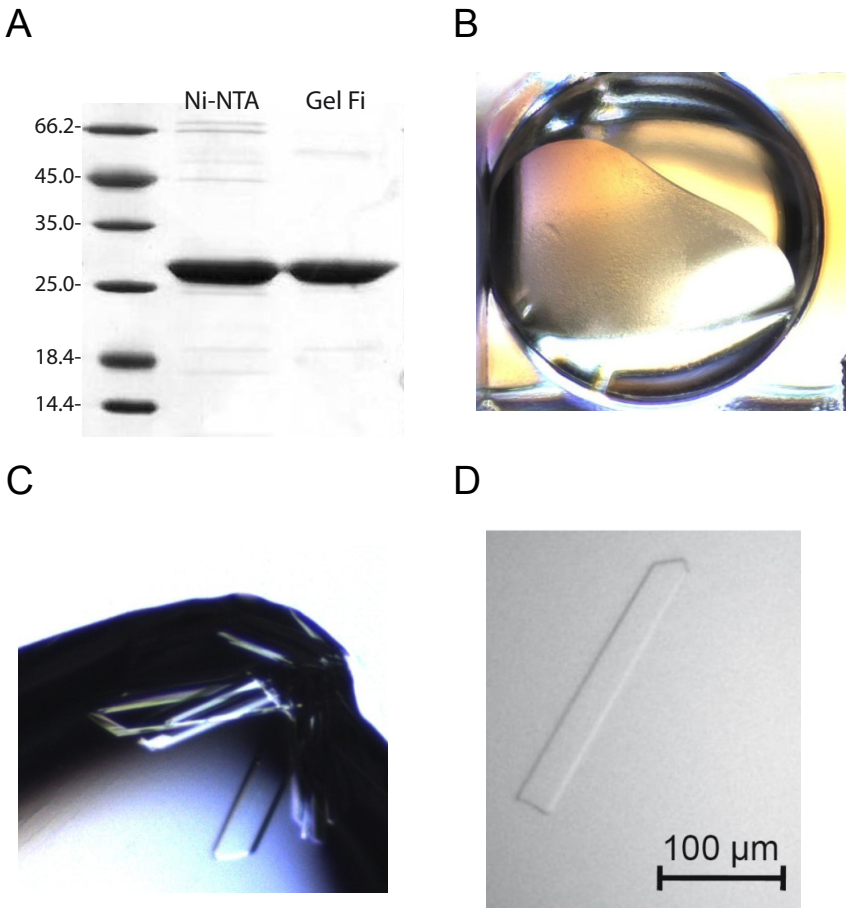

Figure 35. (A) His_6-ChpT step of purification: Ni-NTA = Eluted protein after the first step of purification by Nickel columns; GF = Eluted protein obtained by Gel filtration purification. (**B**) Primordial nucleation phenomena of His_6-ChpT obtained in condition 88 of Cryokit, Qiagen; (**C**) Crystals obtained after optimization of condition and concentration of protein; (**D**) Crystal used for X-ray diffraction, isolated from the drop showed in panel C (modified from Fioravanti *et al*., 2012).

Data processing revealed that the crystals belonged to the orthorhombic space group C2221, with unit-cell parameters a = 103.5, b = 210.2, c = 93.9 Å for His_6-ChpT-Native. Phasing by molecular replacement using known structures of HKs was unsuccessful. Therefore, we solved the His_6-ChpT structure using a heavy-atom derivative. We produced crystals of His_6-ChpT in presence of Eu-DO3A (see Materials and Methods) that presented unit- cell parameters a = 106.4, b = 210.0, c = 94.1 Å, but the same space group of the native crystal. 13 Eu-DO3A sites were found in the asymmetric unit of the derivative, with occupancies ranging from 20 to 100%. There are three His_6-ChpT subunits in the asymmetric unit of the crystal, corresponding to a Matthews coefficient of 3.3 $Å^3$ Da^{-1} and an estimated solvent content of 62.8%. Two subunits

form a homodimer, while the third subunit exploits a twofold symmetry axis of the lattice to generate a similar homodimer. The structure has been deposited in the Protein Data Bank with code 4fpp. The presence of metal ions was suggested by the electron-density map. A fluorescence spectrum measured on the BM30 beamline allowed us to show that the only metal ions present in the cooled sample were nickel ions, which are presumably derived from the purification procedure. His_6-ChpT adopts the overall domain architecture of the intracellular part of a class I histidine kinase (HK; Fig. 36).

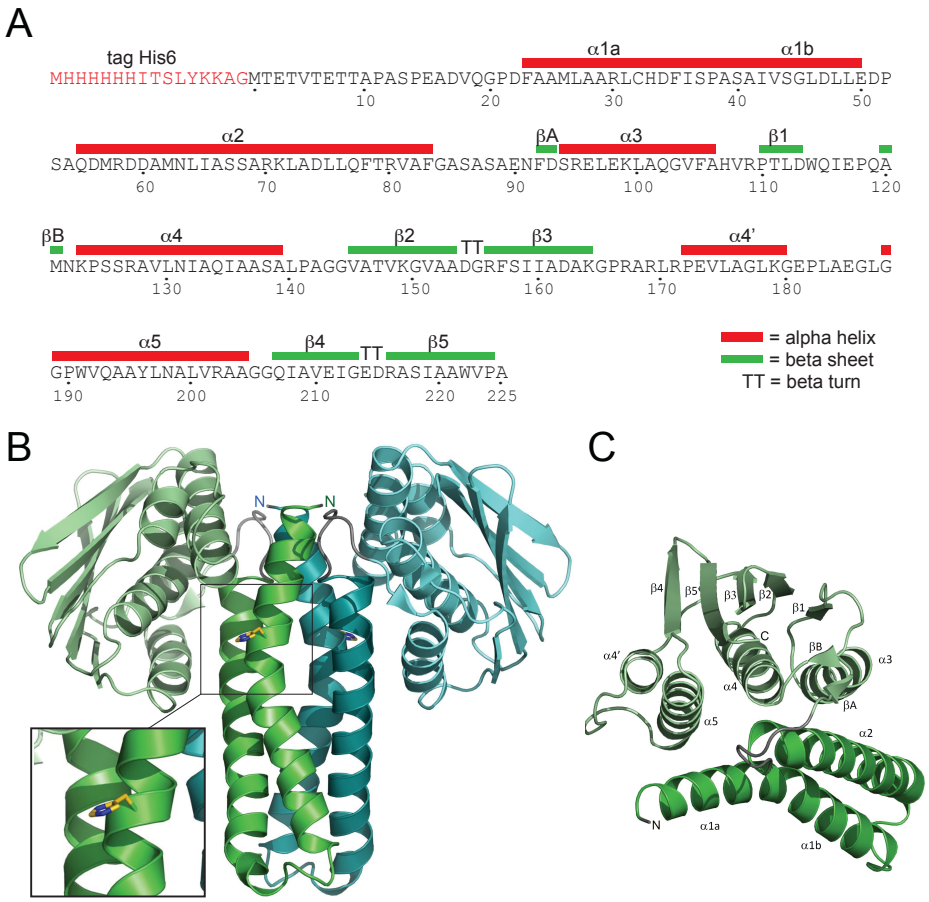

Figure 36. Structure of ChpT. (**a**) Definition of secondary-structure elements in the His_6-ChpT sequence. (**b**) Ribbon representation of the overall ChpT structure viewed perpendicular to the twofold symmetry axis. The two ChpT subunits are displayed in green and blue. This view shows the formation of the four-helix bundle of the DHp domain flanked by the two C-terminal domains. The catalytic His33 residues are shown in stick representation on opposite faces of the DHp domain. The two N-termini are also indicated. (**c**) Representation of one ChpT subunit, with all secondary-structure elements labeled (from Fioravanti *et al.*, 2012).

Each subunit consists of two distinct domains, an N-terminal helical hairpin domain and a C-terminal α/β domain, which are connected by a short linker (residues 84–91). The helical hairpin domain is comprised of residues 20–83 and its two antiparallel α-helices are connected by an eight-residue turn (residues 51–58). The N-terminal residues 1–19 are disordered and were not included in the structure. The dimer interface is exclusively between the two helical hairpin domains and the twofold symmetry axis runs parallel to the helices such that the N-termini are adjacent, forming a four-helix bundle referred to as the dimerization and phosphotransfer (DHp) domain. The DHp domain contains the two H-boxes, with each catalytic His33 located on an opposite face of the four-helix bundle. Helix α1 extends for about 40 Å from the N-terminus to residue 50, displaying a kink induced by Pro38 at the end of the H-box (helix α1, 20–38; helix α2, 39–50). Helix α2 has a similar extension but without any pronounced kink. The four-helix bundle is stabilized mainly by hydrophobic interactions involving Leu27, Leu31, Phe35, Ala39, Ile42, Leu46, Met62, Ala69, Leu72 and Leu76. A structure-similarity search using the PDBeFold protein-structure comparison service at the European Bioinformatics Institute (http:// www.ebi.ac.uk/msd-srv/ssm; Krissinel & Henrick, 2004) revealed that the His_6-ChpT C-terminal (CCT) domain is a close structural homologue of the ATP-binding domain of DesK (r.m.s.d. of 2.15 Å for 109 structurally aligned Cα atoms) (Trajtenberg *et al*., 2010), among many other homologous domains belonging to various sensor type histidine kinases (Fig. 37).

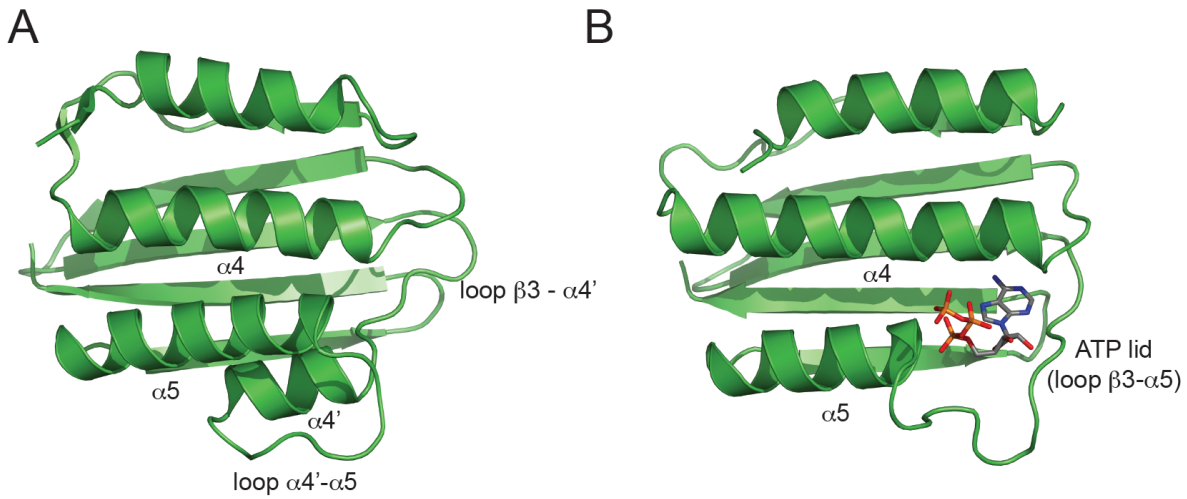

Figure 37. Ribbon representation of the C-terminal domains of (**a**) ChpTand (**b**) DesK (Trajtenberg *et al*., 2010). DesK binds ATP in the ATP-binding pocket defined by the ATP lid (a loop between strand β3 and helix α5) and the central helix α4, while the γ-phosphate is exposed and can be attacked by the catalytic histidine of the DHp domain. In

ChpT the ATP lid is substituted by two additional turns in the N-terminal part of helix α5. There is an additional short α-helix (α4') between strand β5 and helix α5, which together with helix α5 closes the ATP-binding pocket (from Fioravanti *et al*., 2012).

The C-terminal adopts a Bergerat ATPase fold (Dutta & Inouye, 2000), which consists of a α/β sandwich with one layer made up of a mixed five-stranded β-sheet and the other layer consisting of three α-helices (α3–α5). In addition, this domain contains a pair of short antiparallel β-strands (βA and βB). It has been shown that ChpT has no capability to autophosphorylate His33 using ATP (Biondi *et al*., 2006). The ChpT crystal structure reveals that the CCT domain differs structurally when compared with ATPase domains found in HKs. In HKs with autokinase activity each ATPase domain characteristically hosts one ATP molecule between the ATP lid (a loop between strand β3 and helix α5) and the central helix α4, while the γ-phosphate is exposed and can be attacked by the catalytic histidine of the DHp domain. The bottom of the ATP pocket consists of β-strands 3, 4 and 5. In His_6-ChpT the ATP lid is substituted by two additional turns in the N-terminal part of helix α5. These turns occupy the space in which the β- and γ-phosphates are usually located in the CA domain of HKs. Also, there is an additional short α-helix (α4') between strand β5 and helix α5 in ChpT, which together with the latter helix closes the ATP-binding pocket found in the CA domain of HKs. We also obtained crystals of His_6-ChpT in the presence of 2.5 mM ATP or ADP in the crystallization buffer. Analyses of these crystals did not reveal any ATP or ADP bound to His_6-ChpT, which was consistent with the different conformation of the CCT domain (data not shown).

Even if the His_6-ChpT homodimer shares the overall architecture of class I HK, with its four-helix bundle flanked by two ATP-binding-like domains, significant differences are observed in the relative orientation of these domains. In His_6-ChpT the two domains adopt a compact conformation, with helices α3, α4 and α5 from the CCT domain lying along helices α1 and α2, leaving the five-stranded β-sheet of the CCT domain roughly parallel to the helical axis of helix α1. The KinB kinase from *Geobacillus stearothermophilus* (Bick *et al*., 2009) is one of the closest structural homologues of ChpT. Although the ChpT and KinB DHp domains superimpose reasonably well (2.1 Å r.m.s.d. on 52 structurally aligned Cα atoms), the disposition of the C-terminal domains with respect to the DHp domains is very different. Structural alignment of the CCT domain with that of KinB would require an approximate rotation of 55° initiated at the

interdomain linker and an outward translation of 20 Å away from the homodimer twofold axis. Structural studies have reported that the CA domains in HKs adopt different positions with respect to the phosphoacceptor His residue according to the step of the phosphotransfer process (Marina *et al*., 2005). ChpT is devoid of autokinase activity and thus such specific movements between domains are not expected in the context of an autophosphorylation process. However, it cannot be excluded that domain movement still occurs, for example in the partner-recognition process. A key characteristic of two-component systems is the high specificity of the HK–RR interaction (Laub *et al*., 2007). Because of their structural similarities, we assume that the molecular basis of ChpT–target recognition should be similar to that of HK–RR. Structural insight into HK–RR interactions has recently been revealed by studies of the ThkA–TrrA and HK853–RR468 complexes of *Thermotoga maritima* (Marina *et al*., 2005; Casino *et al*., 2009, 2010; Yamada *et al*., 2009) and specificity rewiring of TCSs (Skerker *et al*., 2008; Capra *et al*., 2010; Ashenberg *et al*., 2011). These studies showed that the recognition domain of the response regulator (RR) binds to its partner protein via interactions with helix α1 of the DHp domain below the phosphodonor His residue and also parts of the ATP lid and the interdomain linker in the HKs. Since the ATP-lid region is severely affected in the ChpT structure by the N-terminal extension of helix α5 and the presence of an additional helix α4', we anticipate that these differences may have implications for partner recognition of ChpT. We have demonstrated in this work that His_6-ChpT, an essential phosphotransferase that controls the phosphorylation of CtrA in *C. crescentus*, adopts the class I histidine kinase fold, with a four-helix bundle flanked by two domains displaying a structurally different ATPase fold. This structure paves the way for future biochemical investigations aiming at deciphering the functional aspects of ChpT regulation and function.

The study of CckA-ChpT-CtrA phosphorelay: phosphorylation and dimerization

As described before, *C. crescentus* cells divide producing two distinct cell types. The development of different cellular types is caused by the asymmetrical localization of factors before cell division. Among cell cycle regulators, two-component system proteins are the major

players. In its phosphorylated form, the response regulator CtrA represses the origin of chromosome replication (*Cori*) and activates the expression of tens of genes that are crucial for cell cycle progression. After the G1-S transition, in which CtrA is proteolyzed, its transcription is reactivated by GcrA in early S-phase. CtrA is then phosphorylated by the CckA/ChpT phosphorelay at the new pole of the predivisional cell. This spatial organization of CckA suggests that in predivisional cells CtrA-P levels should be higher at the swarmer new pole. The aim of this project, in collaboration with Pauline Vandame (PhD in Biondi's Lab), was to create biosensors able to detect the phosphorylation level of CtrA *in vivo* and *in vitro*. These sensors, based on the Förster resonance energy transfer (FRET, Förster 1948) approach, exploit the ability of response regulators to dimerize upon phosphorylation. The receiver domain of CtrA (CtrA(RD)) presents in fact, homologous domain of dimerization that is common in many Response Regulators proteins in bacteria (Gao *et al*., 2009; Gao *et al*., 2010). Thus, starting from the hypothesis that CtrA undergoes homodimerization upon phosphorylation and previous works on RD FRET based biosensors (Gao *et al*., 2008), we fused CtrA RD domain with either a donor (CFP) or an acceptor (YFP) fluorescent protein to measure the FRET signal.

A FRET is a non-radiative energy transfer phenomenon that occurs between two fluorophores. This transfer can occur just if the sensors, in our case CtrA(RD)-CFP and CtrA(RD)-YFP, are close enough to each other (less than 10 nm) and the emission spectrum of the donor fluorophore (CtrA(RD)-CFP) overlap the excitation spectrum of the acceptor fluorophore (CtrA(RD)-YFP) (Fig. 38).

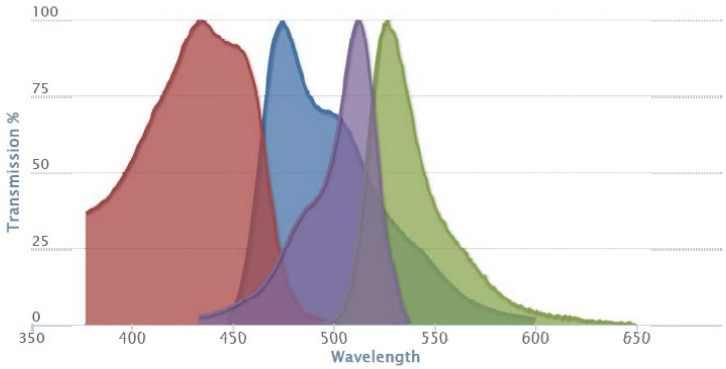

Figure 38. Fluorescence excitation and emission spectrum for the fluorophores CFP [emission peak 475 nm (in blue); excitation peak 435nm (in red)] and YFP [emission peak 527 nm (in green); excitation peak 512 nm (in purple)].

As FRET is a possible pathway for the relaxation of the excited state fluorophores (the donor), the emitted fluorescence will be subjected to modifications of its properties upon FRET. One of these modifications concerns the emission intensities: in fact, upon a FRET event, emission intensity of the donor fluorophore decreases while the acceptor's one increases. The FRET sensitized emission, is a technique based on the measurements of those parameters and the calculation of acceptor and donor emission ratio intensity, to monitor FRET efficiency *in vivo* or *in vitro*.

a) Design of a CtrA phosphorylation sensor

As mention before, based on the hypothesis that CtrA undergoes dimerization upon phosphorylation, we realized CtrA (RD)-CFP and YFP constructions based on previous work (Gao *et al*., 2008), in order to allow *in vitro* and *in vivo* FRET experiments (Fig. 39).

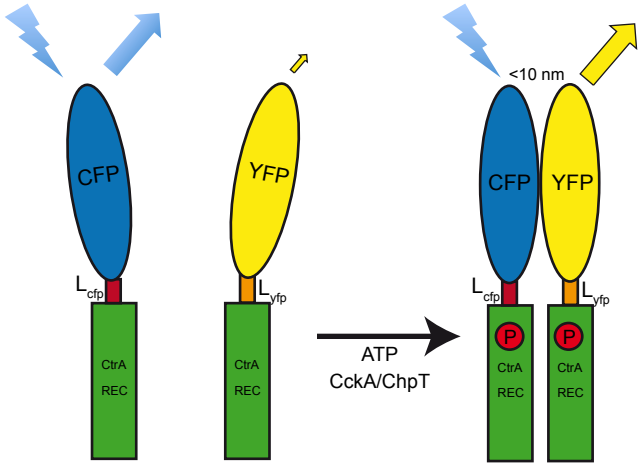

Figure 39. Schematic representation of CtrA(RD)-CFP and CtrA(RD)-YFP sensor. Principles of the FRET-based dimeric sensor. In blue: CtrA(RD)-CFP; in yellow: CtrA(RD)-YFP; in green: response regulator; red P: phosphate group. The different flourophores are linked to the receiver domain by optimized linker sequences as previously described in Gao *et al*., 2008.

N-terminal His_6 tagged versions of the sensor were constructed in order to express them in *E. coli* cells and purified for the *in vitro* experiments (See Materials and Methods). Briefly the strategy is based on the phosphorylation in vitro by the reconstituted phosphorelay (cckA and

ChpT) followed by the measurement of the FRET signal. The CckA N-terminal His_6-Thioredoxin (Txr) receiver domain (RD) and N-terminal His_6-Maltose binding protein (MBP) histidine kinase domain were produced and purified as previously described (Biondi *et al*., 2006) in addition to the N-terminal His_6 tagged ChpT (Fioravanti *et al*., 2012) to reconstitute the *in vitro* phosphorelay CckA-ChpT-CtrA (see Material and Method and figure 40).

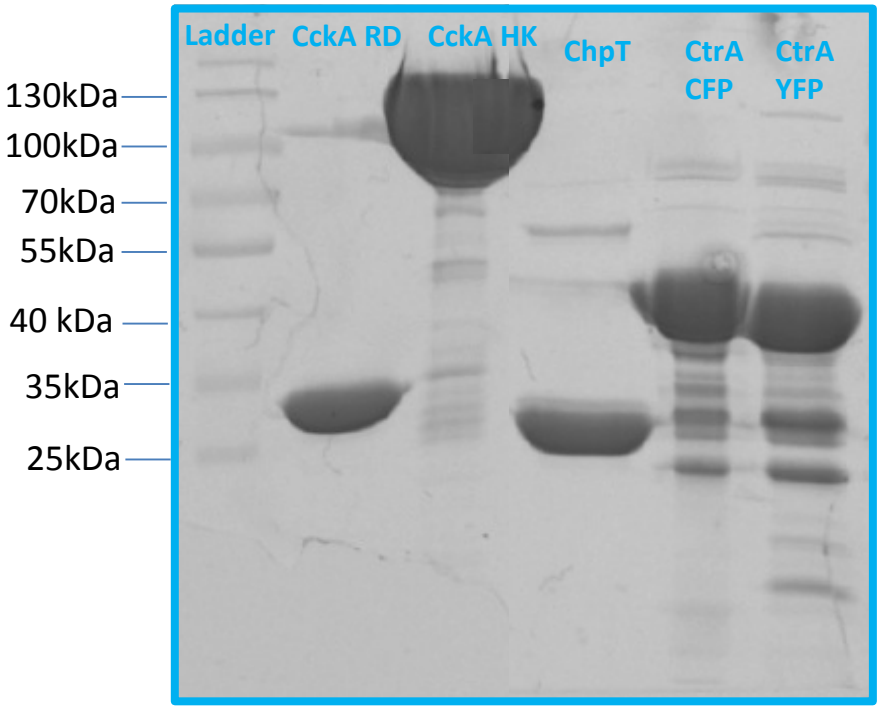

Figure 40. Purification of CtrA phosphorylation cascade components. His_6-Trx-CckA (RD)= 27.4 kDa; His_6-MBP-CckA(HK)=97.7 kDa; His_6-ChpT= 25.3 kDa; His_6-CFP-CtrA(RD)=42.9 kDa; His_6-YFP-CtrA(RD)=43.7 kDa.

For the *in vivo* study different constructions of CtrA(RD)-CFP and YFP sensor were performed in high (pBR322 derivatives, pSRK; Khan *et al*., 2008) and low copy number per bacterium (pRK derivatives, pMR20) vectors to express the FRET sensor in *C. crescentus* cells under the modulation of induction by IPTG or xylose (see Material and Methods and figure 41).

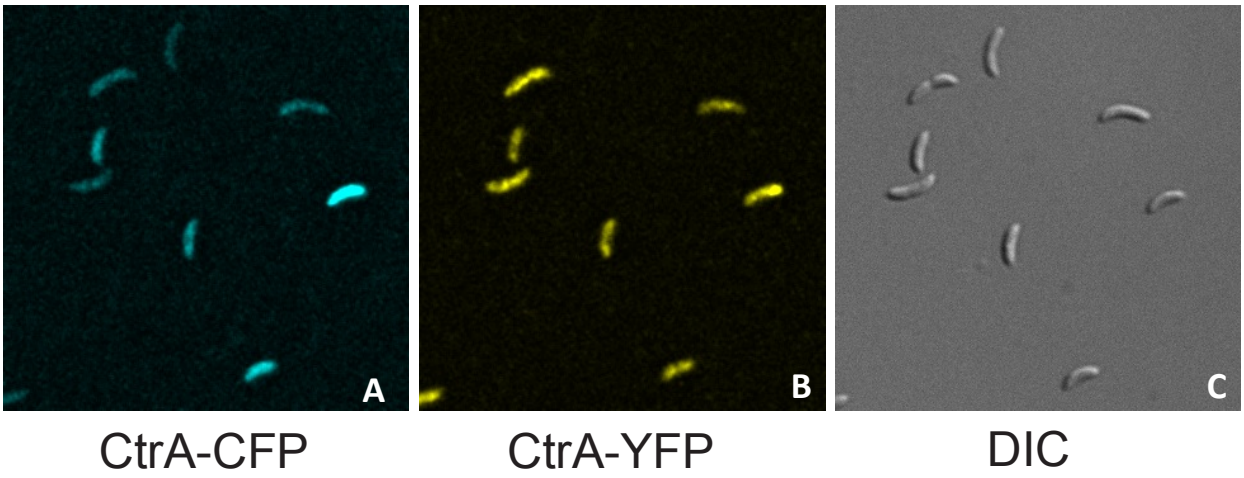

Figure 41. *C. crescentus* EB972 that express CtrA(RD)-CFP in presence of IPTG (**A**) and CtrA(RD)-YFP upon xylose induction (**B**). (**C**) Differential interference contrast (DIC) picture.

b) CtrA YFP and CFP dimerize upon phosphorylation

In order to confirm that phosphorylation, exploited by CckA-ChpT phosphorelay, causes dimerization of CtrA we first verified whether our sensors were able to be phosphorylated *in vitro* by the reconstructed phosphorylation cascade.

A phosphorylation biochemical assay was set up *in vitro*, and after incubating the purified CckA HK domain with ATP in addition to CckA RD and ChpT we were able to separate the phosphorylated form of CtrA(RD)-YFP (shown in the figure 42) or CtrA(RD)-CFP (data not shown) by Phosphate-affinity (Phos™-Tag) SDS-PAGE electrophoresis (see Material and Methods).

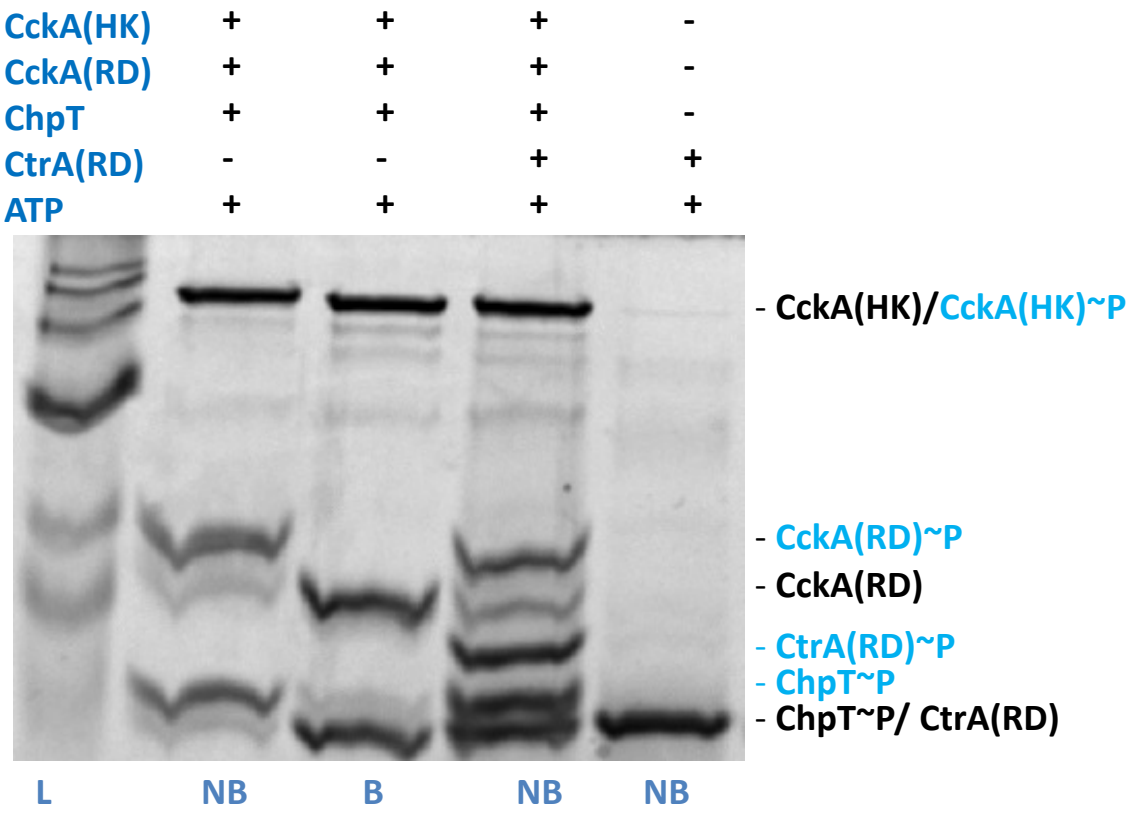

Figure 42. Phos™-Tag SDS-PAGE electrophoresis of the *in vitro* phosphorylation of CtrA-YFP upon reconstitution of the phosphorelay; L= ladder, NB= not boiled sample, B=boiled sample; after phosphorylation we observe a shift of the phosphorylated protein in its run that correspond to the ~P forms of the proteins in the picture.

Once we verified that our phosphorylation cascade was active and that our sensors could be phosphorylated *in vitro*, a FRET-measurement experiment was set up in a 384-well assay. FRET donor CtrA(RD)-CFP and CtrA(RD)-YFP acceptors were incubated in presence of CckA-RD, CckA-HK and ChpT with and without ATP. The plate was then read on a Pherastar Plate reader (BMG Labtech.Gmbh) with excitation at 430 nm and emission 480 nm and 530 nm. Emission ratios of 530 nm/480 nm were calculated and normalized based on the measured fluorescence of the donor and acceptors alone.

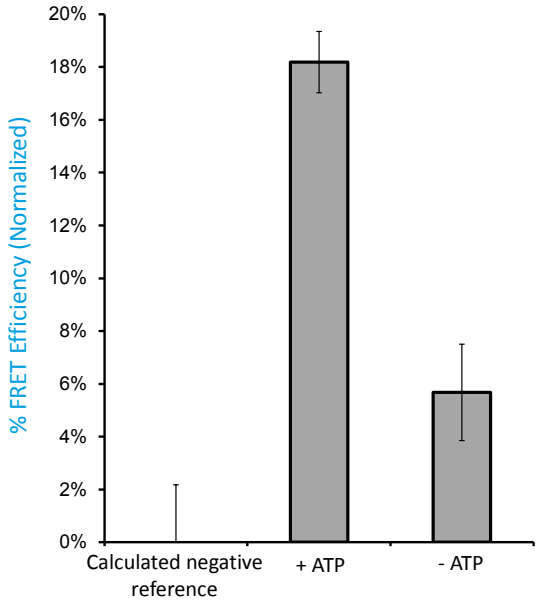

Figure 43. The histogram represents the measured FRET efficiency in the *in vitro* experiment. The negative reference was calculated in presents of the entire phosphorelay, ATP and half of the sensor (CtrA(RD)-YFP or CFP).

As we can see from the results obtained with these experiments represented in figure 43, a significant FRET efficiency can be detected only when ATP is added to the whole phosphorelay and strictly when both pair of the sensor are present (CtrA(RD)-CFP and CtrA(RD)-YFP). This result confirms *in vitro* the prediction that, upon phosphorylation, CtrA undergoes to dimerization.

In order to confirm our result also *in vivo*, in support of Pauline Vandame (Biondi lab), we performed FRET experiment (Fig. 44) on the *C. crescentus* EB972 that expresses, under the control of IPTG and xylose, our sensor CtrA(RD)-CFP and CtrA(RD)-YFP respectively. This strain was compared with similar strain in which YFP has no CtrA(RD) domain (EB911).

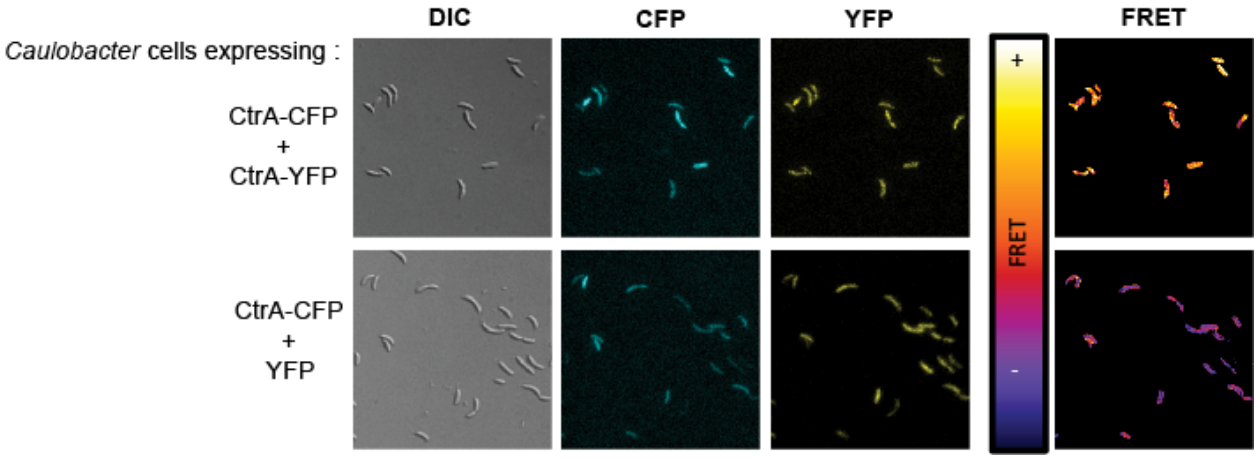

Figure 44. Dimerization upon phosphorylation of CtrA measured by FRET. *In vivo* FRET experiment on *C. crescentus* EB972 Images (upper panel) show a representative field of each condition for DIC, CFP and YFP channels. FRET images are represented with a pseudo-color scale. Images of EB911, our negative control (down panel), show that the FRET efficiency depends from the dimerization of CtrA, since it is not detected where just one version of the sensor is present.

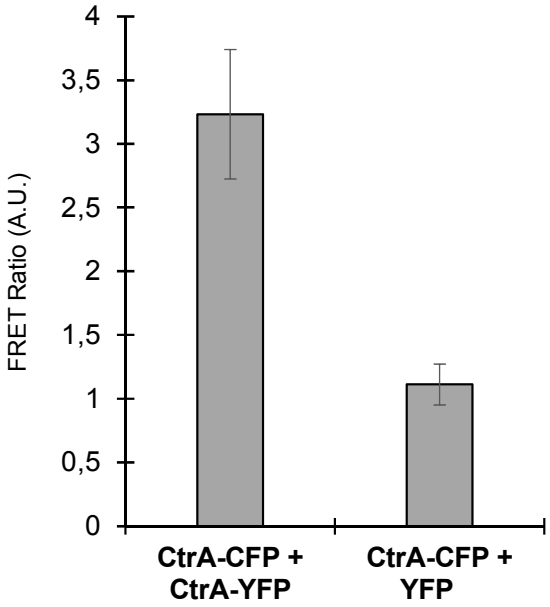

Figure 45. The averaged FRET levels per condition after a cell by cell analysis (30 cells) are represented in the graph.

As we can see in the figure 45, in which FRET measurements in fixed *C. crescentus* cells expressing CtrA-CFP and CtrA-YFP were compared to cells expressing CtrA-CFP and YFP (used as a negative control), we could measure a significant FRET efficiency only in presence of the

complete sensor pair. Therefore the functionality of this sensor was demonstrated also *in vivo,* showing definitively that CtrA undergoes dimerization upon phosphorylation.

c) Study of CtrA dimerization changes during cell cycle.

A lot is known on CtrA expression and activation during the progression of cell cycle (see introduction), but still a direct observation of how the phosphorylation levels of CtrA are changing during this process and what is the spatial distribution of CtrA-P are still missing.
To investigate the CtrA phosphorylation, we used Phos Tag gels (Pini *et al.,* 2013) in order to analyze the stoichiometry of its phosphorylation in cells. In other words with Phos tag gels we can separate the phosphorylated and non-phosphorylated forms of a response regulator.
A wild type CtrA immunoblotting on a Phos-tag gel of synchronized *C. crescentus* cells was set up (Fig. 46).

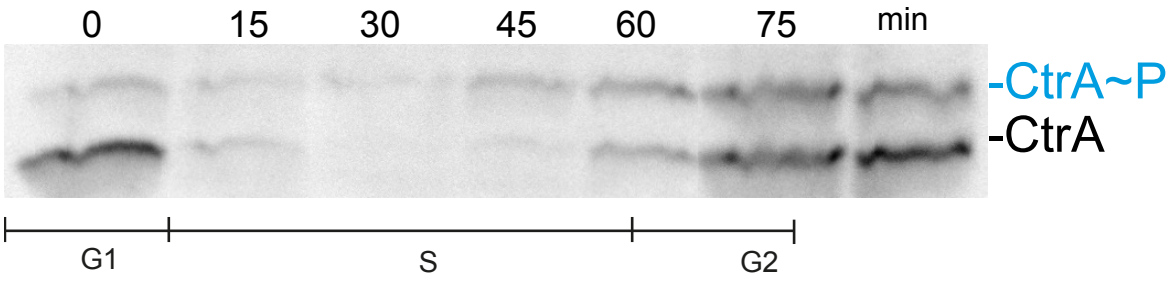

Figure 46. Wild type CtrA immunoblotting on a Phos-Tag gel loaded with synchronized *Caulobacter* samples (rich medium).

The intensity of the phosphorylated bands from the synchronized CtrA wild type immunoblotting /Phos-tag gel was measured (Fig. 47). First we observed that CtrA levels disappeared at the G1-S transition. We confirmed by quantification of the phosphorylated band, that the highest absolute amount of phosphorylated CtrA is in the G2 phase. That, after a little decreasing in G1, phosphorylation of CtrA almost disappeared around 30 min (beginning of S-phase). All those observations are consistent with the oscillation of expression of CtrA and the dynamic of activation by phosphorylation.

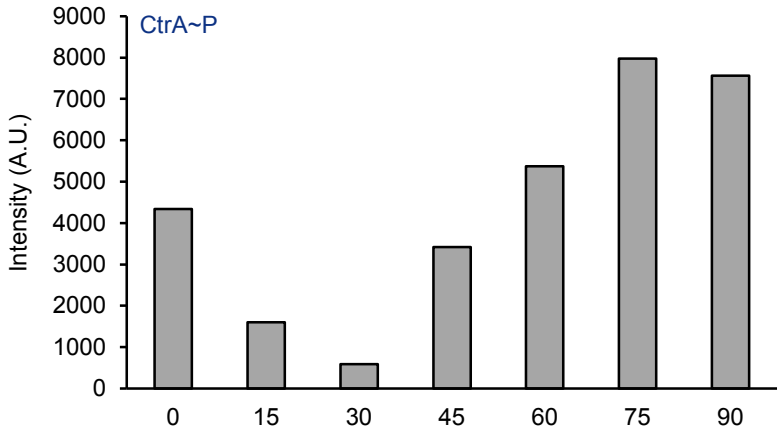

Figure 47. Quantification of the intensity of the phosphorylated bands using Image J. X axis is in minutes. See text for interpretation.

Taking advantage of the Phos-tag technology we also calculated the ratio between the phosphorylated and un-phosphorylated bands for each time point (Fig. 48). Although CtrA is decreasing (G1-S-phase transition) due to proteolysis, the phosphorylation ratio increased. This phenomenon may be due to a higher stability of the phosphorylated form and/or a higher activity of the CckA/ChpT phosphorelay.

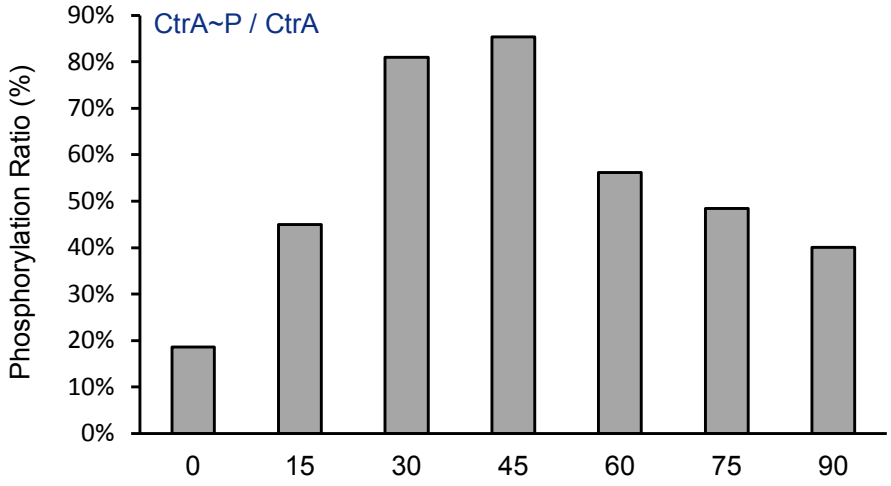

Figure 48. Intensities ratio of the phosphorylated/unphosphorylated bands that correspond to the activity of the phosphorylation cascade. X axis is in minutes. See text for interpretation.

In order to measure the phosphorylation levels by CckA/ChpT over the cell cycle and therefore discriminate between those two possibilities in the G1-S transition, we used *in vivo* the FRET-based biosensor (Fig. 49). It should be considered that our sensor could not be proteolyzed therefore it gives the actual levels of phosphorylation in a constant level of expression of the substrate.

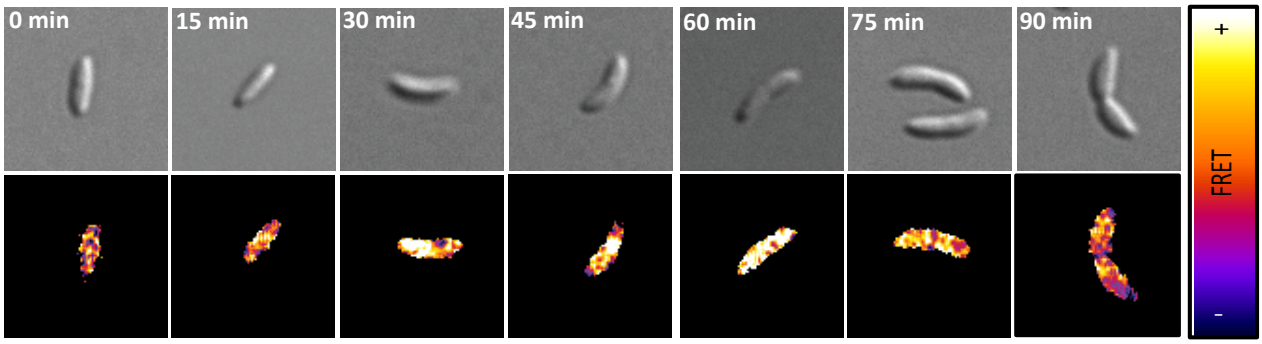

Figura 49. Synchronized *Caulobacter* cells expressing CtrA-CFP and CtrA-YFP. See text for interpretation.

For each time point the average FRET signal was calculated and results are shown in figure 50.

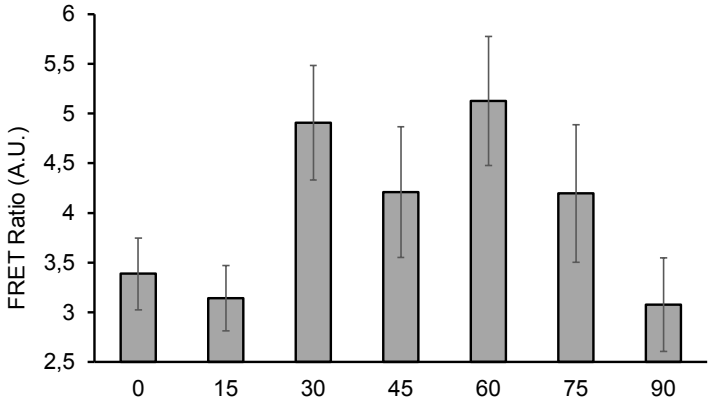

Figure 50. Average FRET levels per time point calculated on 20 cells for each time point. X axis is in minutes.

Analysing the results it appears that at 30 min the capacity of phosphorylation is high, although CtrA is almost absent.

A general conclusion is that CtrA-CFP and CtrA-YFP dimerize upon phosphorylation *in vitro*. This property was used to create a biosensor that was able to detect levels of phosphorylation of CtrA *in vivo*. The CtrA biosensor was indeed able to report the phosphorylation changes during the cell cycle and thus the activity of the phosphorelay composed by CckA and ChpT. Interestingly we detected a decrease of the phosphorylation activity prior/at the G1-S transition. This activity recovered immediately even if CtrA was not present, possibly confining the dephosphorylation/degradation of CtrA and dephosphorylation of CpdR in a very limited time period, just enough to free the origin of replication.

Conclusions and perspectives

A step forward in the comprehension of GcrA role and activity in regulating the cell cycle of *C. crescentus* has been achieved with this thesis. For the first time GcrA has been characterized by combining structural biology, biochemistry and cell biology. We found that GcrA is a mainly disordered transcription factor able to bind specific promoter regions of the chromosome depending on their methylation states (Fioravanti *et al*., 2013). A novel functional interaction between the enigmatic cell cycle regulator GcrA and the N6-adenosine methyltransferase CcrM was reported. We used a combination of ChIP-Seq (chromatin-immunoprecipitation-deep sequencing), biochemical and biophysical experimentation, and genetics to show that GcrA is a dimeric DNA-binding protein that preferentially targets promoters harbouring CcrM methylation sites. We showed that N6-methyl-adenosine promoter marks recruit GcrA *in vitro* and *in vivo*. Interestingly, depending on the target DNA region, a differential affinity of GcrA for different methylation states of the DNA sequences (hemi-methylated in + or - strand or fully-methylated) has been observed. Moreover, we found that, in the presence of a methylated target, GcrA recruits the RNA polymerase to the promoter, consistent with its role in transcriptional activation. In the case of *ctrA*P1, this differential affinity of GcrA for different methylation state of DNA has been confirmed also by DNAse I footprinting. In this experiment GcrA protects specific regions of the probe in a methylation-dependent manner, giving rise to a larger region of protection spanning the -35 to the -10 of the *ctrA*P1 promoter with the fully-methylated (i.e. on both strands) probe. By contrast, the protection of the hemi-methylated (on the plus strand) probe was confined to a region adjacent to the methylation site itself. We conclude that methylation induces different oligomerization or conformational states in strand-specific manner. Based on these results we wanted to see if this behaviour could affect transcription; thus an *in vitro* transcriptional assay of *ctrA*P1 was set up. GcrA was able to enhance an asymmetrical transcription *in vitro* in the presence of different hemi-methylation forms of the *ctrA*P1 promoter, while it apparently acted as a repressor of transcription in the case of a fully methylated template. This behaviour of GcrA may play a role as an additional regulatory mechanism in the predivisional cells where a single fully-methylated chromosome is replicated

in two different hemi-methylated chromosomes located each towards the two poles. Moreover our *in vitro* evidences suggest that besides activating gene expression GcrA could also act as methylation dependent repressor, as for *ctrA*P1 when the chromosome is fully-methylated.

Since methylation-dependent DNA binding is also observed with GcrA orthologs from other *Alphaproteobacteria*, we can conclude that GcrA is the founding member of a new and conserved class of transcriptional regulators that function as molecular effectors of a methylation dependent (non-heritable) epigenetic switch that regulates gene expression during the cell cycle. It will be worth investigating in the future the functional role of GcrA in other model systems such as *S. meliloti* or *B. abortus*, possibly in the context of the infection process.

In this thesis we also discovered another interacting protein of GcrA that was identified in co-immunoprecipitation experiments and named GipX. This protein, essential and cell cycle regulated (in phase with GcrA expression), was studied at the structural and functional level. GipX structure revealed a similarity with aspartate aminotransferase enzymes involved in the biosynthesis of the cell wall. Interestingly, the major difference found in GipX structure from members of this family of enzymes from organisms that do not possess GcrA, correspond to inserted regions exposed on the surface of the protein, which may be involved in recognition an interaction with partners such as GcrA. The interaction of GipX with GcrA has been confirmed also *in vitro*; performing EMSA assays with GcrA and GipX together, we observed the capability of GipX to remove GcrA from the binding to the DNA. However the biological meaning of this interaction is still missing. In the future the functional characterization of mutants of *gipX* combined with GcrA Chip-Seq analysis in GipX loss of function and overexpression strains, should clarify the reality and possibly the role of this interaction.

One of the goals of this thesis was the study on the CtrA phosphorylation cascade, composed by CckA and ChpT; two different approaches has been used, a structural one and a biochemistry/microscopy one. At the structural level, due to the known instability of the protein, we could not obtain new structural information about CtrA; however an optimized protocol of purification was set up for biochemical assays. ChpT crystallization was instead successful, allowing us to solve the structure of this protein. ChpT resulted to be a homodimer that adopts the domain architecture of the intracellular part of class I histidine kinases and that

cannot auto-phosphorylate itself, because it is missing of the ATP binding pocket typical in HK (Fioravanti *et al*., 2012).

Finally in order to study *in vitro* and *in vivo* the phosphorylation cascade CckA-ChpT-CtrA we developed a tool based on FRET able to detect phosphorylated CtrA levels. The FRET-based sensor consisted in a CtrA-CFP and CtrA-YFP pair in which only the receiver domain represents CtrA. By reconstructing *in vitro* the entire phosphorylation cascade we transferred the phosphate to the sensor showing that the two parts can dimerize and produce a FRET signal only when phosphorylated. Such activity was also confirmed *in vivo*, in *C. crescentus* cells. Expressing our sensor in a synchronized population of cells allowed us to measure this event of phosphorylation throughout the cell cycle. These latter results of my thesis represent, in my opinion, a very promising research that may be able to study and understand the dynamics of phosphorylated CtrA in time and space, but also the unknown extracellular signals responsible of the activation/deactivation of the cascade. Moreover this FRET-based biosensor approach can be extended to all response regulators creating a map of phosphorylation levels of each response regulator in *C. crescentus*, but also in other bacteria in which two-component systems are present and presumably creating spatial distribution of phosphorylation. As two-component systems are often implicated in pathogenesis such biosensors could be utilize as reporter sensor for new drugs tests able to selectively inactivate phosphorylation cascades.

Materials and Methods

This section is organized in chapters corresponding to sections of the results. However the next two paragraphs are general and applied to all research projects.

Strains and growth conditions

C. crescentus strains were grown in peptone-yeast extract (PYE, rich medium) at 30°C (Ely B., 1991) or 37°C as necessary, tetracycline (1 µg/ml), kanamycin (25 µg/ml), spectinomycin/streptomycin (100-5 µg/ml) 0.1% glucose, 0.1% xylose, 1 mM isopropyl-b-D-thiogalactoside (IPTG), as required. *E. coli* strains were grown at 20°C, 30°C or 37°C in LB broth supplemented with ampicillin (100 µg/ml), as required. Plasmids were transformed into *C. crescentus* and *E. coli* BL21 (DE3) by electroporation.

Initial crystallization test

The commercial kits of crystallization that have been used in this work are listed below:

- **Cryos Suite** (QIAGEN) contains 96 defined chemicals solutions (see manual of the kit) at high concentrations that allow evaluating component's effects on protein solubility.
- **The Pact Suite** (QUIAGEN) also provides an easy and fast screening but using different 96 chemical solutions (see manual of the kit) with different combinations of polyethylene glycol and ions, in order to test the effect of anions and cations and different pH effects on protein stability.
- **The pH Clear I and II kits** (QIAGEN) allow an easy analysis of the effect of precipitant, concentration and especially a wide range of pH (from 4 to 9) (see manual of the kits).

GcrA is a CcrM methylation–dependent transcription factor controlling cell cycle

Cloning *gcrA*s from *C. crescentus*, *S. meliloti* and *B. abortus*

DNA fragments from *C. crescentus*, *S. meliloti* and *B. abortus* were amplified by PCR using cell lysates or genomic DNA for *Brucella* using Pfu-Turbo (Life Technologies, www.lifetechnologies.com/) following a protocol as recommended by the manufacturer. Plasmids and strains are listed in Table 1.

Table 1. Plasmids and strains

Strains				
	Name	**Organism or plasmid**	**Description**	**Source**
	NA1000	*Caulobacter crescentus*	Reference strain	/
	Rm1021	*Sinorhizobium meliloti*	Reference strain	/
	2308	*Brucella melitensis* biovar *abortus*	Reference strain	Xavier de Bolle
	CB15N	*Caulobacter crescentus*	Reference strain	/
	gcrAts	*Caulobacter crescentus*	GcrA temperature (37) sensitive (mutation T10P), grow at 30C	Lucy Shapiro
	EB510	*Caulobacter crescentus*	CB15N + pMR20 (TetR)	This study
	EB517	*Caulobacter crescentus*	gcrAts + pMR20 (TetR)	This study
	EB514	*Caulobacter crescentus*	CB15N + pMR20-GcrA(S. meliloti) (TetR)	This study
	EB519	*Caulobacter crescentus*	gcrAts + pMR20-GcrA(S. meliloti) (TetR)	This study
	EB516	*Caulobacter crescentus*	CB15N + pMR20-GcrA(B. abortus) (TetR)	This study
	EB521	*Caulobacter crescentus*	gcrAts + pMR20-GcrA(B. abortus) (TetR)	This study
	EB516	*Caulobacter crescentus*	CB15N + pMR20-GcrA(C. crescentus) (TetR)	This study
	EB523	*Caulobacter crescentus*	gcrAts + pMR20-GcrA(C. crescentus) (TetR)	This study
	BL21(D3E)	*Escherichia coli*	Expression strain (induction by IPTG)	/
	UG2212	*Caulobacter crescentus*	CB15N Δ*ccrM*::Ω(SpecR), transduced from LS2144	This study
	LS3707	*Caulobacter crescentus*	CB15N Δ*gcrA*::Ω(SpecR) P_{xyl}-*gcrA* (KanR)	Holtzendorff *et al*., 2004
	LS2144	*Caulobacter crescentus*	CB15N Δ*ccrM*::Ω(SpecR) P_{xyl}-*ccrM* (TetR)	Stephens *et al*., 1996
Plasmids				
	EB343	pMR20 (TetR)	Low copy vector tetR	R. Roberts
	EB494	pMR20-Pxyl-GcrA(S. mel) (TetR)	Low copy vector tetR expressing *S. meliloti gcrA* by a xylose inducible promoter	This study
	EB498	pMR20-Pxyl-GcrA(B. abor) (TetR)	Low copy vector tetR expressing *B. abortus gcrA* by a xylose inducible promoter	This study
	EB502	pMR20-Pxyl-GcrA(C. cres) (TetR)	Low copy vector tetR expressing *C. crescentus gcrA* by a xylose inducible promoter	This study
	EB335	pET-His6-GcrA(Cc)	*E. coli* IPTG-inducible vector expressing Cc *gcrA*	This study

EB488	pET-His6-GcrA(Sm)	*E. coli* IPTG-inducible vector expressing Sm *gcrA*	This study
EB490	pET-His6-GcrA(Ba)	*E. coli* IPTG-inducible vector expressing Ba *gcrA*	This study

Primers are listed in the table 2. PCR products were then transferred in pENTR by Directional TOPO Cloning (Life technologies, www.lifetechnologies.com/), sequence verified and then transferred in pET derivatives His_6-tagged destination vectors for *E. coli* BL21 expression, or pMR20 destination vector for xylose inducible expression in *C. crescentus* strains (Skerker *et al*., 2005).

Table 2. Primers and probe

Primers for GcrAs cloning:	
***S. meliloti* Rm1021 (SMc02139)**	
pSMc02139-CACC- fw	CACCATGAACTGGACTGACGAGCG
pSMc02139-rev	AGCGGAATGAGCAAGGCG
***B. melitensis biovar abortus* (BAB1_0329)**	
pBAB1_0329- CACC- fw	CACCATGAACTGGACAGACGAGCG
pBAB1_0329- rev	GGGGACGCTTCCTGAATTCA
***C. crescentus* CB15N (CC2245)**	
pCC2245-NdeI-fw	CACCATGAGCTGGACCGACGAA
pCC2245-rev2	GTCATCCCGCGCTTTATGC
EMSA probes (70 bp) 5'- 3:	
CCNA_0697:	
ACGTTTCCCCGAACAGGGGCGAAACGAATCGGGACCGAATCAGCGACGTTCGCCGATTCAGTATTTGTTC	
***ctrA* promoter:**	
AGACTGGTTAATGGTGAATGTTTCCCGTCGGAGGAATGGTTAATCTGATTTGCGAATCGGGTGCAAGCCG	
***mipZ* promoter:**	
TGGCTCGGATCCTTCTGCGTCGCGACTCAGCGACTCTTAATCGAAGGTTAACACGATGTTTCCCGCCCCC	
CCNA_0278* and *CCNA_0279:	
CGCGCGCTGGCGTCGGCCGGCGCAGGCTGCGGCTCATGACCACGCCAAGCCGTCGCATCCTGATCTTGGT	
CCNA_1926 and CCNA_1927:	
TTCTGAAGATTTCGCTAGCCTTCCCAAGGGGCAAAGGCGCCTAGACTCGCCCCCAACGAACACAGGGAGG	
DNase I foot printing and RNA transcription assay region (*ctrAP1* promoter), 120 bp, 5'- 3:	
cggtgaaacccttcggccactttgccggagagttaatttaagactggttaatggtgaatgtttcccgtcggaggaatggttaatctgatttgcgAatcgggtgcaagccg cgtcggagcc	

Purification of GcrAs from *C. crescentus*, *S. meliloti* and *B. abortus*

The full-length DNA fragment of *gcrA* (and *gcrA*s from S*. meliloti* and *B. abortus*) was cloned into a pET15 derivative, the pML375 vector (Skerker *et al.,* 2005), obtaining a recombinant protein with a His_6-Thrombin cleavage site tag in N-terminus of the protein. Overexpression of GcrA was induced in E. coli BL21 (DE3) at 600 nm Optical Density (OD_{600}) of 0.6-0.8 by 500 µM IPTG over night (O/N) at 20°C. The cells were harvested by centrifugation and then resuspended in lysis buffer (PBS 1X pH 7.5, 0.2 M NaCl, 1 mM DTT, 0.1% Triton, supplemented with Complete Protease Inhibitor Cocktail (Roche, http://www.roche.com/) and DNase I (Euromedex, www.euromedex.com/) and lysed by Emulsiflex (Avestin, www.avestin.com/) at 10° C.

From the supernatant, GcrA was purified in two steps of purification, first, using Ni^{2+}-nitrilotriacetate affinity resin (Ni-NTA) (Qiagen, www.qiagen.com/) equilibrated with lysis buffer and eluted by PBS 1X (pH 7.5), 0.5 M Imidazole, followed by Gel filtration step using HiLoad 16/60 Superdex 75 prep grade (GE Healthcare, www.gehealthcare.com/) equilibrated with running buffer (0.1 M Tris pH 8.5, 0.2M NaCl, 5% Glycerol) optimized after DLS (See below the experimental procedure).

DLS measurements by the Zetasizer nano ZS (Malvern, www.malvern.com/) with an accuracy of 0.1°C were performed immediately after both the size exclusion step and the concentration step in order to find the best buffer composition. DLS was employed to estimate the thermo-stability of protein samples in different buffer solutions from to 15°C to 64°C, one degree steps. DLS was also used for the estimation of monodispersity of GcrA preparation. SDS-page gels showing the production and/or purification of the GcrAs preparation are reported in the result section (see figure 11 and 22).

SAXS analysis

SAXS experiments were conducted on the SWING beamline at the SOLEIL synchrotron. The Aviex charge-coupled device detector was positioned at a distance of 1.8 m. Data were collected in the q-range 0.008–0.3 Å−1 (λ = 1.033 Å) ($q = 4\pi\sin\theta\ \lambda^{-1}$, where 2θ is the scattering angle) in a fixed-temperature (15°C) quartz capillary (diameter of 1.5 mm and a wall thickness of 10 µm.

GcrA (9.9 mg/ml) was injected onto a size-exclusion column (SEC-3, 150 Å, Agilent), using an Agilent HPLC system, and eluted (0.1 M TRIS pH 8.5, 150 mM NaCl and 10% glycerol) directly into the SAXS flow-through capillary cell at a flow rate of 0.15 ml min^{-1}. SAXS data were collected continuously, with frame duration of 1.5 s and a dead time between frames of 0.5 s. Selected frames corresponding to the main elution peak were averaged. Data reduction to absolute units, frame averaging and subtraction were done using FOXTROT (David and Pérez, 2009). Data are in Table S1 of Fioravanti *et al.*, 2013.

All subsequent data processing, analysis and modeling steps were carried out with PRIMUS and other programs of the ATSAS suite (EMBL Hamburg, Germany).

The experimental SAXS data for all samples were linear in a Guinier plot of the low q region, indicating that the proteins did not undergo aggregation. The radius of gyration RG was derived by the Guinier approximation I(q) = I(0) exp(-q2RG2/3) for qRG < 1.0 using the software PRIMUS (Konarev *et al*., 2003). Interference-free SAXS profiles were estimated by extrapolating the measured scattering curves to infinite dilution. The software GNOM (Svergun, 1992) was used to compute the pair-distance distribution functions, P(r). This approach also features the maximum dimension of the macromolecule, Dmax. Normalized Kratky plot (ie (qRg)2I(q)/I(0) as a function of qRG) was used to assess the conformational behavior of the polypeptide chain. In this representation, the scattering curve of a globular protein yields a characteristic bell-shape profile (Kratky and Porod, 1949), whereas the scattering curve of a disordered/non globular protein exhibits a plateau at large q values. For all constructs, the data measured at different protein concentrations were perfectly superimposable at large q (q>0.15Å), indicating that the buffer subtraction was correct, and therefore that the profiles of the Kratky plot is significant.

Limited proteolysis

Purified His_6-GcrA was digested with proteases Thermolysin (Sigma-Aldrich, www.sigmaaldrich.com/) and Endoproteinase GluC V8 (New England Biolabs, www.neb.com/) (25°C with 0.5 mg/ml GcrA in 20 mM TRIS pH 8, 150 mM NaCl for digestion with Thermolysin and 20 mM Tris (pH 7.6), 1 mM $CaCl_2$ in case of digestion with V8). The protease/substrate ratio was 1:100 (w/w) in each case. At different time intervals, aliquots of the proteolysis reactions

were stopped with loading buffer. The protein samples were then analyzed by SDS-PAGE and the fragments analyzed by Trypsin digestion and mass spectrometry. Proteolysis control of His_6-ChpT (Fioravanti *et al*., 2012) in presence of differentially methylated DNAs was performed as described above.

ChIP-Seq protocol and analysis

Illumina Genome Analyzer IIx or HiSeq 2000 runs of barcoded ChIP-Seq libraries yielded several million reads that were mapped to *C. crescentus* NA1000 (NC_011916) using Blast (data available for download at http://www.iri.cnrs.fr/spip.php?rubrique169&lang=en).
Alignments at 100% identity with the genome spanning the entire length of the read without gaps were selected to build a genome wide coverage profile; only one alignment per reads was considered to avoid artefacts concerning repeated genome segments. The coverage profile obtained was loaded in Matlab(R) and the mspeaks function was used in order to identify peaks i.e. genome regions with high coverage in the experiment. mspeaks is a function that converts raw peak data to a peak list (centroided data) by first smoothing the signal using undecimated wavelet transform with Daubechies coefficients, assigns peak locations, estimates noise and finally eliminates peaks that do not satisfy specified criteria. We used the following parameters: "minimum height" (coverage) of the peak 600 (this was adjusted to obtain a manageable number of peaks, since our analysis does not require to identify all binding locations); "over segmentation" was set empirically to 300 to avoid the identification of multiple peaks actually corresponding to a single bound region. Mspeaks with these parameters returned 50 peaks with height ranging from about 1600 down to a minimum of 600 (as specified by the minimum height parameter); width of the peaks identified by the algorithm ranged from 400 to 1700 nucleotides. The identification of GcrA controlled promoters was accomplished by extracting from the genome-wide coverage profile the regions from 300 nucleotide upstream to 100 nucleotide downstream the first codon of each gene. The total coverage of a gene was defined as the sum of all sequenced nucleotides in that region; after checking for normality, we transformed the total coverage into a Z-score and we retained only genes with Z-score>2 (where $p(Z>2)\approx0.02$), ending with a list of 161 genes.

To compare different ChIP-Seq experiments, we normalized the coverage at each nucleotide by the total coverage of the genome. Then the log2 ratio among different ChiP-seq dataset was calculated (i.e. wild type vs mutant) and Z-score transformed to highlight differences in binding in different conditions (i.e. presence or absence of methylation).

DNA binding in vitro assays

EMSAs were performed using the LightShift Chemiluminescent EMSA Kit (Thermo Scientific). Briefly, different versions and concentration of GcrA were incubated at room temperature in 10 mM Tris pH 7.5, 100 mM KCl, 0.5 mM DTT, 50 ng/µl poly(dI-dC), and 0.05% Nonidet P-40 binding buffer with 5 fmol of a biotin-labeled DNA fragment (1.25µM) for 25 minutes.

After 25 min incubation at room temperature, samples were resolved by a 10% non-denaturing polyacrylamide gel prepared in TBE buffer (450 mM Tris, 450 mM boric acid and 0.01 mM EDTA). The samples were blotted onto a 0.45-µm Biodyne B nylon membrane (Thermo Scientific, www.piercenet.com/) at constant current of 300 mA for 45 min at 4°C, and then cross-linked to the membrane using a 312nm UV Transilluminator (Uvitec, www.uvitec.com.) for 10 min. Membranes were processed as recommended in the Chemiluminescent Nucleic Acid Detection Module Kit (Thermo Scientific, www.piercenet.com/).

Competitive EMSAs were performed as described above, adding a preincubation step of 20 min at room temperature of GcrA and competitor DNAs before the usual 25 min GcrA/biotin-labeled DNA fragment incubation.

EMSA in presence of RNA polymerase core enzyme (Epicentre, www.epibio.com/) was performed by pre-incubating GcrA in presence of RNAP for 20 min at room temperature before the usual incubation with biotin-labeled DNA.

For detecting the binding region of GcrA, a 120bp probe from *ctrA*P1 (see Table 2) was synthesized and labeled with Fam-6 (Eurogentec, www.eurogentec.com/). Single stranded probes containing m6A were also synthesized, which were later assembled into double stranded probes in different combinations. Five fmoles of probes were incubated at room temperature with increasing concentrations of purified GcrA as done with EMSA for 30 min. The samples were digested with approximately 7U of DNaseI (Euromedex, www.euromedex.com/) at room

temp for 3 min. DNaseI was inactivated by adding 0.1 M EDTA followed by incubation at 750C for 10 min. The digested fragments were eluted using the mini-elute columns (Qiagen, www.qiagen.com/). The samples were run in a 3130 Genetic Analyzer (Life Technologies) as described before (Yindeeyoungyeon *et al*., 2000), analyzed by GelQuest (SequentiX, www.sequentix.de/). Sequencing reactions were also performed using Thermo Sequenase Dye Primer Manual Cycle Sequencing Kit (Affymetrix, www.affymetrix.com/) using the probe region as a template and a sequencing primer labeled with FAM at the 5 primes.

Study of C. crescentus GcrA interaction with RNAP

Affinity chromatography for RNA Polymerase detection

Nickel columns loaded by His_6-GcrA were also used for affinity chromatography showed in figure 18. An 1 ml HisPur-Ni-NTA Chromatography Cartridge (Qiagen, www.qiagen.com/), equilibrated with running buffer (0.1 M Tris pH 8.5, 0.15 M NaCl, 5% Glycerol) was loaded at 15°C with 23 mg of histidine-tagged *C. crescentus* GcrA (His_6-GcrA) that was prepared as previously described, and washed with 15 volumes of running buffer. Meanwhile, 2 liters of *C. crescentus* cells (OD_{600} of 0.6) were harvested by centrifugation (5000 rpm, 20 min, 4°C) and resuspended in 30 ml of lysis buffer (0.1 M Tris pH 8.5, 0.15M NaCl, 1 mM DTT, 0.1% Triton, supplemented with Complete Protease Inhibitor Cocktail (Roche, www.roche.com/) and DNase I (Euromedex, www.euromedex.com/)) and lysed by Emulsiflex (Avestin, www.avestin.com/) at 10°C. The lysate was then centrifuged at 9500 rpm, 20 min, 4°C and the supernatant obtained was applied to the column. The column was eluted with running buffer NaCl gradient from 0.15 M and 1 M of NaCl. A last wash was done in presence of Imidazole (0,1 M Tris pH 8,5, 0,15 M NaCl, 5% Glycerol, 0.5 M Imidazole) in order to remove the His6-GcrA and proteins still bound at the column.

The negative control to this experiment was performed doing the same procedure with a 1 ml HisPur Ni-NTA Chromatography Cartridge without His_6-GcrA.

The eluted samples were run in SDS-PAGE gel and transferred to nitrocellulose membrane. The membrane was blocked with PBS, 0.1% NP-40 and 3% dry milk for 1 hour at room temp. The

membrane was incubated with anti-RNA polymeraseβ-subunit antibody (Thermo Scientific, www.pierce-antibodies.com/) against the β-subunit (1:5000) at 40°C overnight. Each membrane was washed 5 times each for 10 min with PBS containing 0.1% NP-40, followed by incubation with the secondary antibody (1:50,000) for 45 min. The membrane was developed following the procedure described under immunoblot section.

Immunoblots

PVDF (polyvinylidenfluoride) membranes (Merck-Millipore, www.merckmillipore.com) were blocked with PBS, 0.05% tween 20 and 5% dry milk for 1h and then incubated for 1h with the primary antibodies diluted in PBS, 0.05% tween 20, 5% dry milk. The membranes were washed 4 times for 5 min in PBS and incubated 1h with the specific secondary antibody diluted in PBS, 0.05% tween 20 and 5% dry milk. The membranes were finally washed again 4 times for 5 min in PBS and revealed with Immobilon Western Blotting Chemoluminescence HRP substrate (Merck Millipore, www.merckmillipore.com/). The antiserum was used at the following dilutions: anti-GcrA (1:10,000). Anti-RNA polymerase beta antibodies (Abcam, www.abcam.com/) were used using the protocol described in "Affinity chromatography for RNA Polymerase detection".

Pull down/ Co-Immunoprecipitation of FLAG tagged protein

A *gcrA*ts allele (GcrA is inactivated at 37°C) was transformed with a pRK derivative low-copy plasmid containing a copy of GcrA fused with a N-terminal M2 flag inducible by xylose (EB690). This strain, containing FLAG GcrA (EB690), was grow overnight to an OD_{600} ~0.8, in a 50 to 100 ml volume. The cells were harvested by centrifugation for 10 min at 9000 g and resuspended in 1X TBS, to be centrifuged again. The strain with M2-GcrA was compared with the same genetic background and plasmid without GcrA (EB689). The pellets were then stored at -20°C for 30 min. All the following steps were done on ice. Pellets were resuspended in 1 ml of cell lysis buffer (50 mM Tris-Cl, pH 7.5, 150 mM NaCl, 1 mM EDTA, pH 8.0, 1% Triton X-100) by thorough vortexing. Lysozyme was added (0.1 mg/ml final conc.) and the samples passed through 18 Gauge (Ga) and 27 Ga needles to facilitate cell lysis and then kept on ice for 30 min. DNAse I (10

μg/ml) and $MgCl_2$ (5 mM final concentration) were added. Samples were centrifuged at 12000 g for 15 min to remove the cell debris. For pre-clearing of the samples, 50 μl of protein A sepharose (CL-4B GE Healthcare) was added to the supernatant and incubated at 40°C in a rotary shaker for 30 min. Samples were centrifuged for 1 min at 500g and the supernatant was transferred into a new Eppendorf tube leaving the sepharose beads. 15 μl of anti-FLAG resin (Sigma) was added to the pre-cleared cell lysate and incubated for 2 hours at 40°C in a rotary shaker. Anti-FLAG resin was prepared following the manufacturer's instructions. The cell lysate and the resin mix were centrifuged at 5000g for 1 min at 40°C; supernatant was removed leaving the resin. The resin was washed 3 times with 500 μl of cell suspension buffer (50 mM Tris-Cl, pH 7.5, 150 mM NaCl, 1 mM EDTA, pH 8.0) by centrifuging at 5000g for 30 sec each. Immunoprecipitated proteins were eluted from the resin by incubating it with 30 μl of FLAG peptide (100 μg/ml in 1X TBS) at 40°C for 1 hour. After centrifugation at 6000 g for 1 min supernatants were collected in a new Eppendorf tube. Samples were run in SDS-PAGE gel, and protein bands were selected and analyzed by mass spectroscopy.

In vitro RNA transcription

The *in vitro* transcription assay was performed to detect the effects of GcrA and CcrM methylation on the transcription of *ctrAP1* promoter. The *ctrAP1* region was synthesized as single stranded forms containing methylated m6A sites, which were later assembled into double stranded forms in combinations such as hemi-methylation in the positive and negative strands and full methylated forms. These different forms were used as template in the *in vitro* transcription study. RNA polymerase was prepared from the *C. crescentus* culture by the TAP tagged method (Rigaut *et al*., 1999). The preparation was checked in a SDS-PAGE gel for the presence of the major subunits and stored in a buffer consisting of 10 mM Tris-Hcl pH 7.9, 500 mM NaCl, 50% Glycerol, 0.1 mM EDTA and 0.1 mM DTT.

Approximately 250 ng of different methylated templates were preincubated with increasing concentrations of purified GcrA (0.125- 0.5 μM) at room temperature for 10 min in a reaction buffer containing 66 mM Tris-acetate (pH 7.9), 40 mM potassium acetate, 20 mM magnesium acetate, 5 mM dithiothreitol (DTT), and 100 μg/ml bovine serum albumin (BSA). After

incubation, 1 µl of *C. crescentus* RNA polymerase (from a preparation of 0.75 mg/ml) was added, and incubation was continued for 5 min at room temperature. Transcription was initiated by adding (final concentration) 1 mM each of ATP, CTP and GTP, and 0.25 mM UTP along with 0.75 mM biotin labeled UTP (Epicentre) to the reaction mixture. Heparin (10 µg) was added to inhibit the re-initiation of transcription. The reaction volume is 10 µl for 30 min at 37°C. Following the transcription reaction the templates were degraded using 2 U DNase I (Epicentre) for 10 min at 37°C. Equal volume of 2X RNA loading dye (95% formamide, 0.5 mM EDTA, 0.025% SDS, 0.025% bromophenol blue & 0.025% xylene cyanoll) was added to the reaction followed by denaturing the samples by heating at 65°C for 3 min. Samples were resolved in a 8% denaturing polyacrylamide gel (8M Urea) in 0.5X Tris-borate-EDTA (TBE) buffer running at 200 V for 75 min. The gel was washed twice, each for 5 min, in 0.5X TBE with shaking to remove urea. The transcripts from the gel were transferred to a 0.45 µm Biodyne B nylon membrane (Thermo Scientific) at a constant voltage of 20 V for 45 min at 40°C. The membrane was cross linked in a UV crosslinker using a setting of 0.120 Joules. Membranes were processed as recommended in the Chemiluminescent Nucleic Acid Detection Module Kit (Thermo Scientific).

Study of the GcrA-Interacting Protein X (GipX)

Expression and purification of His_6-GipX

The full-length DNA fragment of *gipX*, previously annotated CC3611, was amplified using the primers pCC3611-CACC-fw (5'-caccATGAGCATGCCCTTCATCGACC-3) and pCC3611-rev (5-TCAGCCGCCGAAGCTGCGGATCG-3) cloned into pENTR/D (Life Technologies, Carlsbad, California, USA) using Gateway technology, sequence-verified and transferred by LR clonase II reaction into pET300/NT-DEST vector (Life Technologies), producing a recombinant IPTG-inducible gene that is able to express GipX fused to an N-terminal His_6 tag (MHHHHHHITSLYKKAG–). Overexpression of His_6-GipX (42.9 kDa) was induced in E.coli BL21 (DE3) cells at an OD_{600} nm of 0.6 in presence of 500 µM IPTG and cell growth was continued for 3h at 30°C with shaking (215 rev min^{-1}). The cells were harvested by centrifugation for 20 min at 500 rev min^{-1} and 277 K, resuspended in

lysis buffer [PBS 1x pH 7.4, 10 mM imidazole pH 7.4, 1 mM DTT, 0.1% Triton X-100, Complete Inhibitor Cocktail (Roche, Basel, Switzerland) and DNase I (Euromedex, Sauffelweyersheim, France)] and lysed using an Emulsiflex homogenizer (Avestin, Ottawa, Ontario, Canada) at 283 K. The supernatant containing His_6-GipX was purified using Ni^{2+} –nitrilotriacetate (Ni–NTA) affinity resin (Qiagen, Hilden, Germany) equilibrated with lysis buffer and was eluted with 500 mM imidazole (PBS 1x pH 7.4, 500 mM imidazole). A second step of purification was performed by Ion Exchange chromatographic using a HiTrap Q HP column (GE Healthcare, Waukesha, Wisconsin, USA) equilibrated with running buffer [20 mM Tris pH 8]. Following the loading of His_6-GipX fraction obtained with the first step of purification, elution was performed using a linear gradient (0–100%) of 20 mM Tris pH8, 2M NaCl. Finally the protein was desalted using PD-10 desalting column (GE Healthcare, Waukesha, Wisconsin, USA) with the storage buffer [100 mM Tris pH8, 150 mM NaCl, 1 mM DTT, Glycerol 5%]. A thermal shift assay (TSA) was performed to optimize the buffer composition as described previously (Fioravanti et *al*., 2012). An SDS–PAGE of His_6-GipX purification is shown in figure 27.

Crystallization and data collection GipX

Initial crystallization screening of His_6-GipX (57.58 µM and 76.22 µM) were performed by the sitting-drop vapour-diffusion method using the Cryos Suite, pH clear I and II commercial kits (Qiagen, Hilden, Germany) for a total of 288 condition tested. The best crystallization hit was obtained in condition No. 86 of Cryo Suite Kit, consisting of 0.17 M Ammonium acetate, 0.085 M Sodium acetate pH 4.6, 25.5 %(w/v) PEG 4000 and 15 %(v/v) Glycerol. These conditions were subsequently refined using the hanging-drop vapour-diffusion method at 20°C in 24-well plates (Hampton Research, Aliso Viejo, California, USA). Drops were prepared by mixing equal volumes (1 µl each) of protein solution and reservoir solution. The crystals used for data collection were obtained in 0.6 ml precipitant solution consisting of 0.085 M Sodium acetate pH 4.6, 36 %(w/v) PEG 4000 and 15 %(v/v) Glycerol for a concentration of His_6-GipX of 76.22 µM. The crystals were then picked up in a nylon loop and flash-cooled.

Data collection and processing

Data sets were collected at -173 °C on the ID23 Beamline at the European Synchrotron Radiation Facility (Grenoble, France). The data were processed with XDS (Kabsch *et al*., 2010). Crystals diffract to 2.1 Å resolutions and belong to the monoclinic space group P21 with the following unit cell parameters: a = 47.37, b = 89.85, c = 80.90; β= 98.1. Data-collection statistics for data set are presented in Table 3.

Structure determination and refinement

The structure of His_6- GipX was solved by molecular replacement using MOLREP v.9.2 from the CCP4 suite v.6.1.13 (Winn *et al*., 2011). The search model was based on the *P. aeruginosa* WbpE structure (PDB entry 3Nu7; Larkin *et al*., 2010), which shares 41% sequence identity with GipX and from which, chains different form GipX, were replaced by alanine using PDBSET (Winn *et al*., 2011).

Automated model building was performed using ARP/wARP v.7.1 (Langer *et al*., 2008) coupled to the REFMAC5 (Murshudov *et al*., 2011). The two molecules in the asymmetric unit were treated independently during refinement. Rounds of model manipulation were made using Coot (Emsley *et al*., 2010) interspersed with refinement using BUSTER (Bricogne *et al*., 2011.) was used to complete the protein model. We are still working on the refinement of the model, but at this stage we can see that the loop between α-helix 8 and α-helix 9 in monomers A and B (see figure 30) is not well defined, and residues G222–D235 are missing in the electron-density map, probably due to the high flexibility of these regions. Coordinates will be deposited at the protein data bank as soon as possible.

Table 3. Data-collection and preliminary refinement statistics for His_6-GipX. Values in parentheses are for the outermost resolution shell.

Data collection	
Unit-cell parameters (Å ;°)	a = 47.37, b = 89.85, c = 80.90; β= 98.1
Space group	P21
Beamline	ID23 ,ESFR
Wavelength (Å)	0.98400
Temperature (K)	100
Detector	PILATUS 6M-F
Resolution (Å)	45,7-2.1 (2.2–2.1)
No. of unique reflections	37374 (4855)
Completeness (%)	99.6 (99.8)
Multiplicity	7.1 (7.4)
R_{merge}† (%)	18.5 (172%)
R_{meas}‡ (%)	20 (185)
$[I/\sigma(I)]$	8.1 (1.62)
Refinement	
R_{work}§ (%)	22.8
R_{free} (%)	27.0
Mean B (Å ^{2})	47.9
No. of non-H atoms	
Protein	5643
Water	137
R.m.s.d.	
Bond lengths (Å)	0.010
Bond angles (°)	1.19

Values in parentheses are for the last shell. † $R_{merge} = \sum_{hkl} \sum_i |I_i(hkl) - \langle I(hkl)\rangle| / \sum_{hkl} \sum_i I_i(hkl)$, where $I_i(hkl)$ is the observed Intensity and $\langle I(hkl)\rangle$ is the average intensity for multiple measurements. ‡ $R_{meas} = \sum_{hkl}((n(hkl)/(n(hkl) - 1))^{1/2} \sum_{hkl} \sum_i |I_i(hkl) - \langle I(hkl)\rangle| / \sum_{hkl} \sum_i I_i(hkl)$, where n is the number of times a given reflection has been observed. § $R_{work} = \sum_{hkl} ||F_{obs}|-|F_{calc}|| / \sum_{hkl} |F_{obs}|$, where F_{obs} is the observed structure factor and F_{calc} is the calculated structure factor. R_{free} is the same as R_{work}, except calculated using 5% of the data that were not included in any refinement calculations.

Cocrystallization GcrA/ GipX

Initial crystallization trials of His_6-GipX and His_6-GcrA complex (50 µM each) were performed by the sitting-drop vapor-diffusion method using the Cryos Suite, pH clear I and II commercial kits (Qiagen, Hilden, Germany) for a total of 288 condition tested. Unique crystal were obtained in condition No. 74 of Cryo Suite Kit, consisting of 0.19 M Calcium chloride, 0.095 M Hepes pH 7.5, 26.6 %(w/v) PEG 400 and 5 %(v/v) Glycerol at 293K. These conditions were subsequently refined using the hanging-drop vapor-diffusion method at 20°C in 24-well plates (Hampton Research, Aliso Viejo, California, USA). The crystals were then picked up in a nylon loop and flash-cooled

and used for X-ray diffraction at the IRI institute. As reported in the result, these crystals didn't diffract.

DNA binding in vitro assays GcrA/GipX

EMSAs were performed, as described above, using the LightShift Chemiluminescent EMSA Kit (Thermo Scientific). Briefly, the His_6-GcrA was incubated at room temperature with 1.25 µM of a biotin-labeled DNA fragment for 15 min and then, after the addiction of an increasing concentration of His_6-GipX, other 15 min RT. The experiment was also performed adding first His_6-GipX to the mix containing GcrA and then, after the usual incubation time, the biotinylated probe was added to the sample. Samples were resolved and revealed as reported before.

Structural study of phosphorylation cascade that activates CtrA

- *C. crescentus* CtrA

Full length *ctrA* gene and the mutated version of *ctrA* D51A were amplified using primers as previously described (Biondi *et al*., 2006) and cloned in pENTR/D (Life Technologies, Carlsbad, California, USA) using Gateway technology, sequence-verified and transferred by LR clonase II reaction into pET300/NT-DEST vector (Life Technologies). Clones pET300-NT-ctrA and pET300-NT-ctrAD51A were named EB527 and EB624, respectively. Overexpression of the two His_6-CtrA (27.7 kDa) was induced in *E. coli* BL21 (DE3) cells at an OD_{600} nm = 0.6 in presence of 500 µM for the EB527 and 300 µM in the case of EB624 of IPTG and cells were incubated for 3 hours at 30°C with shaking (210 rpm). Cells were then harvested by centrifugation for 20 min, 5000 rpm at 10°C and then resuspended in Lysis buffer [50 mM NaH_2PO_4, 300 mM NaCl, 10 mM imidazole pH 8, 1 mM DTT, 0.1% Triton X-100, Complete Inhibitor Cocktail (Roche) and DNase I (Euromedex)] and lysed by Emulsiflex homogenizer (Avestin,) at 4°C. The supernatant containing the soluble His_6-CtrA was purified using Ni–NTA affinity resin (Qiagen) equilibrated with lysis buffer and eluted after washing with NPI-500 pH 8 (50 mM NaH_2PO_4, 300 mM NaCl, 500 mM imidazole). A second step of purification was performed by gel filtration using a HiLoad 16/60 Superdex 75

prep-grade column (GE Healthcare) equilibrated with an optimized storage buffer different for the two CtrA [50 mM Tris pH 8, 150 mM NaCl, 1 mM DTT, 10%(w/v) glycerol in the case of EB527 and 50 mM Hepes pH 7,5, 100 mM NaCl, 1 mM DTT, 5%(w/v) glycerol] for the EB624 optimized by TSA (Fioravanti *et al*., 2012). An SDS-page gel showing the production and purification of the two proteins is shown in figure 34.

- ***C. crescentus* ChpT**

Expression and purification of His_6-ChpT

The full-length DNA fragment of *chpT*, annotated CC3470 (Chen *et al*., 2009), was amplified using the primers pCC3470-CACC-fw (5'-CACCTTGACCGAGACCGTCACC-3') and pCC3470-rev (5'-GGTTAAGGAGCGGTTTGCTA-3') cloned into pENTR/D (Life Technologies, Carlsbad, California, USA) using Gateway technology, sequence-verified and transferred by LR clonase II reaction into pET300/NT-DEST vector (Life Technologies), producing a recombinant IPTG-inducible gene that is able to express ChpT fused to an N-terminal His_6 tag (MHHHHHHITSLYKKAG–). Overexpression of His_6-ChpT (25.29 kDa) was induced in *E.coli* BL21 (DE3) cells at an OD_{600} nm of 0.6 by the addition of 100 µM IPTG and cell growth was continued overnight at 30°C with shaking (215 rev min^{-1}). The cells were harvested by centrifugation for 20 min at 500 rev min^{-1} and 4°C, resuspended in lysis buffer [50 mM NaH_2PO_4, 300 mM NaCl, 10 mM imidazole pH 8, 1 mM DTT, 0.1% Triton X-100, Complete Inhibitor Cocktail (Roche, Basel, Switzerland) and DNase I (Euromedex, Sauffelweyersheim, France)] and lysed using an Emulsiflex homogenizer (Avestin, Ottawa, Ontario, Canada) at 10 °C. The supernatant containing His_6-ChpT was purified using Ni–NTA affinity resin (Qiagen, Hilden, Germany) equilibrated with lysis buffer and was eluted with NPI-500 pH 8 (50 mM NaH_2PO_4, 300 mM NaCl, 500 mM imidazole). A second step of purification was performed by gel filtration using a HiLoad 16/60 Superdex 75 prep-grade column (GE Healthcare, Waukesha, Wisconsin, USA) equilibrated with running buffer [20 mM HEPES pH 7.5, 150 mM NaCl, 1 mM DTT, 10%(w/v) glycerol]. An SDS–PAGE of His_6-ChpT purification is shown in 35 A.

A thermal shift assay (TSA) was performed to optimize the buffer composition as described previously (Niesen *et al*., 2007). 24 buffer conditions based on sodium acetate, sodium phosphate, Tris, HEPES, Bicine and potassium phosphate at different concentrations and pH values were assayed (data not shown). His_6-ChpTwas added to a final concentration of 56 mM in a 40 ml total reaction volume containing 5x SYPRO Orange dye and measurements were made using a Mx30005P real-time PCR instrument (Stratagene-Agilent, Santa Clara, California, USA), raising the temperature from 25 to 95 °C in 1 °C intervals. The optimized buffer composition was 20 mM HEPES pH 7.5, 150 mM NaCl, 1 mM DTT, 10 %(w/v) glycerol.

Crystallization of ChpT

Initial crystallization trials of His_6-ChpT (0.5 mM) were performed by the sitting-drop vapour-diffusion method using the Cryos Suite kit (Qiagen, Hilden, Germany). The best crystallization hit was obtained in condition No. 88, consisting of 24%(w/v) polyethylene glycol (PEG) 4000, 0.16 M $MgCl_2$, 0.08 M Tris–HCl pH 8.5, 20%(w/v) glycerol. These conditions were subsequently refined using the hanging-drop vapour-diffusion method at 20°C in 24-well plates (Hampton Research, Aliso Viejo, California, USA). Drops were prepared by mixing equal volumes (1 µl each) of protein solution and reservoir solution. 0.6 ml precipitant solution consisting of 15%(w/v) PEG 4000, 0.16 M$MgCl_2$, 0.08 M Tris–HCl pH 8.5, 10%(w/v) glycerol was pipetted into the reservoir well.

For crystallization trials with putative substrates, His6-ChpT was incubated at 20°C for 30 min in the presence of ATP or ADP (2.5 mM) and crystals were obtained under similar conditions. For experimental phasing, a heavy-atom-derivative crystal was prepared by soaking a crystal for 16 min at 18 °C in the crystallization buffer described above with the PEG 4000 concentration increased to 22%(w/v) in the presence of 100 mM Eu-DO3A (europium chelated to 1,4,7,10-tetraazacyclododecan-1,4,7-triacetic acid) obtained from NatX-ray (Girard *et al*., 2003). For the native crystal, we used the crystallization buffer with PEG 4000 increased to 20%(w/v) as a cryoprotectant. The native and heavy-metal-derivative crystals were picked up in a nylon loop and flash-cooled (Niesen *et al*., 2007).

Data collection and processing

Data sets were collected from native (His_6-ChpT-Native) and europium-derivative (His_6-ChpT-Eu-DO3A) crystals at 100 K on the PROXIMA1 beamline at the SOLEIL synchrotron (Gif-sur-Yvette, France) and BM30 at the European Synchrotron Radiation Facility (Grenoble, France), respectively. The data were processed with XDS (Kabsch, 2010). Data-collection statistics for both data sets are presented in Table 4.

Table 4. Data-collection and refinement statistics.

Data collection	His6-Chpt-Eu-DO3A	His6-ChpT-Native
Cell parameters (Å)	106.4 210.0 94.1	103.5 210.2 93.9
Space group	$C222_1$	$C222_1$
Beamline	ESRF BM30	SOLEIL PROXIMA1
Wavelength (Å)	1.776075	0.980110
Temperature (K)	100	100
Detector	ADSC QUANTUM 315r	PILATUS 6M
Crystal-to-detector distance (mm)	177	320
Rotation range per image (°)	1	0.2
Exposure time per image (s)	60	0.2
Images collected	180	1200
Resolution (Å)	47-2.5 (2.6-2.5)	49–2.2 (2.3-2.2)
Unique reflections	70189 (7765)	52206 (6430)
Crystal mosaicity (°)	0.146	0.085
Completeness (%)	99.6 (98.9)	100 (100)
Redundancy	3.7 (3.6)	8.7 (9.2)
I/σI	9.8 (2.7)	12.5 (2.9)
R_{merge} **† (%)**	10.1 (52.0)	10.7 (81.8)
R_{meas} *** (%)**	11.8 (60.9)	11.4 (86.9)
Overall CC_{anom}	0.35	-
CC_{anom} (cutoff 3.0 Å)	0.45	-
Refinement data		
Rwork **‡(%)**		22.79
Rfree **§(%)**		26.38
Mean *B* ($Å^2$)		61.9
N° of non-H atoms		
Protein		4549
Ion		1
Water		159
R.m.s. deviations		
Bond lengths (Å)		0.024

Bond angles (°)	2.034
Ramachandran statistics	
Favored (%)	97.1
Allowed (%)	2.7
Disallowed (%)	0.2

Values in parentheses are for the last shell. † $R_{merge} = \sum_{hkl} \sum_i |I_i(hkl) - \langle I(hkl) \rangle| / \sum_{hkl} \sum_i I_i(hkl)$, where $I_i(hkl)$ is the observed Intensity and $\langle I(hkl) \rangle$ is the average intensity for multiple measurements. * $R_{meas} = \sum_{hkl}((n(hkl)/(n(hkl) - 1))^{1/2} \sum_{hkl} \sum_i |I_i(hkl) - \langle I(hkl) \rangle| / \sum_{hkl} \sum_i I_i(hkl)$, where n is the number of times a given reflection has been observed. ‡ $R_{work} = \sum_{hkl} ||F_{obs}| - |F_{calc}|| / \sum_{hkl} |F_{obs}|$, where F_{obs} is the observed structure factor and F_{calc} is the calculated structure factor. § R_{free} is the same as R_{work}, except calculated using 5% of the data that were not included in any refinement calculations.

Structure determination and refinement

The structure was solved by the single isomorphous replacement method with anomalous scattering (SIRAS) using SHARP/autostructural SHARP (Vonrhein *et al*., 2007). The resolution cutoff used was 3 Å, as suggested by SHELXC during the autoSHARP procedure. The substructure was subsequently determined by SHELXD based on the anomalous signal (Sheldrick, 2008). 13 Eu-DO3A sites were found in the asymmetric unit, with estimated occupancies of between 20 and 100%. The initial phases were improved using density modification and phase extension by solvent flipping with the program SOLOMON (Abrahams & Leslie, 1996) implemented in autoSHARP. Model building was performed using the program ARP/wARP v.7.1 (Langer *et al.,* 2008) coupled to the CCP4 package (Winn *et al*., 2011), specifically using REFMAC5 (Murshudov *et al*., 2011). The structure was manually completed using the program Coot (Emsley *et al.,* 2010) alternating with cycles of refinement. The final refinement statistics are presented in Table 4.

The study of CckA-ChpT-CtrA phosphorelay: phosphorylation and dimerization

The Histidine Kinase domain and the receiver domain of CckA, were cloned and expressed as described previously (Biondi *et al*., 2006).

The DNA fragment corresponding to the receiver domain of CtrA was amplified using the primers PCTRAREC-HindIII-fw (5'-aagcttATGCGCGTACTGTTGATCGAGGATG-3') and pCTRAREC-KpnI-rev (5'-ggtaccCTTCGAACGACGGACCACCGCGT-3'), cloned in pGEM-T-easy (Promega) and

sequenced verified. The same was done for CFP and YFP using PCFP/YFP-NdeI-fw (5'-catATGGTGAGCAAGGGCGAGGAGCT-3') for both and PCFP-tag-HindIII-rev (5'-aagcttgtggccgccgccgccgccCTTGTACAGCTCGTCCATGCCGA-3') and PYFP-tag-HindIII-rev (5'-aagcttgccgcccgagccgcgcgggacgaggccgccgccCTTGTACAGCTCGTCCATGCCGA-3'), respectively. CtrA receiver domain and CFP or YFP were then fused together by restriction/ligation using the enzymes mentioned in the primers name and ligation into the plasmid pSRK-Km (Khan *et al*., 2008). Chimeric genes CFP or YFP fused with CtrA receiver domain were amplified again from pSRK-Km derivatives using the primer PCFP/YFP-CACC-fw (5caccATGGTGAGCAAGGGCGAGGAGCT-3') and cloned into pENTR/D (Life Technologies, Carlsbad, California, USA) using Gateway technology, sequence-verified and transferred by LR clonase II reaction into pET300/NT-DEST vector (Life Technologies), producing a recombinant IPTG-inducible gene that is able to express CtrA fused to an N-terminal His_6 tag (MHHHHHHITSLYKKAG–). For the expression in vivo the fusion proteins were transferred in a pML396 destination vector by LR-clonase reaction as described in the table 5. *C. crescentus* strains were generated by two-plasmids electroporation of pML396 (pRK origin) derivatives and pSRK-Km (pBR322 origin) derivatives as reported in the Table 5.

Table 5. List of all the strain used in the FRET study

Strain name	Organism	Plasmid ,resistence	Gene expressed
	In vivo study		
EB909	*C. crescentus* CB15N	pSRK(p*lac*), Km^{res}	*ctrA*(RR)-CFP
EB910	*C. crescentus* CB15N	pSRK(p*lac*), Km^{res}	*ctrA*(RR)-YFP
EB911	*C. crescentus* CB15N	pSRK(p*lac*), Km^{res}	YFP
EB912	*C. crescentus* CB15N	pSRK(p*lac*), Km^{res}	CFP
EB924	*C. crescentus CB15N*	pML396(plXyl), Tet^{res}	*ctrA*(RR)-CFP
EB925	*C. crescentus CB15N*	pML396(p*Xyl*), Tet^{res}	*ctrA*(RR)-YFP
EB972	*C. crescentus CB15N*	pSRK(p*lac*), Km^{res}	*ctrA*(RR)-CFP
		pML396(p*Xyl*), Tet^{res}	*ctrA*(RR)-YFP
EB1011	*C. crescentus CB15N*	pSRK(plac), Km^{res}	ctrA(RR)-CFP
		pML396(pXyl), Tet^{res}	YFP
	In vitro study		
EB893	*E. coli* BL21	pET300(N-ter), Amp^{res}	*ctrA*(RR)-CFP
EB895	*E. coli* BL21	pET300(N-ter), Amp^{res}	*ctrA*(RR)-YFP
EB1021	*E. coli* BL21	pML310, Amp^{res}	*cckA*-RD
EB1089	*E. coli* BL21	pML333, Amp^{res}	*cckA*-HK

Proteins purification

All the proteins used for the in vitro test were overexpressed in *E.coli* BL21 (DE3) cells at an OD_{600} of 0.6 by the addition of 150-300 µM IPTG and cell growth was continued for 3 hours at 30°C with shaking (215 rev min^{-1}). The cells were harvested then by centrifugation for 20 min at 500 rev min^{-1} at 4°C, resuspended in lysis buffer [20 mM Tris pH8, 500 mM NaCl, 10 mM imidazole pH 8, 0.1% Triton X-100, Complete Inhibitor Cocktail (Roche, Basel, Switzerland) and DNase I (Euromedex, Sauffelweyersheim, France), Glycerol 10%] and lysed using an Emulsiflex homogenizer (Avestin, Ottawa, Ontario, Canada) at 10°C. The supernatant containing His_6-Tagged protein was purified using Ni–NTA affinity resin (Qiagen, Hilden, Germany) equilibrated with lysis buffer and was eluted with Elution Buffer (20 mM Hepes pH8, 500 mM NaCl, 10% (w/v) glycerol, 250 mM Imidazole). A second step of purification was performed by gel filtration using a HiLoad 16/60 Superdex 75 prep-grade column (GE Healthcare, Waukesha, Wisconsin, USA) equilibrated with running buffer [10 mM HEPES pH 8, 50 mM KCl, 1 mM DTT, 0.1 EDTA, 10%(w/v) glycerol]. An SDS–PAGE of the proteins preparation purification is shown in figure 40 of the results section.

***In vitro* fret and analysis**

A 384 well plate containing both references and samples (see Table 6) was read on a Pherastar plate reader (BMG Labtech Gmbh) with excitation at 430 nm and emission 480 nm and 530 nm. For each condition, at least 10 samples were measured 100 times. Mean emission ratio of 530 nm/480 nm were calculated for each sample. Then we subtracted the calculated ratio of the summed fluorescence of the donor and acceptor alone. It allows normalization on a calculated negative FRET reference.

Schematic organization of the *in vitro* fret experiment Table 6; each condition has been done in triplicate. ATP (final concentration 5 mM) was first pre-incubated at room temperature with the phosphorelay and then, to these reactions, the sensor pair of half of it was added.

Following final concentration of protein were used:

- [CckA-RD]=[ChpT]= 2.5 µM
- [CckA-HD]= 5 µM
- [CtrA-CFP]=[CtrA-YFP]= 0.1 µM

Table 6. Schematic organization of the in vitro fret experiment; √ represents the presence of the component in the reaction.

Proteins	1	2	3	4	5	6	7	8	9	10
CckA-RD			√		√	√	√	√	√	√
CckA-HK			√		√	√	√	√	√	√
ChpT			√		√	√	√	√	√	√
CtrA-CFP				√	√	√			√	√
CtrA-YFP							√	√	√	√
ATP		√	√	√		√		√		√
Buffer	√	√	√	√	√	√	√	√	√	√

***In vivo* FRET analysis**

1 ml OD_{600} 0.1-0.2 EB972 and EB1011 Synchronized (Evinger *et al.*, 1977) or mixed population were pelleted and resuspended in PBS 1x pH 7.4. Then they were analysed at 15°C by inverted Leica AF6000 video-microscope (Leica Microsystems, Wetzlar, Germany) with 100x, 1.4 numerical aperture (NA) oil-immersion objective. Fluorescence excitation was performed with a 427 ± 10 and 504± 12 nm bandpass filters through a double band dichroic mirror (440/520 nm). A fast detection filter wheel (respectively with 472 ± 30 nm and 542 ± 27 nm bandpass filters) was used.

YFP/CFP ratio was calculated with the ImageJ routine software developed according to the procedure as described in Kardash *et al*. 2011 except for the final equation that comes from Wouters *et al.*, 2001. The bleed-through coefficients (crossover of the donor and acceptor

fluorophore spectrum) were calculated on strain expressing either Ctra-YFP or CtrA-CFP alone using the same acquisition parameters. For each condition the YFP/CFP ratio curves were calculated cell by cell and data average and standard deviation were calculated by excel. FRET images correspond to the YFP/CFP ratio calculated pixel by pixel and represented in pseudocolor using ImageJ.

Phostag gel

In the Phosphate-affinity polyacrylamide gel electrophoresis (Phos™-Tag SDS-PAGE) the phosphate-affinity site is exploit by a polyacrylamide-bound dinuclear Mn^{2+} complex (Mn^{2+}-Phos-tag) that can enhance mobility shifts of phosphorylated forms of proteins. The phostag gel that are presented in the results were made following the general protocol that is described in Pini *et al*. 2013. For CtrA phosphorylation levels we used antibodies raised against *Caulobacter* CtrA.

Bibliography

- Abrahams JP, Leslie AG. Methods used in the structure determination of bovine mitochondrial F1 ATPase. Acta Crystallogr D Biol Crystallogr. 1996 Jan 1;52(Pt 1):30-42.

- Albu RF, Jurkowski TP, Jeltsch A (2012) The Caulobacter crescentus DNA- (adenine-N6)-methyltransferase CcrM methylates DNA in a distributive manner. Nucleic Acids Res 40: 1708–1716. doi:10.1093/nar/gkr768.

- Ardissone S, Viollier PH. Developmental and environmental regulatory pathways in alpha proteobacteria. Front Biosci (Landmark Ed). 2012 Jan 1;17:1695-714.

- Ashenberg O, Rozen-Gagnon K, Laub MT, Keating AE. Determinants of homodimerization specificity in histidine kinases. J Mol Biol. 2011 Oct 14;413(1):222-35. doi: 10.1016/j.jmb.2011.08.011.

- Bastedo, D. P., and G. T. Marczynski. 2009. CtrA response regulator binding to the Caulobacter chromosome replication origin is required during nutrient and antibiotic stress as well as during cell cycle progression. Mol. Microbiol. 72:139–154.

- Bick MJ, Lamour V, Rajashankar KR, Gordiyenko Y, Robinson CV, Darst SA. How to switch off a histidine kinase: crystal structure of Geobacillus stearothermophilus KinB with the inhibitor Sda. J Mol Biol. 2009 Feb 13;386(1):163-77.

- Biondi EG, Skerker JM, Arif M, Prasol MS, Perchuk BS, Laub MT. A phosphorelay system controls stalk biogenesis during cell cycle progression in Caulobacter crescentus. Mol Microbiol. 2006 Jan;59(2):386-401.

- Biondi, E. G., S. J. Reisinger, J. M. Skerker, M. Arif, B. S. Perchuk, K. R. Ryan, and M. T. Laub. 2006. Regulation of the bacterial cell cycle by an integrated genetic circuit. Nature 444:899–904.

- Blair JA, Xu Q, Childers WS, Mathews II, Kern JW, Eckart M, Deacon AM, Shapiro L. Branched signal wiring of an essential bacterial cell-cycle phosphotransfer protein. Structure. 2013 Sep 3;21(9):1590-601.

- Bricogne G., Blanc E., Brandl M., Flensburg C., Keller P., Paciorek W., Roversi P, Sharff A., Smart O.S., Vonrhein C., Womack T.O. (2011). BUSTER version 2.10 Cambridge, United Kingdom: Global Phasing Ltd.

- Brilli M, Fondi M, Fani R, Mengoni A, Ferri L, Bazzicalupo M, Biondi EG. 2010. The diversity and evolution of cell cycle regulation in alpha-proteobacteria: a comparative genomic analysis. BMC Syst Biol. 4:52.

- Brown PJ, de Pedro MA, Kysela DT, Van der Henst C, Kim J, et al. 2012. Polar growth in the alphaproteobacterial order Rhizobiales. Proc. Natl. Acad. Sci. USA 109:1697–701

- Brown PJB, Kysela DT, Brun YV (2011) Polarity and the diversity of growth mechanisms in bacteria. Semin Cell Dev Biol 22:790–798.

- Brun, Y. V. and R. Janakiraman. 2000. Dimorphic life cycles of Caulobacter and stalked bacteria. p. 297 317. In Prokaryotic Development. Yves V. Brun and Larry Shimkets, eds. ASM Press.

- Brunet YR, Bernard CS, Gavioli M, Lloube`s R, Cascales E (2011) An epigenetic switch involving overlapping fur and DNA methylation optimizes expression of a type VI secretion gene cluster. PLoS Genet 7: e1002205. doi:10.1371/ journal.pgen.1002205.

- Burton GJ, Hecht GB, Newton A: Roles of the histidine protein kinase pleC in Caulobacter crescentus motility and chemotaxis. J Bacteriol 1997, 179:5849-5853.

- Capra EJ, Perchuk BS, Lubin EA, Ashenberg O, Skerker JM, Laub MT. Systematic dissection and trajectory-scanning mutagenesis of the molecular interface that ensures specificity of two-component signaling pathways. PLoS Genet. 2010 Nov 24;6(11):e1001220.

- Casino P, Rubio V, Marina A. Structural insight into partner specificity and phosphoryl transfer in two-component signal transduction. Cell. 2009 Oct 16;139(2):325-36.

- Casino P, Rubio V, Marina A. The mechanism of signal transduction by two-component systems. Curr Opin Struct Biol. 2010 Dec;20(6):763-71.

- Chauhan A, et al. (2006) Interference of Mycobacterium tuberculosis cell division by Rv2719c, a cell wall hydrolase. Mol Microbiol 62:132–147.

- Chen YE, Tropini C, Jonas K, Tsokos CG, Huang KC, Laub MT: Spatial gradient of protein phosphorylation underlies replicative asymmetry in a bacterium. Proc Natl Acad Sci USA 2011, 108:1052-1057.

- Chen, Y. E., C. G. Tsokos, E. G. Biondi, B. S. Perchuk, and M. T. Laub. 2009. Dynamics of two phosphorelays controlling cell cycle progression in Caulobacter crescentus. J. Bacteriol. 191:7417–7429.

- Chien, P., B. S. Perchuk, M. T. Laub, R. T. Sauer, and T. A. Baker. 2007. Direct and adaptor-mediated substrate recognition by an essential AAA protease. Proc. Natl. Acad. Sci. U. S. A. 104:6590–6595.

- Christen B, Abeliuk E, Collier JM, Kalogeraki VS, Passarelli B, Coller JA, Fero MJ, McAdams HH, Shapiro L. The essential genome of a bacterium. Mol Syst Biol. 2011 Aug 30;7:528. doi: 10.1038/msb.2011.58. PubMed PMID: 21878915; PubMed Central PMCID: PMC3202797.

- David and Pérez (2009) Combined sampler robot and high-performance liquid chromatography: a fully automated system for biological small-angle X-ray scattering experiments at the Synchrotron SOLEIL SWING beamline. J. Appl. Cryst. (2009). 42, 892-900.

- David, G., and Pérez, J. (2009). Combined sampler robot and high-performance liquid chromatography: a fully automated system for biological small-angle X-ray scattering experiments at the synchrotron SOLEIL SWING beamline. Journal of applied crystallography 42, 892-900.

- De Nisco NJ, Abo RP, Wu CM, Penterman J, Walker GC. Global analysis of cell cycle gene expression of the legume symbiont Sinorhizobium meliloti. Proc NatlAcad Sci U S A. 2014 Mar 4;111(9):3217-24.

- Demarre G, Chattoraj DK (2010) DNA adenine methylation is required to replicate both Vibrio cholerae chromosomes once per cell cycle. PLoS Genet 6: e1000939. doi:10.1371/journal.pgen.1000939.

- Domian, I. J., K. C. Quon, and L. Shapiro. 1997. Cell type-specific phosphorylation and proteolysis of a transcriptional regulator controls the G1- to-S transition in a bacterial cell cycle. Cell 90:415–424.

- Domian, I.J., Reisenauer, A. and Shapiro, L. (1999) Feedback control of a master bacterial cell-cycle regulator. Proc. Natl. Acad. Sci. U.S.A. 96, 6648–6653.

- Dutta R, Inouye M. GHKL, an emergent ATPase/kinase superfamily. Trends Biochem Sci. 2000 Jan;25(1):24-8.

- Ely B (1991) Genetics of Caulobacter crescentus. Meth Enzymol 204: 372–384.

- Emsley P, Lohkamp B, Scott WG, Cowtan K. Features and development of Coot. Acta Crystallogr D Biol Crystallogr. 2010 Apr;66(Pt 4):486-501

- Evinger M, Agabian N. Envelope-associated nucleoid from Caulobacter crescentus stalked and swarmer cells. J Bacteriol. 1977 Oct;132(1):294-301.

- Fioravanti A, Clantin B, Dewitte F, Lens Z, Verger A, Biondi EG, Villeret V. Structural insights into ChpT, an essential dimeric histidine phosphotransferase regulating the cell cycle in Caulobacter crescentus. Acta Crystallogr Sect F Struct Biol Cryst Commun. 2012 Sep 1;68(Pt 9):1025-9.

- Fioravanti A, Fumeaux C, Mohapatra SS, Bompard C, Brilli M, Frandi A, Castric V, Villeret V, Viollier PH, Biondi EG. DNA binding of the cell cycle transcriptional regulator GcrA depends on N6-adenosine methylation in Caulobacter crescentus and other Alphaproteobacteria. PLoS Genet. 2013 May;9(5):e1003541.

- Flärdh K (2003) Essential role of DivIVA in polar growth and morphogenesis in Streptomyces coelicolor A3(2). Mol Microbiol 49:1523–1536.

- Förster T. (1948) Ann. Phys 2:55–75.

- Fumeaux C, Radhakrishnan SK, Ardissone S, Théraulaz L, Frandi A, Martins D, Nesper J, Abel S, Jenal U, Viollier PH. Cell cycle transition from S-phase to G1 in Caulobacter is mediated by ancestral virulence regulators. Nat Commun. 2014 Jun 18;5:4081

- Gao R, Stock AM. Biological insights from structures of two-component proteins. Annu Rev Microbiol. 2009;63:133-54.

- Gao R, Stock AM. Molecular strategies for phosphorylation-mediated regulation of response regulator activity. Curr Opin Microbiol. 2010 Apr;13(2):160-7.

- Gao R, Tao Y, Stock AM. System-level mapping of Escherichia coli response regulator dimerization with FRET hybrids. Mol Microbiol. 2008 Sep;69(6):1358-72.

- Geourjon C, Deleage G (1995) SOPMA: significant improvements in protein secondary structure prediction by consensus prediction from multiple alignments. Comput Appl Biosci 11: 681–684.

- Ghosh, P. (2004). Process of protein transport by the type III secretion system. Microbiol Mol Biol Rev 68, 771-795.

- Gill JJ, Berry JD, Russell WK, Lessor L, Escobar Garcia DA, et al. (2012) The Caulobacter crescentus phage phiCbK: genomics of a canonical phage. BMC Genomics 13: 542. doi:10.1186/1471-2164-13-542.

- Girard et al. (2003) A new class of lanthanide complexes to obtain high-phasing-power heavy-atom derivatives for macromolecular crystallography. Acta Crystallographica Section D Biological Crystallography, 59,1914-1922.

- Gober JW, Shapiro L (1992) A developmentally regulated Caulobacter flagellar promoter is activated by 39 enhancer and IHF binding elements. Mol Biol Cell 3: 913–926.

- Guillet V, Ohta N, Cabantous S, Newton A, Samama JP. Crystallographic and biochemical studies of DivK reveal novel features of an essential response regulator in Caulobacter crescentus. J Biol Chem. 2002 Nov 1;277(44):42003-10.

- Hallez R, Bellefontaine AF, Letesson JJ, De Bolle X. Morphological and functional asymmetry in alpha-proteobacteria. Trends Microbiol. 2004 Aug;12(8):361-5

- Hallez R, Mignolet J, Van Mullem V, Wery M, Vandenhaute J, Letesson JJ, Jacobs-Wagner C, De Bolle X. The asymmetric distribution of the essential histidine kinase PdhS indicates a differentiation event in Brucella abortus. EMBO J. 2007 Mar 7;26(5):1444-55.

- Hecht GB, Lane T, Ohta N, Sommer JM, Newton A: An essential single domain response regulator required for normal cell division and differentiation in Caulobacter crescentus. EMBO J 1995, 14:3915-3924.

- Hernday A, Braaten B, Low D (2004) The intricate workings of a bacterial epigenetic switch. Adv Exp Med Biol 547: 83–89.

- Hernday A, Braaten B, Low D (2004) The intricate workings of a bacterial epigenetic switch. Adv Exp Med Biol 547: 83–89.

- Hinz, A.J., Larson, D.E., Smith, C.S. and Brun, Y.V. (2003) The Caulobacter crescentus polar organelle development protein PodJ is differentially localized and is required for polar targeting of the PleC development regulator. Mol. Microbiol. 47, 929–941.

- Holtzendorff, J., Hung, D., Brende, P., Reisenauer, A., Viollier, P.H., McAdams, H.H. and Shapiro, L. (2004) Oscillating global regulators control the genetic circuit driving a bacterial cell cycle. Science 304, 983–987.

- Hottes AK, Shapiro L, McAdams HH (2005) DnaA coordinates replication initiation and cell cycle transcription in Caulobacter crescentus. Mol Microbiol 58: 1340–1353. doi:10.1111/j.1365 2958.2005.04912.x.

- Hwang BY, Lee HJ, Yang YH, Joo HS, Kim BG. Characterization and investigation of substrate specificity of the sugar aminotransferase WecE from E. coli K12. Chem Biol. 2004 Jul;11(7):915-25.

- Iniesta, A. A., P. T. McGrath, A. Reisenauer, H. H. McAdams, and L. Shapiro. 2006. A phospho-signaling pathway controls the localization and activity of a protease complex critical for bacterial cell cycle progression. Proc. Natl. Acad. Sci. U. S. A. 103:10935–10940.

- Jacobs C, Domian IJ, Maddock JR, Shapiro L. Cell cycle-dependent polar localization of an essential bacterial histidine kinase that controls DNA replication and cell division. Cell. 1999 Apr 2;97(1):111-20.

- Jacobs C, Hung D, Shapiro L: Dynamic localization of a cytoplasmic signal transduction response regulator controls morphogenesis during the Caulobacter cell cycle. Proc Natl Acad Sci USA 2001, 98:4095-4100.

- Jenal, U. & Fuchs, T. An essential protease involved in bacterial cell-cycle control. EMBO J. 17, 5658–5669 (1998).

- Jensen, R.B. and Shapiro, L. (1999) The Caulobacter crescentus smc gene is required for cell cycle progression and chromosome segregation. Proc. Natl. Acad. Sci. U.S.A. 96, 10661–10666.

- Kabsch, W. (2010). XDS. Acta Cryst. D66, 125-132.

- Kang CM, Nyayapathy S, Lee JY, Suh JW, Husson RN (2008) Wag31, a homologue of the cell division protein DivIVA, regulates growth, morphology and polar cell wall synthesis in mycobacteria. Microbiology 154:725–735.

- Kardash, E.; Bandemer, J.; Raz, E. Imaging protein activity in live embryos using fluorescence resonance energy transfer biosensors. Nat. Protoc. 2011, 6, 1835–1846.

- Khan SR, Gaines J, Roop RM 2nd, Farrand SK. Broad-host-range expression vectors with tightly regulated promoters and their use to examine the influence of TraR and TraM expression on Ti plasmid quorum sensing. Appl Environ Microbiol. 2008 Aug;74(16):5053-62.

- Konarev, P.V., Volkov, V.V., Petoukhov, M.V., and Svergun, D.I. (2006). ATSAS 2.1, a program package for small-angle scattering data analysis. Journal of applied crystallography 39, 277-286.

- Konarev, P.V., Volkov, V.V., Sokolova, A.V., Koch, M.H.J., and Svergun, D.I. (2003). PRIMUS: a Windows PC-based system for small-angle scattering data analysis. Journal of applied crystallography 36, 1277-1282.

- Kozdon JB, Melfi MD, Luong K, Clark TA, Boitano M, Wang S, Zhou B, Gonzalez D, Collier J, Turner SW, Korlach J, Shapiro L, McAdams HH. Global methylation state at base-pair resolution of the Caulobacter genome throughout the cell cycle. Proc Natl Acad Sci U S A. 2013 Nov 26;110(48):E4658-67.

- Kratky, O., and Porod, G. (1949). Diffuse small-angle scattering of X-rays in colloid systems. Journal of colloid science 4.

- Krissinel E, Henrick K. Secondary-structure matching (SSM), a new tool for fast protein structure alignment in three dimensions. Acta Crystallogr D Biol Crystallogr. 2004 Dec;60(Pt 12 Pt 1):2256-68.

- Kysela DT, Brown PJ, Huang KC, Brun YV. Biological consequences and advantages of asymmetric bacterial growth. Rev Microbiol. 2013; 67:417-35

- Langer, G., Cohen, S.X., Lamzin, V.S. & Perrakis, A. (2008) Automated macromolecular model building for X-ray crystallography using ARP/wARP version 7. Nature Protocols. 3, 1171-1179.

- Larkin A, Olivier NB, Imperiali B. Structural analysis of WbpE from Pseudomonas aeruginosa PAO1: a nucleotide sugar aminotransferase involved in O-antigen assembly. Biochemistry. 2010 Aug 24;49(33):7227-37.

- Laub MT, Goulian M. Specificity in two-component signal transduction pathways. Annu Rev Genet. 2007;41:121-45.

- Laub, M. T., Chen, S. L., Shapiro, L. & McAdams, H. H. Genes directly controlled by CtrA, a master regulator of the Caulobacter cell cycle. Proc. Natl Acad. Sci. USA 99, 4632–4637 (2002).

- Laub, M. T., McAdams, H. H., Feldblyum, T., Fraser, C. M. & Shapiro, L. Global analysis of the genetic network controlling a bacterial cell cycle. Science 290, 2144–2148 (2000).

- Letek M, et al. (2008) DivIVA is required for polar growth in the MreB-lacking rodshaped actinomycete Corynebacterium glutamicum. J Bacteriol 190:3283–3292.

- Macara IG, Mili S. 2008. Polarity and differential inheritance-universal attributes of life? Cell 135:801–12.

- Marczynski, G. T., and L. Shapiro. 2002. Control of chromosome replication in *Caulobacter crescentus*. Annu. Rev. Microbiol. 56:625–656.155.

- Marczynski, G.T. (1999) Chromosome methylation and measurement of faithful, once and only once per cell cycle chromosome replication in *Caulobacter crescentus*. J. Bacteriol. 181, 1984–1993.

- Marina A, Waldburger CD, Hendrickson WA. Structure of the entire cytoplasmic portion of a sensor histidine-kinase protein. EMBO J. 2005 Dec 21;24(24):4247-59.

- Marinus MG, Casadesus J (2009) Roles of DNA adenine methylation in host-pathogen interactions: mismatch repair, transcriptional regulation, and more. FEMS Microbiol Rev 33: 488–503. doi:10.1111/ j.1574-6976.2008.00159.x.

- McGrath, P. T., A. A. Iniesta, K. R. Ryan, L. Shapiro, and H. H. McAdams. 2006. A dynamically localized protease complex and a polar specificity factor control a cell cycle master regulator. Cell 124:535–547.

- Meniche X, Otten R, Siegrist MS, Baer CE, Murphy KC, Bertozzi CR, Sassetti CM. Subpolar addition of new cell wall is directed by DivIVA in mycobacteria. Proc Natl Acad Sci U S A. 2014 Aug 5;111(31):E3243-51.

- Menon S, Wang S. Structure of the response regulator PhoP from Mycobacterium tuberculosis reveals a dimer through the receiver domain. Biochemistry. 2011 Jul 5;50(26):5948-57. doi: 10.1021/bi2005575. Epub 2011 Jun 13. Erratum in: Biochemistry. 2011 Aug 16;50(32):7076.

- Mohapatra SS, Fioravanti A, Biondi EG. DNA methylation in Caulobacter and other Alphaproteobacteria during cell cycle progression. Trends Microbiol. 2014 Jun 2. pii: S0966-842X(14)00099-7.

- Mooij WT, Cohen SX, Joosten K, Murshudov GN, Perrakis A. "Conditional Restraints": Restraining the Free Atoms in ARP/wARP. Structure. 2009 Feb 13;17(2):183-9.

- Murshudov GN, Skubák P, Lebedev AA, Pannu NS, Steiner RA, Nicholls RA, Winn MD, Long F, Vagin AA. REFMAC5 for the refinement of macromolecular crystal structures. Acta Crystallogr D Biol Crystallogr. 2011 Apr;67(Pt 4):355-67.

- Neumuller RA, Knoblich JA. 2009. Dividing cellular asymmetry: asymmetric cell division and its implications for stem cells and cancer. Genes Dev. 23:2675–99.

- Nguyen L, et al. (2007) Antigen 84, an effector of pleiomorphism in Mycobacterium smegmatis. J Bacteriol 189:7896–7910.

- Nierman WC, Feldblyum TV, Laub MT, Paulsen IT, Nelson KE, et al. (2001) Complete genome sequence of Caulobacter crescentus. Proc Natl Acad Sci USA 98: 4136–4141. doi:10.1073/pnas.061029298.

- Niesen FH, Berglund H, Vedadi M. The use of differential scanning fluorimetry to detect ligand interactions that promote protein stability. Nat Protoc. 2007;2(9):2212-21.

- Ohta N, Lane T, Ninfa EG, Sommer JM, Newton A: A histidine protein kinase homologue required for regulation of bacterial cell division and differentiation. Proc Natl Acad Sci USA 1992, 89:10297-10301.

- Panis G, Lambert C, Viollier PH (2012) Complete genome sequence of Caulobacter crescentus bacteriophage wCbK. J Virol 86: 10234–10235. doi:10.1128/JVI.01579-12.

- Paredes-Sabja D, Shen A, Sorg JA. Clostridium difficile spore biology: sporulation, germination, and spore structural proteins. Trends Microbiol. 2014 Jul;22(7):406-416.

- Paul R, Jaeger T, Abel S, Wiederkehr I, Folcher M, Biondi EG, Laub MT, Jenal U: Allosteric regulation of histidine kinases by their cognate response regulator determines cell fate. Cell 2008, 133:452-461.

- Pini F, Frage B, Ferri L, De Nisco NJ, Mohapatra SS, Taddei L, Fioravanti A, Dewitte F, Galardini M, Brilli M, Villeret V, Bazzicalupo M, Mengoni A, Walker GC, Becker A, Biondi EG. The DivJ, CbrA and PleC system controls DivK phosphorylation and symbiosis in Sinorhizobium meliloti. Mol Microbiol. 2013 Oct;90(1):54-71.

- Poindexter, J.S. (1964) Biological properties and classification of the Caulobacter group. Microbiol. Mol. Biol. Rev. 28, 231–295.

- Potterton EA, Powell HR, Read RJ, Vagin A, Wilson KS. Overview of the CCP4 suite and current developments. Acta Crystallogr D Biol Crystallogr. 2011 Apr;67(Pt 4):235-42.

- Quon, K. C., B. Yang, I. J. Domian, L. Shapiro, and G. T. Marczynski. 1998. Negative control of bacterial DNA replication by a cell cycle regulatory protein that binds at the chromosome origin. Proc. Natl. Acad. Sci. U. S. A. 95:120–125.

- Quon, K. C., Marczynski, G. T. & Shapiro, L. Cell cycle control by an essential bacterial two-component signal transduction protein. Cell 84, 83–93 (1996).

- Radhakrishnan, S. K., M. Thanbichler, and P. H. Viollier. 2008. The dynamic interplay between a cell fate determinant and a lysozyme homolog drives the asymmetric division cycle of Caulobacter crescentus. Genes Dev. 22:212–225.

- Ramos A, et al. (2003) Involvement of DivIVA in the morphology of the rod-shaped actinomycete Brevibacterium lactofermentum. Microbiology 149:3531–3542.

- Reisenauer, A. & Shapiro, L. DNA methylation affects the cell cycle transcription of the CtrA global regulator in Caulobacter. EMBO J. 21, 4969–4977 (2002).

- Rigaut G, Shevchenko A, Rutz B, Wilm M, Mann M, Séraphin B. A generic protein purification method for protein complex characterization and proteome exploration. Nat Biotechnol. 1999 Oct;17(10):1030-2.

- Robertson G, Hirst M, Bainbridge M, Bilenky M, Zhao Y, et al. (2007) Genomewide profiles of STAT1 DNA association using chromatin immunoprecipitation and massively parallel sequencing. Nat Methods 4: 651–657. doi:10.1038/ nmeth1068.

- Robertson GT, Reisenauer A, Wright R, Jensen RB, Jensen A, et al. (2000) The Brucella abortus CcrM DNA methyltransferase is essential for viability, and its overexpression attenuates intracellular replication in murine macrophages. J Bacteriol 182: 3482–3489.

- Ryan, K. R., Judd, E. M. & Shapiro, L. The CtrA response regulator essential for Caulobacter crescentus cell-cycle progression requires a bipartite degradation signal for temporally controlled proteolysis. J. Mol. Biol. 324, 443–455 (2002).

- Schneider TR, Sheldrick GM. Substructure solution with SHELXD. Acta Crystallogr D Biol Crystallogr. 2002 Oct;58(Pt 10 Pt 2):1772-9.

- Sharma R, Peacock L, Gluenz E, Gull K, Gibson W, Carrington M. 2008. Asymmetric cell division as a route to reduction in cell length and change in cell morphology in trypanosomes. Protist 159:137–51.

- Sheldrick, G.M. (2008). "A short history of SHELX", Acta Crystallogr. D64, 112-122.

- Siam, R. and Marczynski, G.T. (2000) Cell cycle regulator phosphorylation stimulates two distinct modes of binding at a chromosome replication origin. EMBO J. 19, 1138–1147.

- Siam, R., and G. T. Marczynski. 2003. Glutamate at the phosphorylation site of response regulator CtrA provides essential activities without increasing DNA binding. Nucleic Acids Res. 31:1775–1779.

- Skerker JM, Laub MT. Cell-cycle progression and the generation of asymmetry in Caulobacter crescentus. Nat Rev Microbiol. 2004 Apr;2(4):325-37.

- Skerker JM, Perchuk BS, Siryaporn A, Lubin EA, Ashenberg O, Goulian M, Laub MT. Rewiring the specificity of two-component signal transduction systems. Cell. 2008 Jun 13;133(6):1043-54.

- Skerker JM, Prasol MS, Perchuk BS, Biondi EG, Laub MT (2005) Two-component signal transduction pathways regulating growth and cell cycle progression in a bacterium: a system-level analysis. PLoS Biol 3: e334. doi:10.1371/journal.pbio.0030334.

- Sommer JM, Newton A: Pseudoreversion analysis indicates a direct role of cell division genes in polar morphogenesis and differentiation in Caulobacter crescentus. Genetics 1991, 129:623-630.

- Stephens C, Reisenauer A, Wright R, Shapiro L (1996) A cell cycle-regulated bacterial DNA methyltransferase is essential for viability. Proc Natl Acad Sci USA 93: 1210–1214.

- Stephens, C., Reisenauer, A., Wright, R. and Shapiro, L. (1996) A cell cycleregulated bacterial DNA methyltransferase is essential for viability. Proc. Natl. Acad. Sci. U.S.A. 93, 1210–1214.

- Stock, A. M., V. L. Robinson, and P. N. Goudreau. 2000. Two-component signal transduction. Annu. Rev. Biochem. 69:183–215

- Svergun D.I. (1992) Determination of the regularization parameter in indirect-transform methods using perceptual criteria. J. Appl. Crystallogr. 25, 495-503.

- Svergun, D.I. (1992). Determination of the regularization parameter in indirect-transform methods using perceptual criteria. Journal of applied crystallography 25, 495-503.

- Tajbakhsh S, Rocheteau P, Le Roux I. Asymmetric cell divisions and asymmetric cell fates. Annu Rev Cell Dev Biol. 2009;25:671-99.

- Tan IS, Ramamurthi KS. Spore formation in Bacillus subtilis. Environ Microbiol Rep. 2014 Jun;6(3):212-25.; Sella SR, Vandenberghe LP, Soccol CR. Life cycle and spore resistance of spore-forming Bacillus atrophaeus. Microbiol Res. 2014 May 10.

- Thanbichler M, Shapiro L (2006) MipZ, a spatial regulator coordinating chromosome segregation with cell division in Caulobacter. Cell 126: 147–162. doi:10.1016/j.cell.2006.05.038.

- Theillet FX, Kalmar L, Tompa P, Han KH, Selenko P, Dunker AK, Daughdrill GW and Uversky VN. 2013. The alphabet of intrinsic disorder I. Act like a Pro: On the abundance and roles of proline residues in intrinsically disordered proteins. Intrinsically Disordered Proteins 1, e24360.

- Trajtenberg F, Graña M, Ruétalo N, Botti H, Buschiazzo A. Structural and enzymatic insights into the ATP binding and autophosphorylation mechanism of a sensor histidine kinase. J Biol Chem. 2010 Aug 6;285(32):24892-903

- Tsokos CG, Perchuk BS, Laub MT: A dynamic complex of signaling proteins uses polar localization to regulate cell-fate asymmetry in Caulobacter crescentus. Dev Cell 2011, 20:329-341.

- Varughese KI, Madhusudan, Zhou XZ, Whiteley JM, Hoch JA. Formation of a novel four-helix bundle and molecular recognition sites by dimerization of a response regulator phosphotransferase. Mol Cell. 1998 Oct;2(4):485-93.

- Viollier, P.H., Sternheim, N. and Shapiro, L. 2002; Identification of a localization factor for the polar positioning of bacterial structural and regulatory proteins. Proc. Natl. Acad. Sci. U.S.A. 99, 13831–13836.

- Vonrhein C, Blanc E, Roversi P, Bricogne G. Automated structure solution with autoSHARP. Methods Mol Biol. 2007;364:215-30.

- Wheeler RT, Shapiro L: Differential localization of two histidine kinases controlling bacterial cell differentiation. Mol Cell 1999, 4:683-694.

- Winn MD, Ballard CC, Cowtan KD, Dodson EJ, Emsley P, Evans PR, Keegan RM, Krissinel EB, Leslie AG, McCoy A, McNicholas SJ, Murshudov GN, Pannu NS, Wouters FS, Verveer PJ, Bastiaens PI. Imaging biochemistry inside cells. Trends Cell Biol. 2001 May;11(5):203-11.

- Winn MD, Ballard CC, Cowtan KD, Dodson EJ, Emsley P, Evans PR, Keegan RM, Krissinel EB, Leslie AG, McCoy A, McNicholas SJ, Murshudov GN, Pannu NS, Potterton EA, Powell HR, Read RJ, Vagin A, Wilson KS. Overview of the CCP4 suite and current developments. Acta Crystallogr D Biol Crystallogr. 2011 Apr;67(Pt 4):235-42.

- Wouters FS, Verveer PJ, Bastiaens PI. Imaging biochemistry inside cells. Trends Cell Biol. 2001 May;11(5):203-11.

- Wright R, Stephens C, Shapiro L (1997) The CcrM DNA methyltransferase is widespread in the alpha subdivision of proteobacteria, and its essential functions are conserved in Rhizobium meliloti and Caulobacter crescentus. J Bacteriol 179: 5869–5877.

- Wu J, Ohta N, Zhao JL, Newton A: A novel bacterial tyrosine kinase essential for cell division and differentiation. Proc Natl Acad Sci USA 1999, 96:13068-13073.

- Xu Q, Carlton D, Miller MD, Elsliger MA, Krishna SS, Abdubek P, Astakhova T, Burra P, Chiu HJ, Clayton T, Deller MC, Duan L, Elias Y, Feuerhelm J, Grant JC, Grzechnik A, Grzechnik SK, Han GW, Jaroszewski L, Jin KK, Klock HE, Knuth MW, Kozbial P, Kumar A, Marciano D, McMullan D, Morse AT, Nigoghossian E, Okach L, Oommachen S, Paulsen J, Reyes R, Rife CL, Sefcovic N, Trame C, Trout CV, van den Bedem H, Weekes D, Hodgson KO, Wooley J, Deacon AM, Godzik A, Lesley SA, Wilson IA. Crystal structure of histidine phosphotransfer protein ShpA, an essential regulator of stalk biogenesis in Caulobacter crescentus. J Mol Biol. 2009 Jul 24;390(4):686-98. doi: 10.1016/j.jmb.2009.05.023.

- Yamada S, Sugimoto H, Kobayashi M, Ohno A, Nakamura H, Shiro Y. Structure of PAS-linked histidine kinase and the response regulator complex. Structure. 2009 Oct 14;17(10):1333-44.

- Yang ZR, Thomson R, McNeil P, Esnouf RM. RONN: the bio-basis function neural network technique applied to the detection of natively disordered regions in proteins. Bioinformatics. 2005 Aug 15;21(16):3369-76.

- Yindeeyoungyeon W, Schell MA (2000) Footprinting with an automated capillary DNA sequencer. BioTechniques 29: 1034–1036, 1038, 1040–1041.

- Zhou, Y., S. Gottesman, J. R. Hoskins, M. R. Maurizi, and S. Wickner. 2001. The RssB response regulator directly targets sigma(S) for degradation by ClpXP. Genes Dev. 15:627–637.

- Zweiger G, Marczynski G, Shapiro L (1994) A Caulobacter DNA methyltransferase that functions only in the predivisional cell. J Mol Biol 235: 472–485. doi:10.1006/jmbi.1994.1007.

Acknowledgments

Behind every finishing line there is a new start and a lot of people to thank…

First of all, I would like to thank the great scientists of my PhD committee that honoured me with their presence and advices: Professor Barras, Professor Bodart, Professor Viollier, Professor De Bolle, Doctor Villeret and Doctor Biondi.

A special thanks to Prof De Bolle and Prof Viollier that in these past years, as members of my PhD advising committee, have been offering me precious helps for my scientific growth.

I wish to thank also the “Region Nord-Pas De Calais” that contributed to my PhD fellowship.

Thanks to...

Emanuele, friend, brilliant scientist and husband.

The people in my lab that made these years very special to me: Coralie, Francesco, Saswat, Pauline, Thibaut and Elisa.

Morkos, Haoling and Riccardo, an extension of the lab family.

The precious collaborators, technical/administrative assistant Corentin, Bernard, Marie-Andrée, Laurence and Ines.

My big, odd, spread all around the world “ohana”. I’m the luckiest in the word to have all of you.

Antonella

Résumé

L'épigénétique et les modifications post-traductionnelles jouent un rôle essentiel dans la régulation du cycle cellulaire chez les Alphaproteobacteries

Caulobacter crescentus est l'organisme modèle d'étude de cycle cellulaire chez les Alphaproteobacteries. Le contrôle de ce cycle cellulaire implique un réseau complexe d'effecteurs pouvant interagir à différent niveau de régulation. Chaque cycle de division utilise ce circuit moléculaire pour aboutir à la formation de deux cellules filles différentes : une cellule flagellée en phase G1, et une cellule pédonculée en phase S qui entame immédiatement un nouveau cycle de réplication de l'ADN. Le principal régulateur du cycle cellulaire asymétrique est CtrA, qui dans sa forme phosphorylée inhibe la réplication de l'ADN en se fixant à l'origine de réplication du chromosome et active la transcription de dizaines de gènes indispensables à la progression du cycle cellulaire. CtrA est phosphorylé par le phospho-relais CckA/ChpT, localisé au pôle flagellé de la cellule prédivisionnelle. L'organisation spatiale de CckA suggère qu'à ce stade, les formes phosphorylées de CtrA seraient plus majoritairement présentes au pôle flagellé. De plus, CtrA est dégradé lors de la transition G1-S pour être ensuite retranscrit grâce à l'action d'un autre régulateur majeur appelé GcrA, dont le rôle n'était que peu connu au début de ce travail de thèse. Nous décrivons ici l'étude des mécanismes épigénétiques, qui impliquent la combinaison des activités de GcrA et de la méthyltransférase CcrM, ainsi que l'étude des modifications post-traductionnelles de CtrA, dans la régulation de ce cycle cellulaire asymétrique.

Étude fonctionnelle et structurale de la protéine GcrA et de ses partenaires protéiques

Dans ce travail, nous avons mis en évidence l'interaction fonctionnelle entre GcrA et le N6-adenosine méthyltransférase CcrM, protéines toutes deux hautement conservées chez les Alphaproteobacteries et activées respectivement au début et à la fin de la phase S. La combinaison d'expériences de biochimie, de biophysique, d'immunoprécipitation de la chromatine et de génétique nous a permis de révéler que GcrA est une protéine dimérique qui se fixe à l'ADN, et qui montre une affinité préférentielle, à la fois *in vitro* et *in vivo*, pour les promoteurs qui ont été méthylés par CcrM. Nous avons également montré que GcrA active la transcription des gènes sous le contrôle de ces promoteurs, en recrutant l'ARN polymérase. La fixation à l'ADN, dépendante de la méthylation est également observée avec les orthologues de GcrA présents chez d'autres Alphaproteobacteries, telles que *Brucella abortus* ou *Sinorhizobium meliloti*. GcrA est donc le membre fondateur d'une classe jusque-là inconnue de facteurs de transcription méthylation-dépendants impliqués dans la phase S du cycle cellulaire. Enfin GcrA

interagit également avec une protéine récemment caractérisée et appelée GipX. Le gène codant cette protéine est essentiel à la croissance de *Caulobacter*, et cette protéine pourrait jouer un rôle dans la régulation de l'activité de GcrA et dans la biosynthèse de la paroi bactérienne.

Résultats

GcrA est une protéine dimérique de structure principalement désordonnée

L'analyse bioinformatique de GcrA de *C. crescentus a* révèlé plusieurs régions (Fig. 1). GcrA a été produite, purifiée et étudiée par SAXS (Fig. 2). L'analyse a révélé une organisation dimérique avec un repliement désordonné.

a

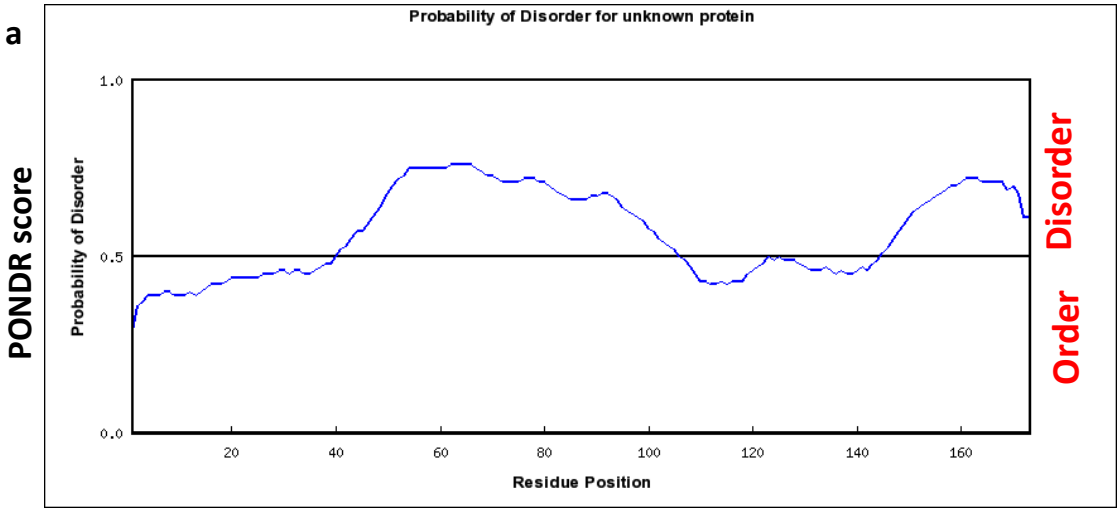

b

```
          10        20        30        40        50        60        70
           |         |         |         |         |         |         |
MSWTDERVSTLKKLWLDGLSASQIAKQLGGVTRNAVIGKVHRLGLSGRAAPSQPARPAFKAPRPARPAAQ
hccchhhhhhhhhhhhttcchhhhhhhhhhcchhhhhhhhhhhetccccccccccccccccccccccccc

AMPSAPRRVTPVEAPTSVPVAAAPAPLPAFRHEEPGSATVLTLGAHMCKWPIGDPSSEGFTFCGRRSSEG
ccccccccccccccccccccccccccccccccccttceeeeehccccccccccccccceeetcccccccc

PYCVEHARVAYQPQQTKKKSGGAELARSLRRYI
cccchhhheeeccccccccchhhhhhhhhhhh


Legend:
   Alpha helix     (h): 28.90%
   Extended strand (e): 6.94%
   Beta turn       (t): 3.47%
   Random coil     (c): 60.69%
```

Figure 1. Étude bioinformatique de la séquence de GcrA. (a) Prédiction des régions désordonnées par RONN. GcrA peut être divisée en 3 zones de structuration différente : une région N-terminale structurée, une région centrale désordonnée et une région C-terminale partiellement désordonnée. (b) La prédiction de structures secondaires GcrA par SOPMA confirme la prédiction de désordre par RONN et prédit des hélices alpha dans la région N-terminale et quelques éléments de structure secondaire dans la région C-terminale.

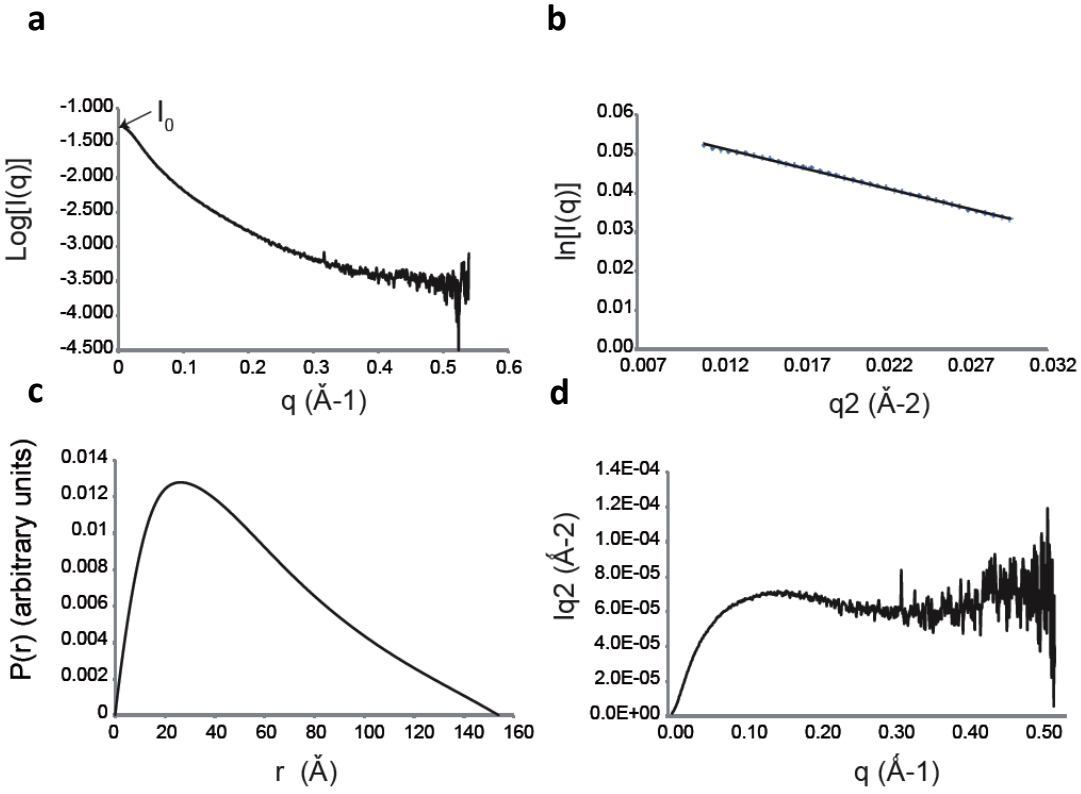

Figure 2. GcrA est un dimère intrinsèquement désordonné de forme allongée. Données de diffusion de rayons X aux petits angles (SAXS) de GcrA en solution. **(a)** Pour GcrA le poids moléculaire estimé correspond à une organisation en dimère (42KDa) **(b)** La représentation de Guignier. **(c)** La fonction de distribution des distances P(r) montre que les particules en solution ont une forme allongée. **(d)** La représentation de Kratky pour GcrA montre l'allure typique observée pour des protéines désordonnées (Fioravanti *et al*., 2013).

GcrA définit une nouvelle classe de protéines de liaison spécifique à l'ADN.

L'affinité des régions d'ADN du chromosome de *C. crescentus* détectées par ChIp-Seq (Fioravanti et al., 2013) pour GcrA ont également été testées par EMSA (Fig. 3). Cette analyse a révélé que GcrA se fixe spécifiquement aux séquences qui sont enrichies en sites de méthylation par CcrM.

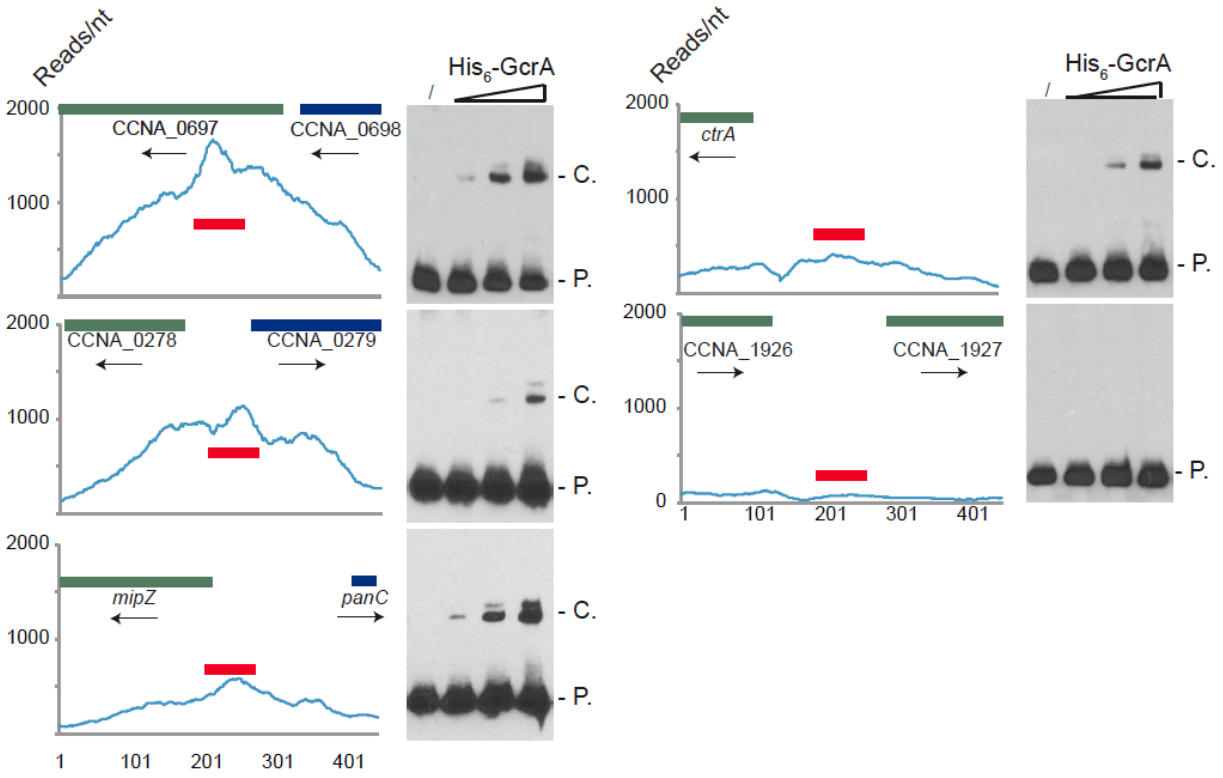

Figure 3. Essais de décalage de mobilité électrophorétique (EMSA pour Electrophoresis mobility shift assay) des 5 régions révélées par ChIP–Seq avec His_6-GcrA. Les résultats de l'EMSA obtenus avec des concentrations croissantes de GcrA purifiée en utilisant des sondes (ligne rouge) conçues dans des régions à grand nombre de lectures dans les résultats de ChIP-Seq. (Fioravanti *et al.*, 2013).

La liaison de GcrA à l'ADN de GcrA est améliorée par les méthylations CcrM-dépendantes

Nous avons ensuite étudié si la liaison GcrA à l'ADN dépendait de la méthylation (Fig. 4). Les sondes correspondant à CCNA_0697, le promoteur P1 de CtrA et le promoteur de mipZ ont été testés.

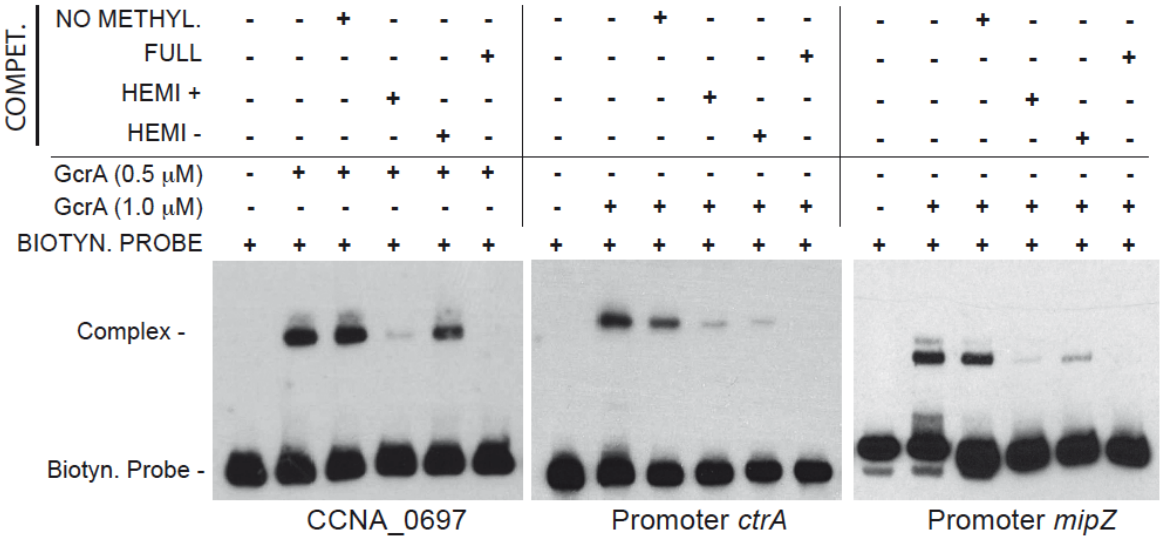

Figure 4. La liaison de GcrA à l'ADN dépend de l'état de méthylation CcrM. Trois régions (*CCNA_0697, CtrA, mipZ*) contenant des sites de méthylation de CcrM ont été testées dans une expérience de compétition. L'ADN compétiteur identique à la sonde dans divers états de méthylation a été mélangé avec des sondes biotinylées et GcrA pour évaluer la compétition. Pour CCNA_00697 nous avons utilisé 0,375 M de compétiteurs, tandis que pour les promoteurs de *CtrA* et *mipZ,* nous en avons utilisé 1,25 uM. Les constantes de dissociation (Kd) des sondes méthylées de *CtrA* et *mipZ* sont présentées dans la figure S9 de Fioravanti et al., 2013).

L'analyse a révélé que GcrA se lie avec plus d'affinité aux séquences méthylées, en particulier les séquences totalement méthylées.

GcrA se lie à la RNA polymerase

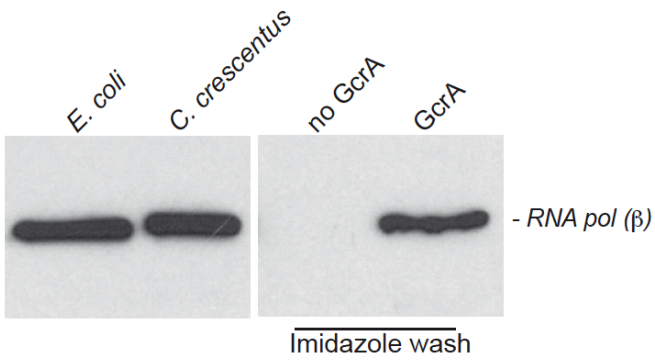

Figure 5. GcrA interagit avec l'ARN polymérase. Immunoblots utilisant des anticorps de la sous-unité β ARNP sur plusieurs échantillons. A gauche les lysats cellulaires de cellules de *E. coli* et des cellules de *C. crescentus*, sont positifs à l'anticorps. A droite, des échantillons de lysats cellulaires de *C. crescentus* CB15N déposés sur une colonne contenant His6-GCRA et ensuite lavés avec du NaCl (jusqu'à 1 M) et de l'imidazole pour éluer la His6-GCRA et ses partenaires protéiques putatifs. Cette procédure a également été réalisée avec une colonne vide (piste « no GcrA »). La colonne chargée de nickel avec His6-GCRA a été utilisé pour détecter la liaison de l'ARN polymerase à GcrA (Fioravanti et al., 2013).

Etude de l'interaction de GcrA de *C. crescentus* avec RNAP

Nous avons marqué GcrA avec un épitope M2 N-terminal et immuno-précipité avec un lysat de *C. crescentus* dans le but d'identifier des protéines partenaires. En comparant un contrôle négatif (EB689) avec un contrôle positif (EB690) comme montré dans la figure 6 nous avons pu identifier plusieurs protéines comme la RNA polymerase et CC3611.

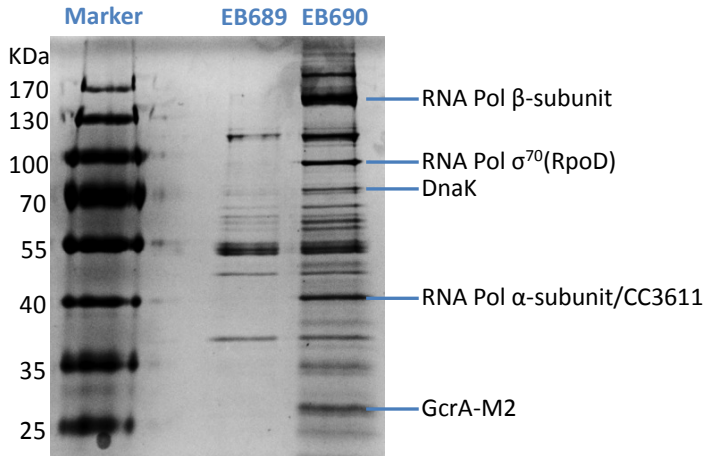

Figure 6. **Essai de co-immuno precipitation utilisant les Anticorps anti M2**. Les bandes du gel SDS-PAGE coloré à l'argent immuno-precipitées avec GcrA-M2 ont été identifiées par analyse en spectrométrie de masse.

Nous avons ensuite reconstitué la machinerie RNAP in vitro et montré que GcrA est capable de promouvoir la transcription dans un mécanisme dépendant de la méthylation (Fig.7).

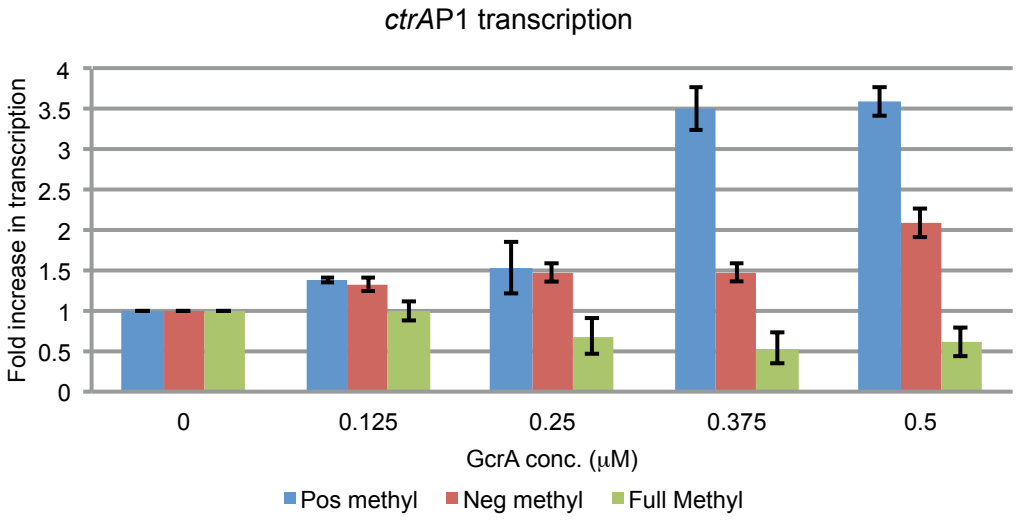

Figure 7. Essais de *transcription in vitro en utilisant* la RNA polymerase holoenzyme de *C. crescentus* en présence de concentrations croissantes de GcrA. Les triplicats de chaque condition montrés dans la figure 25 ont été quantifiés par ImageJ et représentés en quantités relatives.

Etude de la GcrA-Interacting Protein X (GipX, CC3611)

La protéine CC3611, appellee GipX a été purifiée et cristallisée pour résoudre sa structure tridimensionnelle (Fig. 8). L'analyse de la structure a révélé de nombreuses similitudes avec les amino transférases.

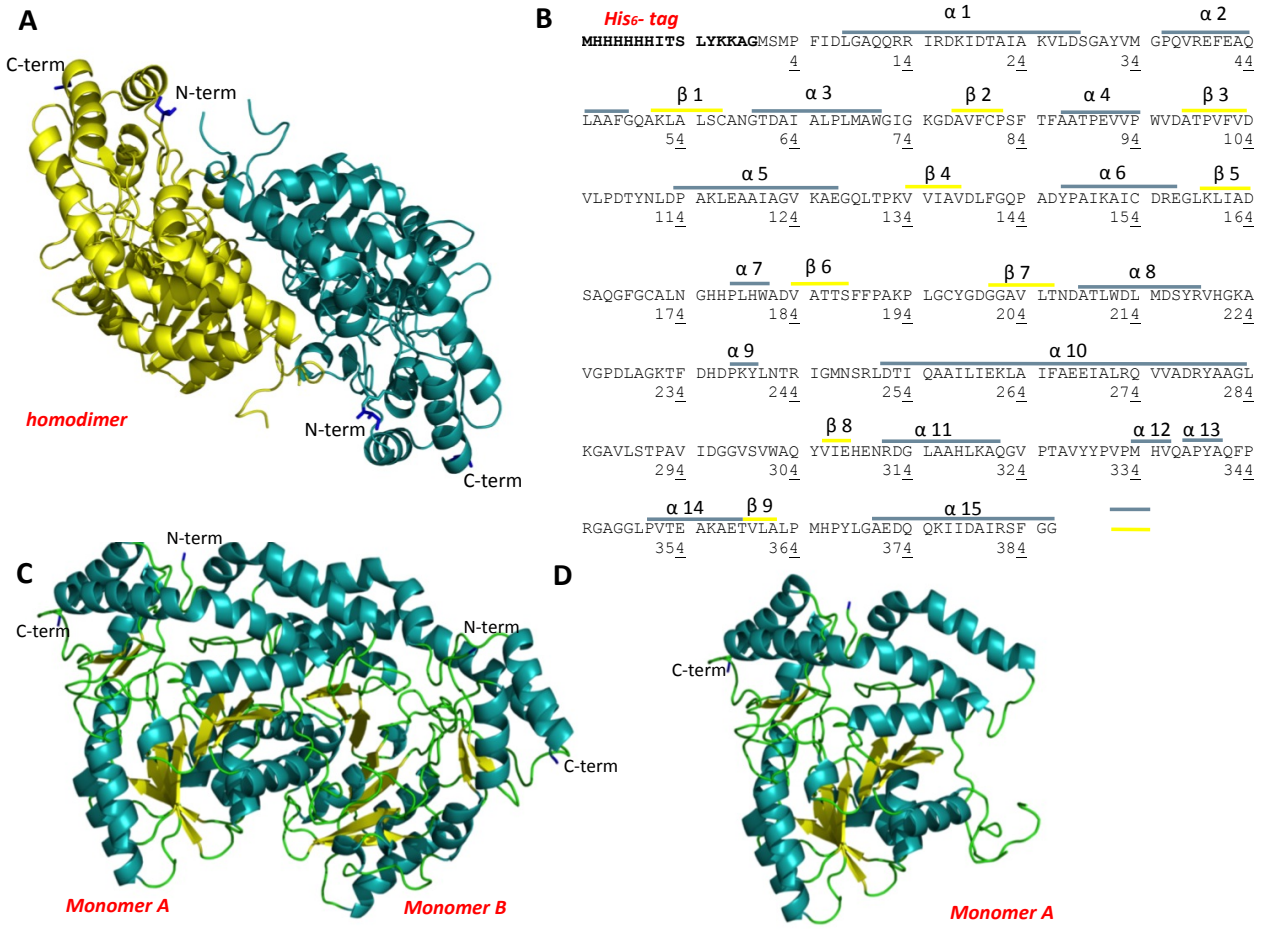

Figure 8. Structure de GipX. (a) Représentation en ruban de l'homodimère de His_6-GipX , les monomères sont représentés en cyan et jaune; (**b**) les éléments de structure secondaire de la proteine sont représentés par des lignes de couleur au dessus de la sequence primaire du monomère de His_6-GipX : helices α en cyan, feuillets β en jaune; (**c**) Representation en ruban de His_6-GipX homodimère, (**d**) Representation en ruban du monomére A, les éléments de structure secondaire sont représentés avec le même code couleur que **b**)

Enfin, nous avons utilisé la sonde *mipZ* pour vérifier que GipX est capable d'interférer avec la fixation de GcrA à l'ADN (Fig. 9).

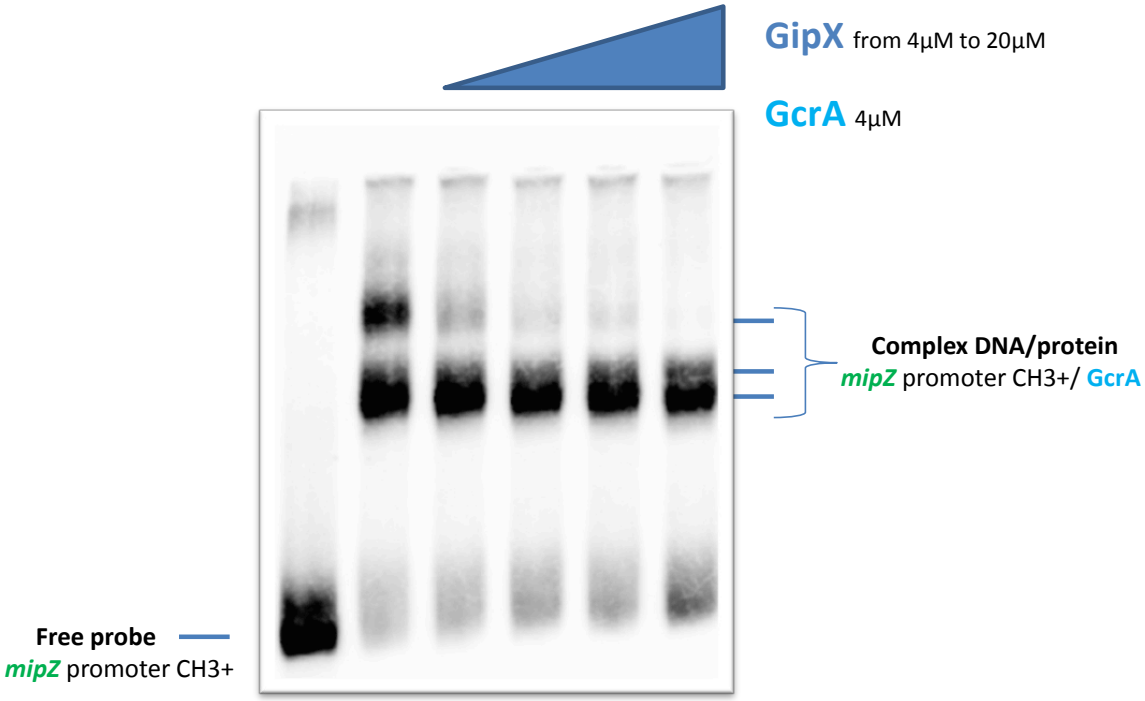

Figure 9. GipX est capable d'entrer en competition avec l'ADN pour l'interaction avec GcrA. Essais EMSA de GcrA avec le promoteur de mipZ en présence de GipX.

Etude de la phosphorylation de CtrA

Enfin, concernant l'étude des modifications post-traductionnelles de CtrA, nous décrivons également la structure protéique de ChpT ainsi que le développement d'un biosenseur capable de détecter les niveaux de phosphorylation *in vivo*. Ce biosenseur est basé sur la capacité des régulateurs de réponses à dimériser lorsqu'ils sont phosphorylés. Nous avons construit deux protéines de fusion basées sur le domaine receveur de CtrA étiqueté dans un cas avec une CFP et la YFP dans un second cas. Ces protéines ont d'abord été purifiées et phosphorylées *in vitro* afin de confirmer la dimérisation dépendante de la phosphorylation par mesure de FRET. Nous avons ensuite validé la fonctionnalité de ce biosenseur *in vivo*, en exprimant les deux protéines de fusion dans des populations de bactéries synchonisées ainsi que dans des souches présentant des contextes génétiques différents. Nos résultats ouvrent la possibilité d'étendre cette méthode pour l'étude *in vivo* de la phosphorylation des régulateurs de réponses dans d'autres systèmes bactériens.

Résultats :

Etude structurale de la cascade de phosphorylation qui active CtrA

C. crescentus ChpT

Le phospho-relai CtrA est composé de CckA, ChpT and CtrA. ChpT est un homodimère qui adopte l'architecture du domaine de la partie intracellulaire de l'histidine kinase de classe I. La structure de ChpT est décrite dans Fioravanti et al., 2012.

Nous avons construit un biosenseur de la phosporylation de CtrA basé sur le FRET décrit dans la figure 10.

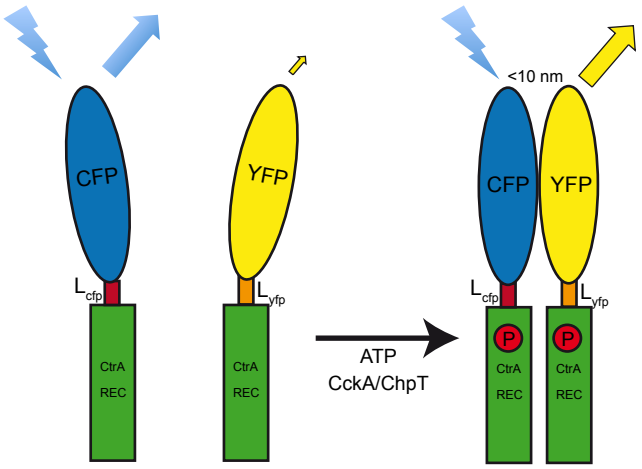

Figure 10. Représentation schématique du senseur CtrA(RD)-CFP et CtrA(RD)-YFP. En bleu: CtrA(RD)-CFP; en jaune CtrA(RD)-YFP; en vert: regulateur de reponse; en rouge: le groupement phosphate.

Nous avons purifié les composants de ce bio-senseur et nous les avons phosphorylés avec CckA et ChpT purifiés. Le signal FRET a été mesuré et est montré dans la figure 11.

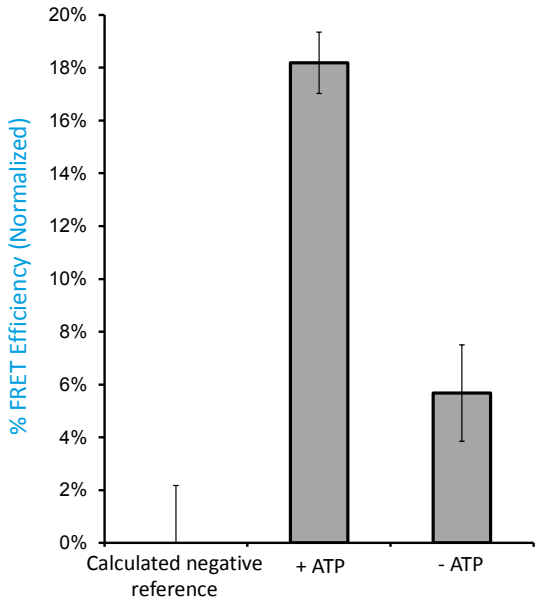

Figure 11. L'histogramme représente la mesure de l'efficacité FRET dans l'expérience *in vitro*. La référence négative a été calculée en présence du phospho-relai entier, de l'ATP et la moitié du senseur (CtrA(RD)-YFP or CFP).

Nous avons également exprimé le senseur *in vivo* (Figure 12) et quantifié le signal FRET par quantification dans différentes cellules (Fig. 13).

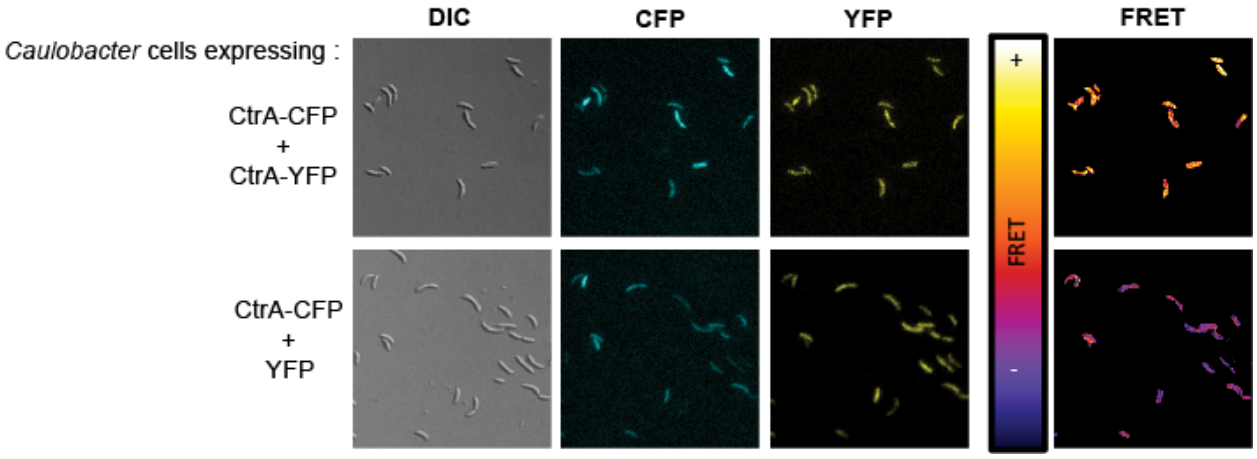

Figure 12. Dimerisation due à la phosphorylation de CtrA mesurée par FRET. L'expérience de FRET *in vivo* sur *C. crescentus*. YFP a été utilisé comme contrôle négatif.

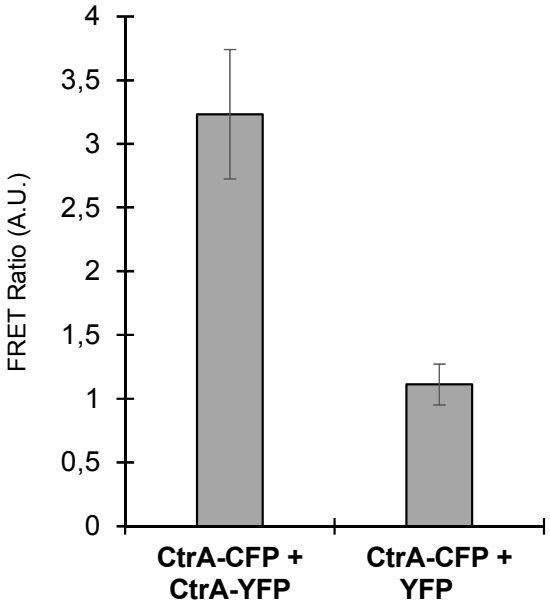

Figure 13. Représentation des niveaux moyennés de FRET par condition après l'analyse cellule par cellule (30 cellules)

Nous avons également comparé les mesures FRET avec les mesures de phosphorylation *in vivo* de CtrA (Fig.14).

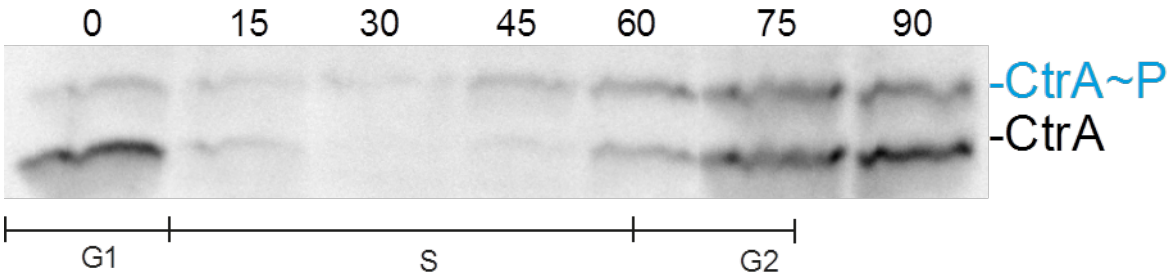

Figure 14. Immunoblot de CtrA wt sur gel Phos-Tag chargé avec des échantillons de Caulobacter synchronisés (milieu riche).

Nous avons quantifié l'intensité des bandes de phosphorylation (Fig. 15) et les quantités relatives des niveaux CtrA/CtrA-P (Fig. 16).

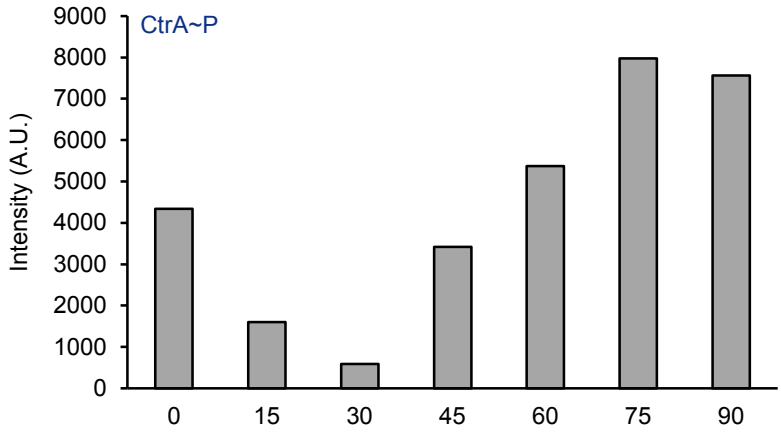

Figure 15. Quantification de l'intensité des bandes phosphorylées avec Image J en fonction du temps (en minutes) voir le texte pour l'interprétation.

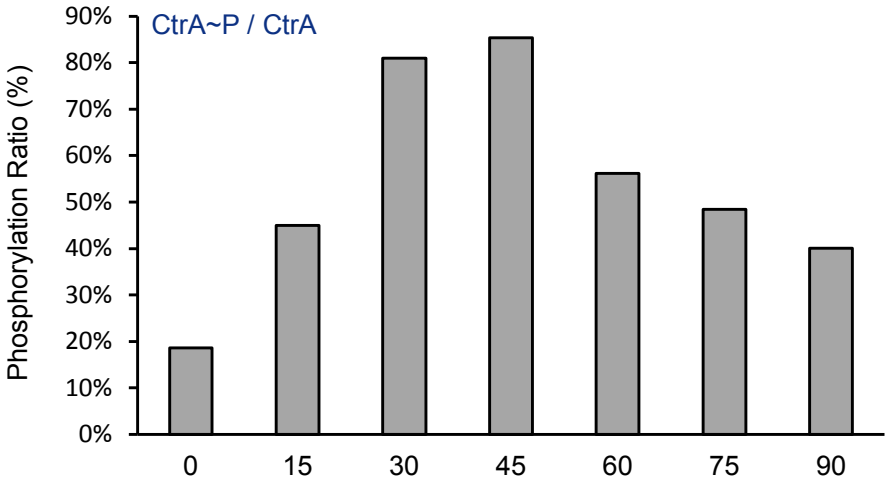

Figure 16. Ratio des intensités des bandes phosphorylées/non phosphorylées correspondant à l'activité de la cascade de phosphorylation en fonction du temps (en minutes).

Nous avons ensuite comparé les mesures avec le bio-senseur FRET (Fig.17) et quantifié les intensités (Fig. 18). Nous avons montré que le senseur est capable de détecter les niveaux de CtrA et leur variation au cours de cycle cellulaire.

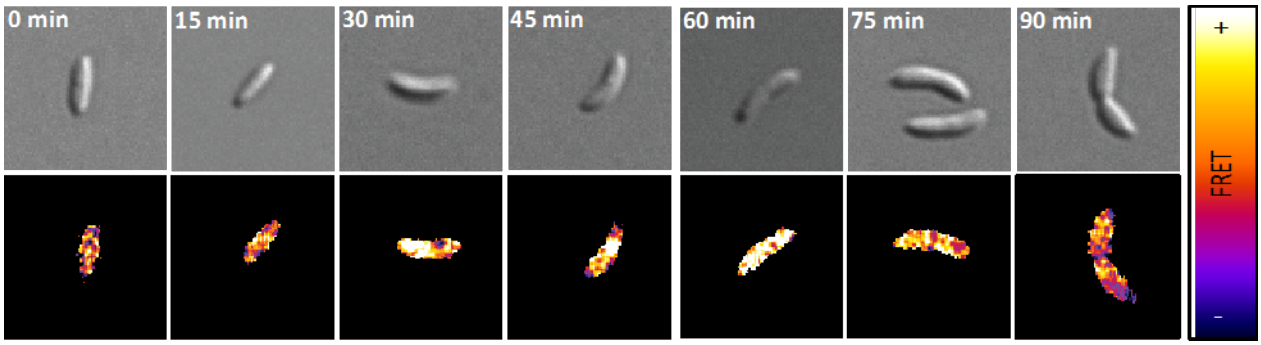

Figure 17. Cellules de *Caulobacter* synchronysées exprimant CtrA-CFP et CtrA-YFP.

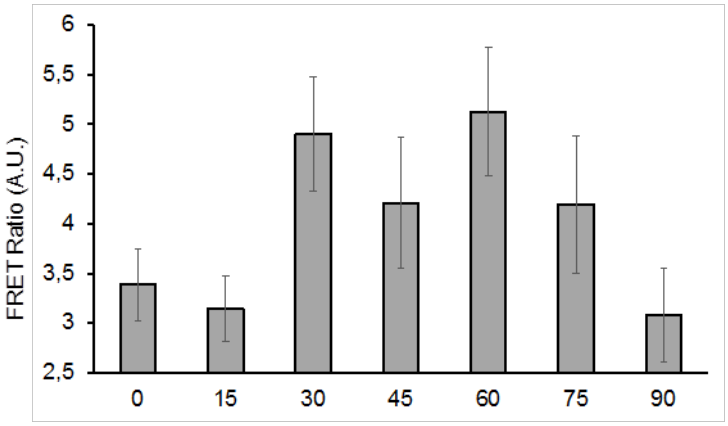

Figure 18. Niveaux moyens de FRET en fonction du temps (en minutes) calculés sur 20 cellules à chaque temps.

Conclusions et perspectives

Un grand pas en avant vers la compréhension du rôle et de l'activité GcrA dans la régulation du cycle cellulaire de *C. crescentus* a été réalisé dans cette thèse. Pour la première fois GcrA a été caractérisée par la combinaison d'approches de biologie structurale, de biochimie et de biologie cellulaire. Nous avons montré que GcrA est un facteur de transcription essentiellement désordonné, capable de se lier spécifiquement aux régions promotrices du chromosome et ce, en fonction de leur état de méthylation (Fioravanti et al., 2013).

Dans cette thèse, nous avons aussi mis en évidence une autre protéine interagissant avec GcrA qui a été identifiée dans des expériences de co-immunoprécipitation et nommée GipX. Cette protéine essentielle et régulée par le cycle cellulaire (en phase avec l'expression de GcrA), a été étudiée au niveau structural et fonctionnel. La structure de GipX a révélé une similitude avec les aspartate aminotransférases impliquées dans la biosynthèse de la paroi cellulaire. De façon intéressante, les différences majeures dans la structure GipX avec les membres de cette famille d'enzymes issus d'organismes qui ne possèdent pas GcrA, correspondent à des régions insérées exposées à la surface de la protéine, qui pourrait être impliquées dans la reconnaissance et l'interaction avec des partenaires comme GcrA.

L'un des objectifs de cette thèse a été d'étudier la cascade de phosphorylation de CtrA, composée par CckA et ChpT. Nous avons développé un outil basé sur le FRET capable de détecter le taux de CtrA phosphorylés. Cette approche biosenseur basée sur le FRET pourra être étendue à tous les régulateurs de réponse en créant une carte des niveaux de phosphorylation de chaque régulateur de réponse de C. crescentus, mais aussi dans d'autres bactéries où des systèmes à deux composants sont présents et agissent en créant une répartition spatiale de la phosphorylation.

Se référer à la version en anglais pour la bibliographie.